INFORMATION TO USERS

This manuscript has been reproduced from the microfilm master. UMI films the text directly from the original or copy submitted. Thus, some thesis and dissertation copies are in typewriter face, while others may be from any type of computer printer.

The quality of this reproduction is dependent upon the quality of the copy submitted. Broken or indistinct print, colored or poor quality illustrations and photographs, print bleedthrough, substandard margins, and improper alignment can adversely affect reproduction.

In the unlikely event that the author did not send UMI a complete manuscript and there are missing pages, these will be noted. Also, if unauthorized copyright material had to be removed, a note will indicate the deletion.

Oversize materials (e.g., maps, drawings, charts) are reproduced by sectioning the original, beginning at the upper left-hand corner and continuing from left to right in equal sections with small overlaps.

Photographs included in the original manuscript have been reproduced xerographically in this copy. Higher quality 6" x 9" black and white photographic prints are available for any photographs or illustrations appearing in this copy for an additional charge. Contact UMI directly to order.

Bell & Howell Information and Learning
300 North Zeeb Road, Ann Arbor, MI 48106-1346 USA
800-521-0600

UMI®

DISSERTATION

EXPERIMENTAL AND THEORETICAL DEVELOPMENT OF A TRACER GAS METHOD FOR MEASURING TRAPPING EFFICIENCY IN INTERNAL COMBUSTION ENGINES

Submitted by

Daniel B. Olsen

Mechanical Engineering

In partial fulfillment of the requirements

for the Degree of Doctor of Philosophy

Colorado State University

Fort Collins, Colorado

Spring 1999

COLORADO STATE UNIVERSITY

February 25, 1999

WE HEREBY RECOMMEND THAT THE DISSERTATION PREPARED UNDER OUR SUPERVISION BY DANIEL B. OLSEN, ENTITLED "EXPERIMENTAL AND THEORETICAL DEVELOPMENT OF A TRACER GAS METHOD FOR MEASURING TRAPPING EFFICIENCY IN INTERNAL COMBUSTION ENGINES" BE ACCEPTED AS FULFILLING IN PART REQUIREMENTS FOR THE DEGREE OF DOCTOR OF PHILOSOPHY.

Committee on Graduate Work

Co-Adviser

Adviser

Department Head

ABSTRACT OF DISSERTATION

EXPERIMENTAL AND THEORETICAL DEVELOPMENT OF A TRACER GAS METHOD FOR MEASURING TRAPPING EFFICIENCY IN INTERNAL COMBUSTION ENGINES

An investigation into a tracer gas method for determining trapping efficiency in 4-stroke and 2-stroke cycle engines is described. Potential difficulties with the technique are identified and analyzed. These potential difficulties include incomplete cylinder tracer reaction, exhaust tracer instability, and inconsistent exhaust sampling. Tracer gas global chemical kinetic mechanisms are reviewed and used as a means for tracer gas selection. Multiple step chemical kinetic mechanisms are implemented to predict tracer destruction in the cylinder and tracer consumption in the exhaust. The tracer gases investigated are nitrous oxide (N_2O) and monomethylamine (CH_3NH_2). As a benchmark the oxygen tracer technique, where oxygen in the intake air is used as the tracer, is evaluated for application to 4-stroke cycle engines. Equations and procedures for performing tracer gas measurements and analysis are developed.

Test results are presented for a GM 5.7 l, 8 cylinder, 4-stroke cycle, gasoline engine and a Cooper-Bessemer GMV-4TF 141 l, 4-cylinder, 2-stroke cycle, natural gas engine. Results include evaluation of tracer cylinder reaction efficiency, assessment of the extent of tracer exhaust reaction, and trapping efficiency measurements. Of the tracers considered, N_2O is determined to be optimal for both applications. The tracer gas method

is utilized to determine the engine speed at which maximum short-circuiting occurs in the 4-stroke cycle engine. Results of scavenging investigations using the tracer gas method are described for the 2-stroke cycle engine for various operating conditions. The scavenging investigations include evaluation of trapping efficiency, delivery ratio, scavenging efficiency, and trapped equivalence ratio. The engine operating condition variations investigated are changes in boost, speed, back pressure, and port restriction.

Daniel B. Olsen
Department of Mechanical Engineering
Colorado State University
Fort Collins, CO 80523
Spring 1999

ACKNOWLEDGMENTS

I thank God for blessing me with the many opportunities that I have had at CSU and the abundance of talented, encouraging people whom have supported me. It is difficult to know where to begin and how to include everyone. I would like to thank my committee members for their guidance and technical input throughout this work. I have been able to draw from the expertise of each member over the course of my Ph.D. program. Much of this work has depended on the collection of quality test data from internal combustion engines, which is generally not an individual effort. It requires, particularly in the case of large bore engine testing, the involvement of several skilled individuals. Two full-time staff members at the Engines and Energy Conversion Laboratory (EECL) who played critical roles in the 2-stroke cycle large bore engine testing were Gary Hutcherson and Jason Holden. I would like to thank Paulius Puzinauskas, who at the time was a full time EECL staff member and committee member, for his key contributions to the automotive 4-stroke cycle engine program. There have been numerous students involved in the testing, both graduate and under graduate. Three graduate students who played important roles in the 2-stroke cycle large bore engine testing were Dean Huntley, Kevin Johnson, and Stephanie Mick. Additionally, I would like to express my appreciation to Peugeot Sport for funding the 4-stroke cycle engine test program and the Pipeline Research Counsel International of the American Gas Association and the Gas Research Institute for funding the 2-stroke cycle engine testing.

I would like to thank my wife, Kim, for her support and patience over the last few years. Our lives were enriched with the birth of our daughter, Rachel, on October 16, 1996. This decreased the amount of time for school and dissertation work, but at the same time was quite an inspiration. I would like to thank my parents, Mr. and Mrs. Larry Olsen, for always encouraging me to pursue a Ph.D.

TABLE OF CONTENTS

LIST OF TABLES

LIST OF FIGURES

NOMENCLATURE

Symbols

Λ	delivery, or scavenging, ratio
ω	engine speed in revolutions per second
$\rho_{a,i}$	inlet air density
$(A/F)_{ov}$	mass based overall air/fuel ratio
$(A/F)_{stoic}$	stoichiometric mass based air/fuel ratio
$(A/F)_{tr}$	mass based air/fuel ratio trapped in the engine cylinder
ρ_{amb}	ambient air density
η_{cr}	cylinder reaction efficiency
η_f	fuel conversion efficiency = $W_c/(m_f Q_{HV})$
ξ	cylinder reaction inefficiency
$(F/A)_{stoic}$	stoichiometric mass based fuel/air ratio
$(F/A)_{tr}$	mass based fuel/air ratio trapped in the cylinder
ΔG^0	change in Gibbs free energy
ρ_{pc}	calculated charge density at exhaust port closing using exhaust manifold pressure and intake manifold temperature
ε_r	mass fraction of tracer destroyed in exhaust
η_{sc}	charging efficiency
η_{sc}	scavenging efficiency
η_{tr}	trapping efficiency
η_v	volumetric efficiency = $m_a/(\rho_{a,i} V_d)$
dm_{del}/dt	measured air mass flow through engine
f_{mf}	misfire fraction
f_{sc}	short-circuited fraction
m_a	mass of air delivered per cycle
m_{del}	total mass of delivered air or air/fuel mixture per cycle
m_e	exhaust mass per cycle
m_f	mass of fuel inducted into the cylinder per cycle
m_{ref}	reference mass
m_{res}	combined mass of combustion products and unused air and fuel from the previous cycle remaining in the cylinder after the scavenging process
m_{ret}	mass of delivered air or air/fuel mixture trapped per cycle
m_{sc}	mass of delivered air or A/F mixture short-circuited per cycle
$m_{t,c}$	mass of tracer which survives in cylinder due to cylinder reaction inefficiency
$m_{t,del}$	mass of tracer delivered per cycle
$m_{t,e}$	mass of tracer in exhaust after exhaust tracer destruction
$m_{t,mf}$	mass of tracer which survives in cylinder due to misfire

$m_{t,sc}$	mass of tracer short-circuited per cycle
$m_{t,tr}$	mass of tracer trapped in cylinder = $m_{t,del}$ - $m_{t,sc}$
m_{tr}	trapped mass in the cylinder
MW_a	molecular weight of intake air
MW_e	molecular weight of exhaust
MW_t	molecular weight of tracer
N	crankshaft rotational speed in revolutions per second
N_{cyl}	number of cylinders
P	indicated engine power or pressure
P^0	reference pressure (1 atm)
Q_{HV}	fuel heating value
R	universal gas constant
SG_{c1}	specific gravity of the sample taken before combustion
SG_{c2}	specific gravity of the sample taken after combustion
SG_e	specific gravity of exhaust = MW_e/MW_a
SG_f	specific gravity of the fuel
T	temperature
V_c	total cylinder volume
V_d	displaced volume
V_{pc}	cylinder volume at exhaust port closing
W_c	indicated work per cycle
X_{c1}	tracer mole fraction in sample taken before combustion
X_{c2}	tracer mole fraction in sample taken after combustion
$X_{e,1}$	mole fraction of tracer entering exhaust
$X_{e,2}$	mole fraction of tracer exiting exhaust
X_{N2}	mole fraction of nitrogen
X_{N2O}	mole fraction of nitrous oxide
X_{O2}	mole fraction of oxygen
$X_{t,e}$	mole fraction of tracer in exhaust
$X_{t,i}$	mole fraction of tracer in intake air
$X_{t,tr}$	mole fraction of tracer trapped in engine cylinder before fuel addition
y_{res}	residual gas fraction

Abbreviations

AGA	American Gas Association
ATC	After Top Center
BMEP	Brake Mean Effective Pressure
CH_3NH_2	Monomethylamine
CO	Carbon monoxide
EES	Engineering Equation Solver
EPA	Environmental Protection Agency
EPO	Exhaust Port Opening
EVO	Exhaust Valve Opening

FTIR	Fourier Transform Infra-Red
GRI	Gas Research Institute
IC	Internal Combustion
IMEP	Indicated Mean Effective Pressure
ISAC	Indicated Specific Air Consumption
LOPP	Location Of Peak Pressure
N_2O	Nitrous oxide
NO_x	Oxides of nitrogen
RRKM	Rice-Ramsperger-Kassel-Marcus
THC	Total Hydrocarbon
TST	Transition State Theory
UV	Ultraviolet

CHAPTER 1

INTRODUCTION

Internal combustion (IC) engines play a vital role in our society. The list of common applications is extensive, ranging in size from chainsaw, snow blower, and motor scooter engines to stationary gas pipeline, locomotive, and ship engines. The term IC engine can be expanded to include a number of engine types, including gas turbines. However, in this work the term refers exclusively to reciprocating IC engines. A significant and highly publicized drawback of IC engines is the emission of pollutants and ensuing degradation of air quality. Producing IC engines that run efficiently and minimize pollutant emissions is important to the conservation of fossil fuels and improvement of air quality. Although engine efficiency and pollutant emissions have improved dramatically over the last few decades, there is still much room for further improvement.

The trapped air/fuel (A/F) ratio is the parameter that perhaps has the greatest influence on emissions. The trapped A/F ratio is the ratio of the mass of air to the mass of fuel in the engine cylinder after the intake valves, or ports, close and fuel delivery is complete. This is the air and fuel mixture that is actually burned in the cylinder. The overall A/F ratio, which may be significantly different, is the A/F ratio that reflects the

total supply of air and fuel to the engine. The trapped A/F ratio is commonly expressed as the trapped equivalence ratio, or simply equivalence ratio, and is defined as

$$\phi = \frac{\left(A/F\right)_{stoic}}{\left(A/F\right)_{tr}} \tag{1.1}$$

where

$(A/F)_{tr}$ = mass based air/fuel ratio trapped in the engine cylinder[1]
$(A/F)_{stoic}$ = stoichiometric mass based air/fuel ratio.

The trapped equivalence ratio can also be expressed in terms of fuel/air ratios

$$\phi = \frac{\left(F/A\right)_{tr}}{\left(F/A\right)_{stoic}} \tag{1.2}$$

where

$(F/A)_{tr}$ = mass based fuel/air ratio trapped in the cylinder
$(F/A)_{stoic}$ = stoichiometric mass based fuel/air ratio.

Expressing the A/F ratio as equivalence ratio provides a means to compare performance and emissions from engines that run on different fuels. The dramatic influence that trapped equivalence ratio has on the primary emissions, carbon monoxide (CO), total hydrocarbon (THC), and oxides of nitrogen (NO_x) is illustrated in Figure 1.1, taken from Heywood[1]. Thus, to study emissions from IC engines the trapped equivalence ratio must be known. Precisely characterizing the trapped equivalence ratio for an engine can influence design and operating decisions driven by emission reduction goals.

Another emission constituent that has been receiving more attention in recent years is formaldehyde (CH_2O)[2,3]. Formaldehyde emissions, like the other pollutants, are

[1] All fuel/air and air/fuel ratios discussed are mass based unless otherwise indicated.

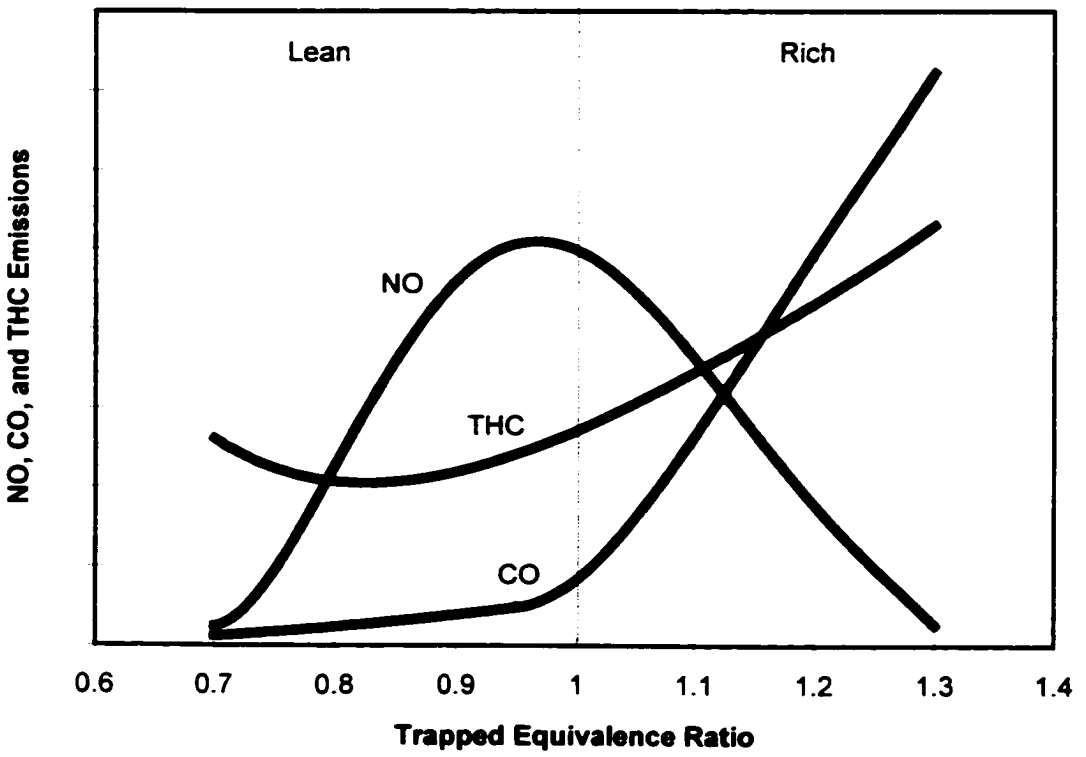

Figure 1.1 Qualitative Variations in Emissions with Trapped Equivalence Ratio.

heavily influenced by the trapped equivalence ratio. The EPA is scheduled to publish regulations for formaldehyde emissions by the year 2000. This is particularly important for natural gas engines. Formaldehyde is a primary intermediate in the chemical kinetic combustion mechanism for methane, the primary constituent in natural gas. Emissions of significant levels of formaldehyde are common in large bore natural gas engines used for natural gas compression and power generation[4]. Formaldehyde is also present at significant quantities in the exhaust of engines running on oxygen-bound fuels such as methanol.

In 4-stroke cycle engines and premixed 2-stroke cycle engines the measurement of the trapped equivalence ratio is not difficult, because the trapped A/F ratio is typically very close to the overall A/F ratio. Assuming the trapped and overall A/F ratios to be equal, direct measurement of the air and fuel flow into the engine or exhaust gas analysis can be used to evaluate the trapped A/F ratio directly. In fuel-injected 2-stroke cycle engines, this is not the case. The combustion products are scavenged with pure air, and fuel is added after the scavenging process. The trapped A/F ratio is dependent on the effectiveness of the scavenging process to remove combustion products and replace them with fresh air. The evaluation of the trapped A/F ratio is dependent on the trapping efficiency according to the equation

$$\left(A/F\right)_{tr} = \left(A/F\right)_{ov} \eta_{tr} \tag{1.3}$$

where

$(A/F)_{OV}$ = mass based overall air/fuel ratio,

and the trapping efficiency is defined as

$$\eta_{tr} = \frac{m_{ret}}{m_{del}} \tag{1.4}$$

where

m_{ret} = mass of delivered air or air/fuel mixture trapped per cycle
m_{del} = total mass of delivered air or air/fuel mixture per cycle.

For 2-stroke cycle fuel-injected engines the trapping efficiency indicates the fraction of air flowing through the engine that is trapped in the cylinder and can be used in the combustion process. This parameter is very difficult to measure. In the past, accurate

measurement has required major engine modifications and testing in a laboratory environment. The tracer gas method is a technique by which the trapping efficiency can be measured without major engine modifications.

The reasons to measure trapping efficiency in 4-stroke cycle engines and 2-stroke cycle premixed engines are important, but different from those for 2-stroke cycle fuel-injected engines. In these engines the mass of premixed air and fuel that is not burned in the engine reduces efficiency and contributes to THC emissions. By implementing the tracer gas method this contribution to THC emissions can be quantified. The tracer gas method is an experimental technique that supports the ongoing effort to increase efficiency and reduce pollutant emissions in IC engines.

1.1 The Tracer Gas Method

The tracer gas method investigated is an experimental technique used to measure trapping efficiency. As discussed above, the trapping efficiency denotes the fraction of gas flowing through an engine that can be utilized in the combustion process. The fraction of the charge that can not be utilized in the combustion process is referred to as the short-circuited fraction, which is simply

$$f_{sc} = 1 - \eta_{tr} \tag{1.5}.$$

The short-circuiting process generally occurs during scavenging and is often called scavenged short-circuiting. A simple representation of this process is shown in Figure 1.2.

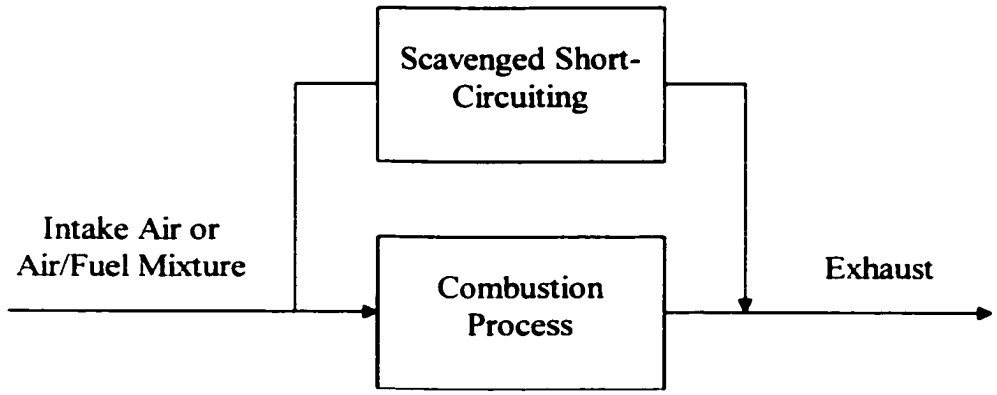

Figure 1.2 Short-Circuiting Process

Historically, trapping efficiency has been a difficult parameter to evaluate. This is because trapping efficiency varies with the level of in-cylinder mixing, gas velocities, exhaust tuning, and other physical phenomena that are difficult to predict. Numerous techniques involving in-cylinder sampling have been successfully implemented to measure trapping efficiency[5]. Although these have proven to be reliable as long as a significant portion of the cylinder contents is removed with each sample, they generally require major engine modification and a laboratory environment. In-cylinder sampling can be intrusive to the combustion process and is costly to carry out. The engine cylinder typically must be physically modified to accommodate a sample valve. The biggest advantage of the tracer gas method is that it does not require major engine modification to execute and is adaptable to field applications. The experimental setup is external to the engine, eliminating the need for major engine modification.

In the tracer gas method a small amount of tracer is continuously fed into and mixed with the intake air or fuel/air mixture. The tracer that is trapped in the cylinder is destroyed during combustion and the short-circuited portion survives in the exhaust.

Ideally, the tracer is completely destroyed at combustion temperatures and stable at exhaust temperatures. The short-circuited gas can be quantified by comparing the tracer mole fraction in the intake to that in the exhaust. A tracer that is completely destroyed when trapped in the cylinder and stable in the exhaust is referred to as an "ideal tracer".

1.2 Application to 4-Stroke Cycle Engines

In a 4-stroke cycle engine, there is typically a period in which both the intake and exhaust valves are open simultaneously, called the overlap period. If there is a positive pressure differential between the intake system and exhaust system during that period, short-circuiting can occur. Figure 1.3 shows an illustration of short-circuiting during the overlap period. Short-circuiting reduces the effective volumetric efficiency, which is directly proportional to engine power. This is seen in the expression for indicated power for a 4-stroke cycle engine[1]

$$P = \frac{\eta_f \eta_v N V_d Q_{HV} \rho_{a,i} \left(F/A\right)_{tr}}{2} \tag{1.6}$$

where

η_f = fuel conversion efficiency = $W_c/(m_f Q_{HV})$
η_v = volumetric efficiency = $m_a/(\rho_{a,i} V_d)$
N = crankshaft rotational speed in revolutions per second
W_c = indicated work per cycle
m_f = mass of fuel inducted into the cylinder per cycle
V_d = displaced volume
Q_{HV} = fuel heating value
$\rho_{a,i}$ = inlet air density.

In many engines the intake and exhaust manifolds are designed to maximize this pressure differential during overlap. This provides additional scavenging and helps initiate the

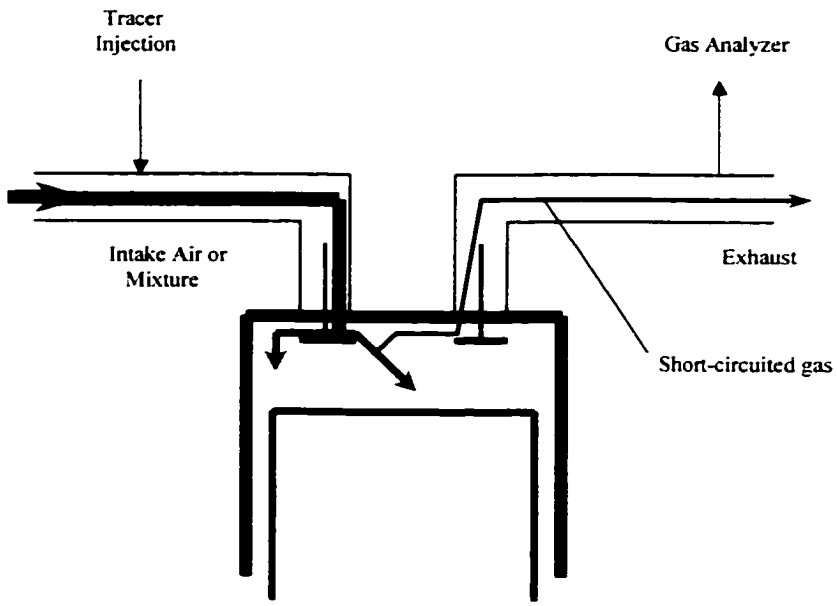

Figure 1.3 Short-Circuiting During Overlap Period

intake process; however, it can also result in wasted fuel. The overlap period and consequently the short-circuited fraction can be adjusted through valve timing to balance its effects on fuel economy, THC emission, and power output. The correct balance is application dependent. The volumetric efficiency can be tailored to a particular application. Valve overlap increases volumetric efficiency at high speeds and reduces volumetric efficiency at low speeds. Consequently, slow speed engines tend to have short overlap periods and high speed engines tend to have large overlap periods. Quantifying the short-circuited fraction helps determine if the engine operation reflects the intended design with regard to valve overlap effects.

The oxygen concentration in the exhaust has been used to calculate the short-circuited fraction in 4-stroke cycle engines[9]. This is similar to the tracer gas method,

only the tracer is the oxygen present in the intake air. The oxygen in the intake air, approximately 21%, flows into an engine cylinder. The oxygen that is trapped in the cylinder reacts with the fuel during combustion, while the fuel that is short-circuited mixes with the exhaust and flows out the engine. The concentration of oxygen in the exhaust is a measure of the level of short-circuiting. This method is most practical when the engine is run at a stoichiometric or rich fuel/air ratio to eliminate exhaust oxygen from charge dilution, or excess air. Additionally, the technique works best when the fuel and air are well mixed in the cylinder to reduce oxygen in the exhaust from incomplete combustion.

1.3 Application to 2-Stroke Cycle Engines

In 2-stroke cycle engines, power is produced on every engine revolution. To achieve this engine cycle the incoming fresh charge must displace, or scavenge, the combustion products from the previous charge. Invariably part of the incoming charge either passes directly out the exhaust port or mixes with combustion products and subsequently exits through the exhaust port. There is also a portion of the products of combustion that remains in the cylinder after scavenging. Figure 1.4 shows an example of scavenging flow in a loop scavenged 2-stroke engine. By design, 2-stroke cycle engines have a much higher fraction of short-circuited gas than 4-stroke cycle engines do.

The short-circuited fraction, degree of mixing, and residual fraction are normally not known in a 2-stroke cycle engine. If the short-circuited fraction can be measured the trapping efficiency can be easily calculated. Two other quantities of interest are the

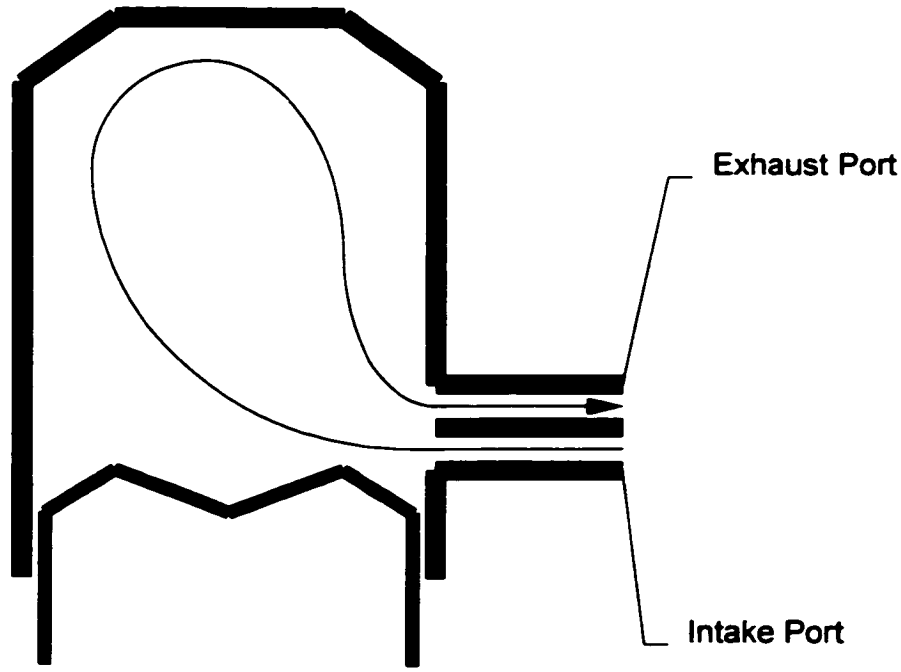

Figure 1.4 Intended Scavenging Flow for a Loop Scavenged Engine

scavenging efficiency and the delivery, or scavenging, ratio. The scavenging efficiency provides an indicator of how effective the scavenging system is at removing combustion products and filling the cylinder with fresh charge. It is defined as

$$\eta_{sc} = \frac{m_{rel}}{m_{tr}} \tag{1.7}$$

where m_{tr} is the trapped mass in the cylinder when the exhaust ports close, including residual combustion products from the previous cycle. The residual gas fraction follows directly from the scavenging efficiency as

$$y_{res} = \frac{m_{res}}{m_{tr}} = 1 - \eta_{sc} \tag{1.8}$$

where m_{res} is the combined mass of combustion products and unused air and fuel from the previous cycle remaining in the cylinder after the scavenging process. The delivery, or scavenging, ratio is defined as

$$\Lambda = \frac{m_{del}}{m_{ref}} \tag{1.9}$$

where m_{ref} is a reference mass. Often the trapped cylinder mass is used as the reference mass. Defining the reference mass in this way, the scavenging efficiency can be expressed as

$$\eta_{sc} = \Lambda \eta_{tr} \tag{1.10}.$$

Therefore, by measuring the necessary parameters to calculate the delivery ratio (discussed in Chapter 6), the scavenging efficiency can be calculated upon implementing the tracer gas method. The scavenging efficiency is an important quantity because it is directly proportional to indicated power per cylinder for 2-stroke cycle engines, which can be written as

$$P = \eta_f \eta_{sc} N V_c Q_{HV} \rho_{a,i} \left(F/A\right)_{tr} \tag{1.11}$$

where V_c is the total cylinder volume at port closure. Another parameter often used in scavenging analysis is the charging efficiency, defined as

$$\eta_{ch} = \frac{m_{ret}}{V_d \rho_{amb}} \tag{1.12}$$

where ρ_{amb} is the ambient air density. Note that charging efficiency is relative to the cylinder mass based on ambient air density, which is typically constant throughout a particular engine test. Thus, varying the inlet air, or boost, pressure has a direct impact on the charging efficiency. In contrast, scavenging efficiency is a mass fraction based solely

on the cylinder contents at port closure. It is a direct measure of the ability of a particular engine design to replace combustion products with fresh charge, regardless of boost.

1.4 Literature Survey

A literature survey on the tracer gas method is carried out. The review focuses on literature where trapping efficiency measurements utilizing the tracer gas method are reported. Additionally, literature is reviewed where the trapping efficiency is measured with other techniques, including in-cylinder sampling. Techniques for measuring scavenging efficiency are also considered, because of the close relationship between trapping and scavenging efficiency.

1.4.1 The Tracer Gas Method. Schweitzer and DeLuca[6] originally developed the tracer gas method in 1942 for measuring the trapping efficiency of large diesel engines. Although the tracer gas method has been available for over half a century, the use of the technique does not appear to be common. Only six references were found where trapping efficiency measurements with the tracer gas method were performed[6,7,8,9,10,11]. This is probably due to difficulties experienced with the technique. Among these difficulties were the requirement of a wet chemistry method to detect monomethylamine (CH_3NH_2), which has been the tracer predominantly used, and monomethylamine consumption in the exhaust system. In hindsight, the use of monomethylamine may not have been optimal.

Schweitzer and DeLuca used monomethylamine as the tracer gas. A wet chemistry method for monomethylamine detection was implemented. In this detection technique a sample of intake or exhaust gas was bubbled through an aqueous sulfuric acid

solution held in a Van Slyke-Cullen urea flask. Monomethylamine reacted with sulfuric acid to form monomethylamine sulfate, eventually neutralizing the solution. The level of monomethylamine in the gas was quantified by measuring the flowrate and time required to neutralize the solution. A Gardner 4-stroke diesel engine, equipped with a zero overlap cam, was used for method development. The zero overlap cam, assuming no valve leakage, eliminated short-circuiting and consequently any tracer measured in the exhaust resulted from incomplete cylinder reaction. In addition to this, assuming the cylinder gases were well mixed, there was no exhaust gas stratification (i.e. the exhaust composition is uniform) which reduces the possibility of sampling errors. The burning efficiency of monomethylamine in the Gardner diesel engine was found to vary from 94.0 to 98.3% for corresponding variations in brake mean effective pressure (BMEP) of 37 to 75 psi. Monomethylamine was determined to be stable in the exhaust at temperatures less than 700 K. The trapping efficiency was measured in a 10.5 inch bore, 12.0 inch stroke, single cylinder 2-stroke cycle crankcase scavenged Vonn Severin diesel engine. In preliminary testing on the Vonn Severin diesel engine the exhaust was found to be stratified. The monomethylamine concentration was much higher 6 inches downstream of the exhaust port than it was 3 feet downstream of the exhaust port. To remedy this, samples were simultaneously extracted at 4 points along the exhaust pipe and subsequently mixed together to give an average concentration. Trapping efficiency was determined to be 0.83 with a delivery ratio of 0.54, assuming a cylinder reaction efficiency of 0.97. Schweitzer and DeLuca estimated the method to be accurate to within 1%.

In a Thesis by Irish *et al.*[7] a comparison was made between four different methods for measuring trapping efficiency on a single cylinder 2-stroke gasoline engine. The four methods were (I) the tracer gas method with monomethylamine, (II) in-cylinder sampling during compression, (III) in-cylinder sampling during expansion, and (IV) the indicated specific air consumption (ISAC) method. The engine was operated from 1000 to 1400 rpm and the delivery ratio was varied from 1.0 to 1.8. The ISAC method involves comparing the indicated power from the 2-stroke cycle engine with a 4-stroke cycle engine with the same piston and cylinder geometry and a zero overlap cam running at the same operating conditions. The tracer gas method was problematic in that the monomethylamine was reacting and being absorbed by condensed water in the exhaust. The same wet chemistry method employed by Schweitzer and DeLuca was used for monomethylamine detection. In order to get results consistent with the other three methods, a sophisticated exhaust sampling system was designed. The system consisted of a 5/16" ID tube which passed into the exhaust manifold and split into four smaller tubes, each terminating 1.5 inches downstream from a different exhaust port. This system resulted from several iterations on system design with the end goal to get results comparable with the other techniques. Acceptable results were achieved with the exception of measurements made at small and large delivery ratios (1.0 and 1.8). The resulting exhaust sample system was developed with the intention of matching the results from the other methods on a specific engine design. It is unclear whether the resulting exhaust sample system would be transportable to other engine designs. The final results showed that the difference between any two methods for a particular operating point was never more than 6%, barring the two exceptions above for the tracer gas method.

Isigami *et al.*[8] implemented the tracer gas method with monomethylamine to measure trapping efficiency in a Fuji Heavy Industry Co., crankcase loop scavenged, 2-stroke cycle, single cylinder engine with a 10 cm stroke and 8.0 cm bore rated at 6 hp at 2000 rpm. The tracer gas measurements were compared with trapping efficiency measurements with an in-cylinder electro-magnetic sampling valve. Off-engine testing was performed to determine at what temperature monomethylamine begins to dissociate. It was determined that significant dissociation occurs above 520 K. The results of these tests were used to correct for exhaust dissociation when the exhaust temperature was above 520 K. Good agreement was obtained between the sample valve technique and the tracer gas method, within ±2%. The data were collected at partial load and a delivery ratio of 1.93. Although the exhaust temperatures were not given, relatively low temperatures would be expected under these conditions.

In the work by Huber[9] trapping efficiency was measured on both a 4-stroke and a 2-stroke cycle engine using oxygen and butane (C_4H_{10}), respectively, as tracers. Experimental errors were evaluated for both cases. A 4-stroke, Lloyd 37 in^3, 2 cylinder, gasoline engine was equipped with a zero overlap cam to determine the extent of tracer reaction in the cylinder. With the zero overlap cam exhaust oxygen concentration ranged from 0.1 to 0.3%, which translates to cylinder reaction efficiencies of approximately 99.5 and 98.5%, respectively. A test to determine the exhaust stability was also carried out for oxygen. Huber concluded that if the exhaust temperature exceeds 770 K, then there would be significant exhaust reactions between oxygen and unburned or short-circuited fuel and trapping efficiency could no longer be determined. For 2-stroke testing, a JLO Model

L151, 9 in^3, single cylinder, crankcase-scavenged diesel engine and a Hanomag D722, 227 in^3, two cylinder, blower scavenged diesel engine were the two engines primarily used. Huber evaluated the extent of the butane cylinder reaction by plotting the fraction of exhaust butane over intake butane vs. excess air ratio. The excess air ratio, though not defined in the paper, is most likely the inverse of equivalence ratio. For excess air ratios between 1 and 3, a minimum of less than 5% of the intake butane was detected in the exhaust. Huber described this as a worst case cylinder reaction inefficiency because a significant portion of the 5% unreacted butane is likely to be from scavenge short-circuiting. The butane exhaust reaction was also evaluated and it was determined that when the temperature of the exhaust climbed above 720 K, significant exhaust reaction occurred. Both the tracer exhaust reaction and cylinder reaction inefficiency were accounted for in the final measurements of trapping efficiency. Only the results from the blower scavenged 2-stroke cycle engine were presented. The trapping efficiency ranged from .44 to .46 for speeds varying from 1050 to 1500 rpm at an excess air ratio of about 2.

Bazika and Rodig[10] performed the tracer gas method on a 2-stroke fuel-injected test engine, at 1500 rpm, at a delivery ratio of 1.3, and with a mean effective pressure of 441 kPa. The scavenging characteristics were altered by changing the height of the exhaust ports. They utilized CO as the tracer gas. The cylinder reaction efficiency was investigated with a 4-stroke cycle engine with a zero overlap cam. These tests showed complete destruction of the injected CO in the engine cylinder from full down to half power. No difficulty with CO consumption in the exhaust system was reported. For a

16% increase in the height of the exhaust ports an increase in the short-circuited fraction from 0.60 to 0.64 was observed.

The scavenging of a Rootes TS-3, 3-cylinder opposed piston 2-stroke compression ignition engine was studied by Wallace and Cave[11] utilizing the tracer gas method. Carbon monoxide was used as the tracer gas at an inlet concentration of 0.1%. The combination of an external compressor and a variable restriction in the exhaust were used to vary the delivery ratio and the level of boost. Measured charging efficiencies were reported vs. delivery ratio for four different boost ratios (1.5, 2.0, 2.5, and 3.0) and three different speeds (1000, 1500, and 2000). Charging efficiency for this work is not defined the same way as it is in Heywood[1], given earlier. Rather, the trapped volume is used instead of the displaced volume and the manifold density is used instead of ambient density. Defining charging efficiency in this way makes it nearly identical to scavenging efficiency. The boost ratio had the largest effect on charging efficiency. For example, at 1500 rpm and a delivery ratio of 1.6 the charging efficiency decreased from about 0.90 to 0.73 for an increase in boost ratio from 1.5 to 3.0. A marked influence of air/fuel ratio in the engine cylinder on completeness of combustion of CO was observed.

The main drawback of CO as a tracer gas is that it is already present in the exhaust in significant quantities, even for lean combustion. The CO content of the exhaust with no CO injected into the intake air must be measured for each data point to be considered. It then must be subtracted from the tracer gas exhaust measurements. This makes the testing extremely difficult when studying engine operating condition variations that have a large effect on CO emissions, such as equivalence ratio variations.

1.4.2 Other Techniques. Another experimental method to measure trapping efficiency, which does not require major engine modifications, is the use of skip-cycle operation[12]. In this technique the engine fires only once in several cycles. At the end of a series of nonfired cycles preceded by a normal cycle, the residual fraction is assumed to be the residual fraction during normal operation raised to one plus the number of skip-cycles. In other words, a power law decay of the residual fraction is assumed to take place during the skip-cycles. The scavenging efficiency, which is one minus the residual fraction, is proportional to indicated mean effective pressure (IMEP). The scavenging efficiency is evaluated by comparing the IMEP for skip-cycle operation to that for normal operation. The assumptions made for this technique, besides the power law decrease in residual fraction mentioned above, are that heat transfer, flow resistance, and flow dynamics are not significantly influenced by skip-cycle operation. This brings to light an inherent advantage of the tracer gas method, which is that the test can be carried out under normal engine operation. During skip-cycle operation the temperature in the cylinder is significantly reduced, which decreases the gas density and most likely changes the flow characteristics.

A technique that is employed to characterize scavenging in a number of different ways is in-cylinder sampling. Two basic methods of in-cylinder sampling are used. One is to remove a small amount of gas at a given crank angle for a short duration every cycle. Thus, continuous sampling each cycle provides an effectively constant flow of sampled gas at the desired crank angle. The problem with this sampling technique is

that the sample represents the composition of the local region around the sample valve, and not necessarily the entire cylinder volume. Trapping and scavenging efficiencies are bulk quantities, and the average composition of the entire cylinder volume is desired. The other sampling technique is to remove a significant portion of the cylinder contents during compression or expansion over a longer duration. The sample must be large enough to represent the average composition of the entire cylinder. This sampling technique is preferred for evaluating trapping and scavenging efficiencies, because a larger sample is more likely to be representative of the average cylinder composition. There have been numerous methods utilizing in-cylinder sampling for scavenging evaluations, and several are discussed below. However, this review is in no way comprehensive of the available literature.

In recent work by Tobis *et al.*[13] where in-cylinder sampling was implemented to measure scavenging characteristics, 5 to 10% of the cylinder charge was extracted during expansion and 12 to 30% during compression. Sampling during compression affected engine operation for several successive cycles because a significant portion of the cylinder volume was removed. However, prior to sampling the engine was generally stable, so the sample extracted reflected stable operation and not the unstable operation that followed sampling. Scavenging and trapping efficiencies were measured at various delivery ratios on a 1.2 liter 2-stroke cycle engine with Schnürle loop scavenging.

The use of in-cylinder sampling in combination with tracer gas injection was employed by Kannappan[14]. In this technique a small amount of tracer (acetylene) was continuously fed into the intake air. Then during compression a large sample of the

cylinder contents was extracted through a valve in the head. The scavenging efficiency was calculated by taking the mole fraction of tracer in the sample over the mole fraction of tracer in the intake air. It was assumed that the tracer trapped in the cylinder during the previous cycle was totally destroyed during combustion. The validity of this assumption was investigated using a 4-stroke diesel engine with a zero overlap cam. With the 4-stroke cycle engine running at constant load and speed the intake air acetylene concentration was increased from zero in small increments until acetylene was detected in the exhaust, indicating that the tracer was not fully consumed in the cylinder. At 100% load, the acetylene intake air concentration limit was 1.3% by weight. This concentration was reduced by half for the 2-stroke cycle engine tests to allow for variations in cylinder temperature. A poppet type valve was used for taking samples that had a diameter equal to $1/4^{th}$ the bore diameter and a valve flow area $1/64^{th}$ of the piston area. With this sample valve it was possible to remove 65% of the cylinder mass when the valve was actuated during compression. Scavenging tests were performed on a crankcase scavenged, 2-stroke cycle diesel engine rated to develop 5 hp at 700 rpm and 7 hp at 980 rpm. The crankcase of the engine served as a mixing chamber for air and acetylene.

Booy[15] describes the use of in-cylinder sampling without tracer gas injection for small 2-stroke cycle engines. Two relatively large gas samples are taken from separate cycles during the compression stroke and from the exhaust gases before dilution by the scavenging flow. The CO_2 mole fraction in each sample is analyzed. The ratio of the mole fraction of CO_2 in the cylinder during compression to the mole fraction of CO_2 in the

cylinder during expansion and exhaust blowdown is a measure of the residual gas fraction. One minus the residual gas fraction is equal to the scavenging efficiency.

A technique that only requires the sampling of the exhaust during blowdown was used by Houtsma[16] to study the scavenging efficiencies in three different engines with three different scavenging configurations. The three configurations were loop scavenging, opposed piston type uniflow scavenging, and uniflow scavenging with the exhaust valves in the cylinder head. A specially designed check valve was utilized for sampling in the exhaust port during blowdown. The valve was designed to only open at blowdown pressures, and to be closed at scavenging pressures. The result was that the gas sampled consisted primarily of trapped combustion products. Analysis was then carried out on the sampled combustion products to determine the scavenging efficiency. For a delivery ratio of 1.0, the scavenging efficiencies were 0.57, 0.65, and 0.70 for the loop, opposed piston uniflow, and the cylinder head exhaust valve uniflow scavenged engines, respectively. At higher delivery ratios, the differences in scavenging efficiencies tend to diminish. For a delivery ratio of 1.5, the scavenging efficiencies were 0.70, 0.73, and 0.82 for the loop, opposed piston uniflow, and the cylinder head exhaust valve uniflow scavenged engines, respectively.

In work by Nuti and Martorano[5], three different methods utilizing exhaust gas composition to calculate the short-circuited fraction were evaluated on a small 2-stroke cycle engine. The first two methods were intended for scavenging with premixed fuel and air, while the third method addressed scavenging with pure air for fuel-injected 2-stroke cycle engines. In the first method, the short-circuited fraction was calculated by

measuring the exhaust mass flow of THC emissions and dividing it by the mass flow of fuel into the engine. This assumed that that unburned hydrocarbons in the exhaust consisted primarily of fuel short-circuited during scavenging. The second technique assumed that a combustion reaction occurred such that the exhaust products consisted only of CO, CO_2, THC, O_2, H_2, H_2O, and N_2. The short-circuited fraction was calculated as the ratio of carbon in the form of THC's to the total amount of carbon in the exhaust from THC's, CO, and CO_2. Thus, the assumption that THC levels in the exhaust result only from scavenge short-circuiting was made here as well. The difference in the two techniques was that the second does not require measurement of fuel flow. Short-circuited fractions were evaluated using the first two methods at wide-open throttle from 3000 to 6000 rpm. At 4000 rpm the short-circuited fractions from the first and second methods were 0.27 and 0.24, respectively. The third method assumed the same combustion reaction as for the second method, but because the fuel was injected after port closure it was not assumed to be present in the short-circuited fraction. The short-circuited fraction was calculated by evaluating the mass flow of oxygen flowing out the exhaust over the mass flow of oxygen entering the engine. At 4000 rpm, a delivery ratio of 1.3, and wide open throttle the short-circuited fraction arrived at using the third method was 0.47. The author did not indicate whether the engines were crankcase scavenged or blower scavenged. The test results analyzed with the first and second methods were most likely generated with a crankcase scavenged premixed engine and the test results arrived at using the third method were probably generated with a blower scavenged fuel-injected engine.

The main advantage of the techniques used by Nuti and Martorano is their simplicity. The required measurements are the exhaust emissions that are normally measured in an emissions test. The main disadvantage is limited accuracy stemming from the many assumptions made during the analysis. Additionally the methods offer no way to account for local and bulk quenching in the cylinder, phenomena thought to be predominate in large bore natural gas engines due to poor mixing and lean engine operation.

1.5 Summary

The most current work on the application of the tracer gas method described in the literature was published in 1971, nearly three decades ago. There have been numerous advances in instrumentation that has made the implementation of the tracer gas method more practical, particularly in the area of gas detection. Bench-top Fourier transform infrared (FTIR) spectrometers are widely available, easy to use, and capable of detecting monomethylamine as well as other potential tracer gases. In the reviewed literature, a typical problem encountered with monomethylamine was excessive reaction in the exhaust. The use of carbon monoxide as a tracer was hindered by problems of incomplete cylinder destruction and separating exhaust CO from scavenged short-circuited CO. Finding a tracer gas that is more stable in the exhaust, yet still consumed in the cylinder, and not a normal exhaust constituent would further improve the practicality and accuracy of the tracer gas method.

This work introduces a new tracer gas, nitrous oxide (N_2O), which appears promising when compared with tracers employed to date. Monomethylamine is considered in this study because historically it has been used the most as a tracer for 2-stroke cycle engines. Oxygen is studied because of its prior use in 4-stroke cycle engines and because it requires little effort to include in testing. However, oxygen is not included in the chemical kinetic modeling. The kinetic modeling focuses on monomethylamine and nitrous oxide. Oxygen was not modeled because of the additional computational effort that is required. Oxygen reaction in the cylinder is heavily dependent on mixing of fuel and air, which would need to be modeled to accurately predict oxygen consumption in the cylinder. A tracer that is destroyed by thermal decomposition is ideal because the destruction is dependent only on temperature. Oxygen is not regarded as a good prospect for a tracer gas because of its limitation to rich equivalence ratios and the apparent reactivity in the exhaust, as was shown by Huber[9]. For these two reasons, the required additional effort was not invested to model the reaction of oxygen in the engine.

The research described in this dissertation has the following objectives: (1) develop equations necessary for calculating trapping efficiency and define and account for non-ideal tracer effects; (2) discuss tracer gas selection and the merits of nitrous oxide as a tracer gas candidate, (3) use chemical kinetics to analyze cylinder and exhaust reactions, (4) implement the technique on both 4-stroke and 2-stroke cycle engines with different tracer gases and experimentally quantify non-ideal tracer effects, (5) update the tracer gas method to utilize modern instrumentation and testing techniques,

and (6) demonstrate the tracer gas method as an accurate, practical, field applicable technique for measuring trapping efficiency. The 4-stroke cycle engine considered is a 5.7 liter, carbureted gasoline engine. The 2-stroke cycle engine studied is a 141 liter, large bore natural gas engine, with direct fuel injection and Curtis scavenging (a marriage of cross and loop scavenging).

CHAPTER 2

QUANTIFYING TRAPPING EFFICIENCY

Implementing the tracer gas method results in a direct measurement of the short-circuited fraction. The trapping efficiency can be written in terms of the short-circuited fraction

$$\eta_{tr} = 1 - f_{sc} = 1 - \frac{m_{sc}}{m_{del}} \tag{2.1}$$

where

m_{SC} = mass of delivered air or A/F mixture short-circuited per cycle.

To calculate the trapping efficiency using experimental data, it must be expressed in terms of measured quantities. The required data to calculate the trapping efficiency assuming the tracer behaves ideally are the tracer mole fraction in the exhaust and intake air, the specific gravity of the exhaust, and the overall F/A ratio. An equation for trapping efficiency in terms of measured quantities will be developed starting with Equation 2.1 for trapping efficiency and assuming 100% tracer cylinder destruction, no tracer exhaust consumption, and uniform mixing of the tracer in the exhaust and intake air. The tracer is typically injected into the intake air prior to fuel addition, even if the engine is carbureted. This assumption will be made throughout the analysis. The short-circuited fraction can be redefined in terms of tracer flow through the engine per cycle as

$$f_{sc} = \frac{m_{t,sc}}{m_{t,del}} \tag{2.2}$$

where

$m_{t,sc}$ = mass of tracer short-circuited per cycle
$m_{t,del}$ = mass of tracer delivered per cycle.

The masses of tracer short-circuited and delivered correspond to the masses of tracer in the exhaust and intake air, respectively. The mass of tracer in the exhaust depends on the total exhaust mass, the mole fraction of tracer in the exhaust, and the ratio of tracer to exhaust molecular weight. The mass of tracer in the intake air depends on the mass of air delivered, the mole fraction of tracer in the intake air, and the ratio of tracer molecular weight to that of air. Substituting the proper relationships into Equation 2.2, the short-circuited fraction becomes

$$f_{sc} = \frac{X_{t,e}\left(MW_t / MW_e\right)m_e}{X_{t,i}\left(MW_t / MW_a\right)m_a} \tag{2.3}$$

where

MW_t = molecular weight of tracer
MW_e = molecular weight of exhaust
MW_a = molecular weight of intake air
m_a = mass of air delivered per cycle
m_e = exhaust mass per cycle
$X_{t,e}$ = mole fraction of tracer in exhaust
$X_{t,i}$ = mole fraction of tracer in intake air.

The mass balance for the cylinder can be written in terms of the overall F/A ratio, $(F/A)_{ov}$,

$$m_e = m_a\left\{1+\left(F/A\right)_{ov}\right\} \tag{2.4}.$$

In most fuel-injected 2-stroke cycle engines the overall F/A ratio is considerably less than the trapped F/A ratio because of excess scavenging air; therefore, it is important to make the distinction between the two. In addition to this the overall F/A ratio is easier to measure, or calculate from the exhaust emissions. The tracer mass flow has been neglected in the cylinder mass balance because it is typically small, 0.05 to 0.3% by volume of the intake air. Substituting Equation 2.4 into Equation 2.3 and eliminating the exhaust mass, mass of delivered air, and molecular weight of the tracer gas, the expression becomes

$$f_{sc} = \frac{X_{t,e} MW_a \left\{1 + \left(F/A\right)_{ov}\right\}}{X_{t,i} MW_e} \tag{2.5}$$

Replacing the ratio of molecular weight of exhaust to molecular weight of intake air with exhaust specific gravity and substituting the short-circuited fraction back into Equation 2.1 results in an equation for calculating trapping efficiency in the tracer gas method which is

$$\eta_{tr} = 1 - \frac{X_{t,e}\left\{1 + \left(F/A\right)_{ov}\right\}}{X_{t,i} SG_e} \tag{2.6}$$

where

SG_e = specific gravity of exhaust = MW_e/MW_a.

The required quantities to calculate trapping efficiency using Equation 2.6 are measurable using readily available laboratory instrumentation. The specific gravity of the exhaust is

typically between 0.96 and 0.99. Depending on the required accuracy it may be adequate to assume the exhaust specific gravity is equal to one.

2.1 Cylinder Reaction Efficiency

The extent of tracer destruction in the cylinder must be examined very closely, especially when the magnitude of short-circuiting is not large. Typically there is a certain fraction of the tracer trapped in the cylinder which survives. Selecting a tracer where this fraction is minimized or predictable is critical. The destruction of tracer in the bulk cylinder charge depends primarily on temperature, concentration, and the chemical kinetics of the tracer gas. The destruction of tracer which is near the walls may be affected by many of the same mechanisms which prevent the fuel from reacting completely giving rise to total hydrocarbon (THC) emissions. Mechanisms which can contribute to THC emissions, proposed by Cheng *et al.*[17] are

1. Crevice volumes
2. Oil layer absorption/desorption
3. Organic deposit adsorption/desorption
4. Wall quenching
5. Quenching from local regions in mixture being too rich or too lean for flame to propagate
6. Liquid fuel which did not fully evaporate either as suspended droplets or condensed on walls
7. Exhaust valve leakage.

Of these mechanisms, numbers 2 and 6 are not important to the tracer gas problem. The work cited above by Cheng *et al.* is specific to gasoline. For the three tracers being considered, nitrous oxide, monomethylamine, and oxygen, the vapor pressure is

significantly higher than gasoline. Consequently the absorption of tracer in oil layers is likely to be negligible, ruling out mechanism number 2. The tracer in general is not in liquid form, which eliminates the possibility of incomplete tracer evaporation, which is mechanism number 6. The other mechanisms, 1, 3, 4, 5, and 7 could potentially contribute to tracer gas cylinder reaction inefficiency. Mechanism number 5 is likely to have a larger impact on oxygen. Oxygen destruction is strongly dependent on the local F/A ratio as well as temperature and chemical kinetics, which makes it different from monomethylamine and nitrous oxide. Fuel rich and lean zones as well as low temperature regions can prevent oxygen from being completely destroyed.

The cylinder reaction efficiency is defined as

$$\eta_{cr} = [\textit{mass of tracer reacted}]/[\textit{mass of tracer retained in cylinder}] \quad (2.7).$$

For 4-stroke cycle engines a zero overlap cam is typically used to characterize the cylinder reaction. Presumably any tracer in the exhaust of an engine using a zero overlap cam is due to incomplete cylinder reaction. The exhaust is sampled near the port so the exhaust reaction is likely to be negligible. Since there is no short-circuiting, exhaust gas stratification is not a concern with regard to sampling errors. This is an important point that will be discussed later. Applying the above analysis for calculating trapping efficiency to a non-short-circuiting condition considering the above assumptions leads to an expression for cylinder reaction efficiency in terms of measured parameters

$$\eta_{cr} = 1 - \frac{X_{t,e}\left\{1 + \left(F/A\right)_{ov}\right\}}{X_{t,i} SG_e} \quad (2.8).$$

This is exactly the same expression as Equation 2.6 for the trapping efficiency, but since the zero overlap cam is in place all tracer present is a result of incomplete reaction in the cylinder.

For 2-stroke cycle engines a different technique for evaluating the cylinder reaction efficiency must be used. One possible technique is in-cylinder sampling before and after combustion. The definition of the cylinder reaction efficiency in Equation 2.7 remains the same. The main difference is that the mass is constant throughout the process, assuming that the sample taken before combustion occurs after fuel addition. The A/F ratio dependency is eliminated and the equation for cylinder reaction efficiency becomes

$$\eta_{cr} = 1 - \frac{X_{c2} SG_{c1}}{X_{c1} SG_{c2}} \tag{2.9}$$

where

X_{c1} = tracer mole fraction in sample taken before combustion
X_{c2} = tracer mole fraction in sample taken after combustion
SG_{c1} = specific gravity of the sample taken before combustion
SG_{c2} = specific gravity of the sample taken after combustion.

Note that the cylinder composition after port closure may contain a significant residual gas fraction, in which case the mole fraction of tracer in the in-cylinder sample extracted during compression will be significantly different than the tracer mole fraction in the intake air.

An alternative technique for extracting the sample after combustion is with a checkvalve in the exhaust port during blowdown. The checkvalve is set to open only when the pressure in the port is elevated above intake manifold pressure, which only occurs during blowdown. The checkvalve is typically oriented into the flow and as close

as possible to the cylinder inner diameter so the dynamic pressure, which is large when the port initially opens, can be recovered and utilized to open the checkvalve. One possible error with this technique results from the presence of residual scavenging air from the previous cycle near the port. As the piston uncovers the exhaust port the combustion products begin to exit the cylinder, subsequently raising the pressure in the port. At the same time the flow of combustion products entrains residual scavenging air from the previous cycle. It seems likely that a small portion of the scavenging air will flow through the check valve. This error can be reduced by locating the checkvalve close to the port. The error can also be reduced by setting the checkvalve to open at pressures significantly above intake manifold pressure. This way a slight delay occurs during blowdown allowing a portion of the residual scavenging air to be swept downstream of the checkvalve before it opens.

2.2 Exhaust Sampling Effects

In general, inconsistent exhaust sampling results from gas composition and pressure variations in the exhaust system. In a 2-stroke cycle engine or in a 4-stroke cycle engine with a conventional cam with overlap installed, the exhaust gas just downstream of the exhaust port is stratified. For 2-stroke cycle engines there is a portion of gas exiting the cylinder during blowdown which is primarily combustion products. This gas is followed by scavenging air mixed with combustion products, changing the composition as time progresses. Depending on the delivery ratio and scavenging effectiveness, the last part of the scavenging flow exiting the cylinder could be nearly pure air or A/F mixture. If the sample tap is near the port, it sees gas composition and pressure that vary over time.

As the exhaust flows down the pipe, mixing occurs and the stratification is reduced. In multi-cylinder engines an averaging of both concentration and pressure occurs where gas from the different cylinders combine.

In 4-stroke cycle engines the nature of the breathing process is more clearly defined because of the prescribed valve motion. There is a cylinder combustion products portion and a portion from scavenged short-circuiting during valve overlap. The scavenged short-circuited portion is likely to contain both fresh charge and combustion products. Initially these two portions are not mixed. Tracer mole fraction measurements at the port are not likely to reflect average tracer mole fractions in the bulk exhaust mass flow because of the different residence times and pressure variations at the sample tap. Figure 2.1 illustrates qualitatively the different residence times for the two portions of exhaust gas in a 4-stroke cycle engine. The short-circuited gas resides near the port for approximately three fourths of the cycle whereas the combustion products are only near the port for about one fourth of the cycle. Exhaust sampling is more accurately carried out at some distance downstream after the gas is mixed and pressure pulsations have attenuated.

2.3 Tracer Destruction in the Exhaust

Tracer reaction in the exhaust has been a difficult problem to overcome in much of the previous work on the tracer gas method. When a portion of the tracer reacts in the exhaust upstream of the sample tap, the resulting trapping efficiency calculated is too high. A common remedy to this problem has been to sample close to the port. As discussed above, this technique has inherent problems of its own for either 2-stroke or

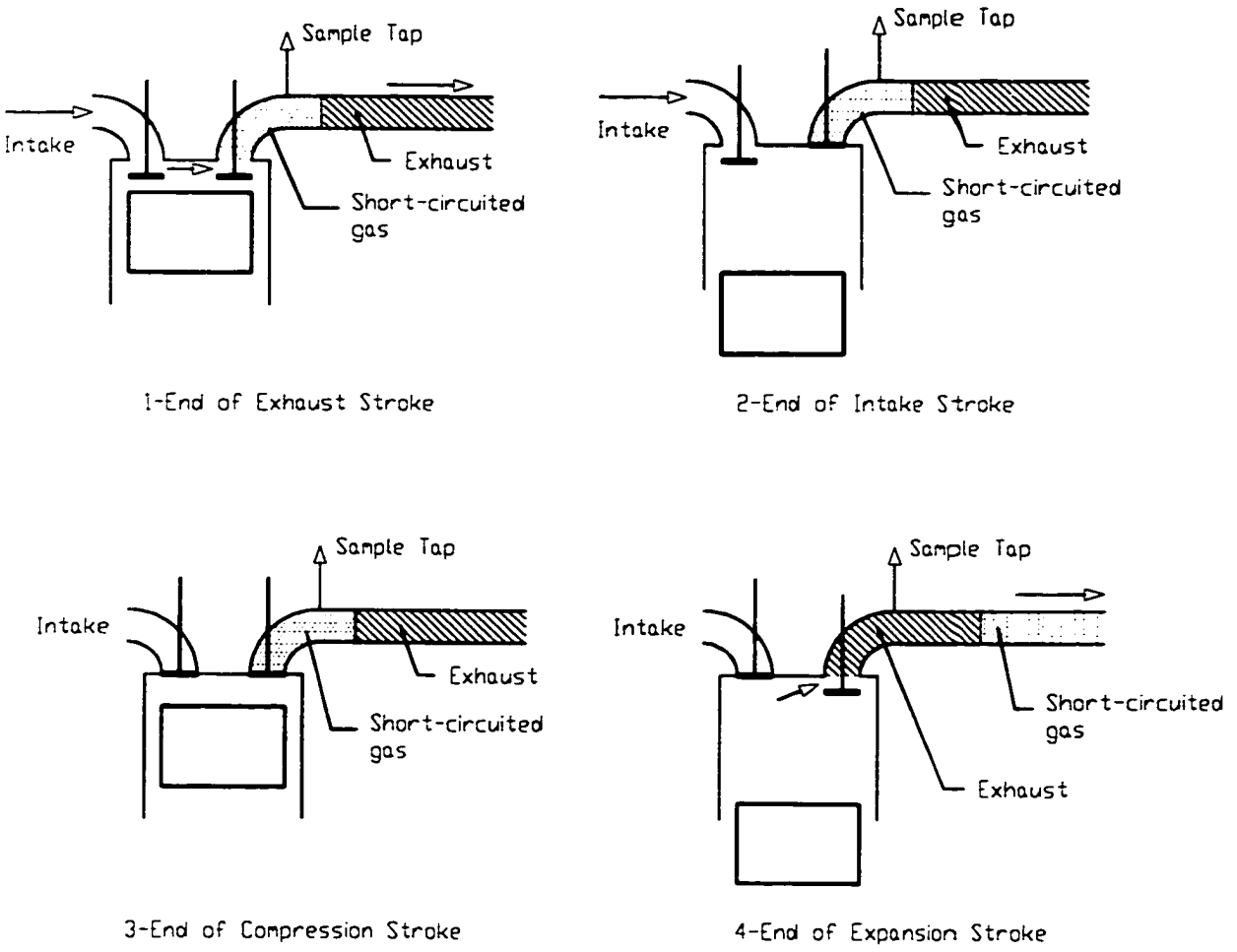

Figure 2.1 Illustration of Disproportionate Gas Residence Times at Sample Tap.

4-stroke cycle engines. To evaluate the exhaust reaction, the exhaust must be sampled at two locations, one close enough to the port for the exhaust to still be hot, and another downstream where the exhaust has cooled and the tracer mole fraction is stable. During this evaluation precautions must be taken to alleviate the sampling errors discussed earlier. Another possibility for evaluating the exhaust reaction is to perform the testing off-engine with a steady flow system. For 4-stroke cycle engines, a zero overlap cam can

be used which eliminates the short-circuited fraction and thus stratification in the exhaust. Another possibility is to put a mixer between the exhaust port and the first sample tap.

The fraction of tracer destroyed in the exhaust can be expressed as

ε_r =*[mass of tracer reacted in exhaust]/[mass of tracer entering exhaust]*

which, in terms of measured parameters is

$$\varepsilon_r = \frac{X_{e,1} - X_{e,2}}{X_{e,1}} \tag{2.10}$$

where

$X_{e,1}$ = mole fraction of tracer entering exhaust
$X_{e,2}$ = mole fraction of tracer exiting exhaust.

The fraction of tracer destruction in the exhaust may vary significantly as engine operating conditions change. However, if it is fairly constant or known for the operating condition of interest then it can be used as a correction factor in calculating trapping efficiency.

2.4 Misfire Correction

It may be desirable to measure the trapping efficiency under engine operating conditions that result in a significant number of misfires. When a misfire occurs the temperature in the cylinder is much lower than during normal combustion. The tracer most likely does not react or dissociate in the cylinder, and subsequently flows out the exhaust. This results in a higher concentration of tracer in the exhaust, yielding a trapping efficiency that is too low. Misfires are typically detected by measuring the cylinder pressure with a piezoelectric pressure transducer and recording the number of cycles with

peak cylinder pressure below a certain threshold. That threshold is typically set at about 10 to 25% above motored peak pressure. The number of misfires divided by the total number of cycles sampled is defined as the misfire fraction, f_{mf}.

2.5 Accounting for Non-Ideal Tracer Effects in Trapping Efficiency Evaluation

An equation for trapping efficiency can be developed which includes the non-ideal tracer effects, or tracer gas method corrections, discussed above. Figure 2.2 depicts tracer mass flow through the engine. The variables shown in the figure are defined as

$m_{t,mf}$ = mass of tracer which survives in cylinder due to misfire
$m_{t,c}$ = mass of tracer which survives in cylinder due to cylinder reaction inefficiency
$m_{t,e}$ = mass of tracer in exhaust after exhaust tracer destruction.

Mass quantities per cycle are used for simplicity, although it is more correct to discuss mass flow rates in this case because of the way the misfire fraction is calculated. All tracer in the cylinder is assumed to survive during a misfire. This assumption is validated with chemical kinetic modeling results in Chapter 4. The first step is to obtain an expression for the short-circuited tracer to be substituted into Equation 2.2, the definition for short-circuited fraction. The mass of tracer exiting the exhaust is the sum of the tracer mass components entering the exhaust, processed by the exhaust destruction fraction

$$m_{t,e} = \left(m_{t,sc} + m_{t,mf} + m_{t,c}\right)\left(1 - \varepsilon_r\right) \qquad (2.11).$$

The mass exiting the cylinder due to misfire is the trapped cylinder mass times the misfire fraction. The mass exiting the cylinder due to cylinder reaction inefficiency is the trapped

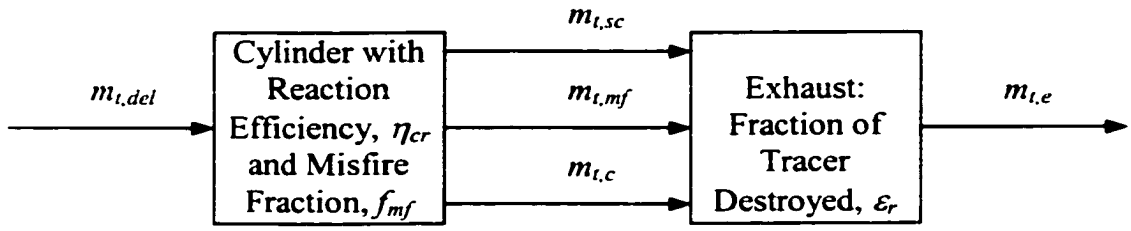

Figure 2.2 Tracer Mass Flow Through Engine Accounting for Non-Ideal Tracer Effects.

cylinder mass times one minus the cylinder reaction efficiency. Incorporating these relationships into Equation 2.11 and solving for the mass of tracer short-circuited

$$m_{t,sc} = \frac{m_{t,e}}{1-\varepsilon_r} - m_{t,tr}\left(1-\eta_{cr}+f_{mf}\right) \tag{2.12}$$

where

$m_{t,tr}$ = mass of tracer trapped in cylinder = $m_{t,del}$ - $m_{t,sc}$.

After substituting the relationship for the tracer trapped in the cylinder, solving for the tracer short-circuited, and plugging the resulting expression into Equation 2.2, the relationship for the short-circuited fraction becomes

$$f_{sc} = \frac{\dfrac{m_{t,e}}{1-\varepsilon_r} - m_{t,del}\left(1-\eta_{cr}+f_{mf}\right)}{m_{t,del}\left(\eta_{cr}-f_{mf}\right)} \tag{2.13}.$$

Incorporating this into Equation 2.1 for trapping efficiency, substituting the equations

$$m_{t,e} = m_a\left\{1+\left(F/A\right)_{ov}\right\}X_{t,e}\left(MW_t/MW_e\right)$$

and

$$m_{t,del} = m_a X_{t,i}\left(MW_t/MW_a\right),$$

and performing the appropriate cancellations the resulting equation for trapping efficiency is

$$\eta_{tr} = 1 - \frac{\left\{1 + \left(F/A\right)_{ov}\right\} X_{t,e}}{\left(1-\varepsilon_r\right)\left(\eta_{cr} - f_{mf}\right) SG_e X_{t,s}} + \frac{1 - \eta_{cr} + f_{mf}}{\eta_{cr} - f_{mf}} \qquad (2.14).$$

Equation 2.13 can be employed to look at the sensitivity of the three quantifiable corrections considered, exhaust destruction fraction (ε_r), cylinder reaction inefficiency ($1-\eta_{cr}$), and the misfire fraction (f_{mf}). Figures 2.3, 2.4, and 2.5 show how sensitive the overall method error is to each of the errors in Equation 2.13 at assumed actual short-circuited fractions of 0.50, 0.25, and 0.05, respectively. As each correction is varied, the other corrections are held constant at zero. The deviation of the uncorrected short-circuited fraction from the actual short-circuited fraction was calculated. Short-circuited fraction is analyzed rather than trapping efficiency because it is the quantity most directly measured. This analysis examines the accuracy of the short-circuited fraction evaluation that results when no effort is made to compensate for non-ideal tracer effects. This is determined by calculating the difference between the short-circuited fractions evaluated from Equations 2.1 and 2.6 and from Equation 2.13. In this analysis the F/A ratio was assumed to be 0.02 and the exhaust specific gravity was assumed to be 0.97. While a non-ideal tracer effect was varied, the other two were held constant at zero.

The calculations show that as the short-circuited fraction gets smaller, the overall method error becomes more sensitive to cylinder reaction inefficiency and the misfire fraction. The sensitivity to the exhaust reaction is unaffected by the changes in

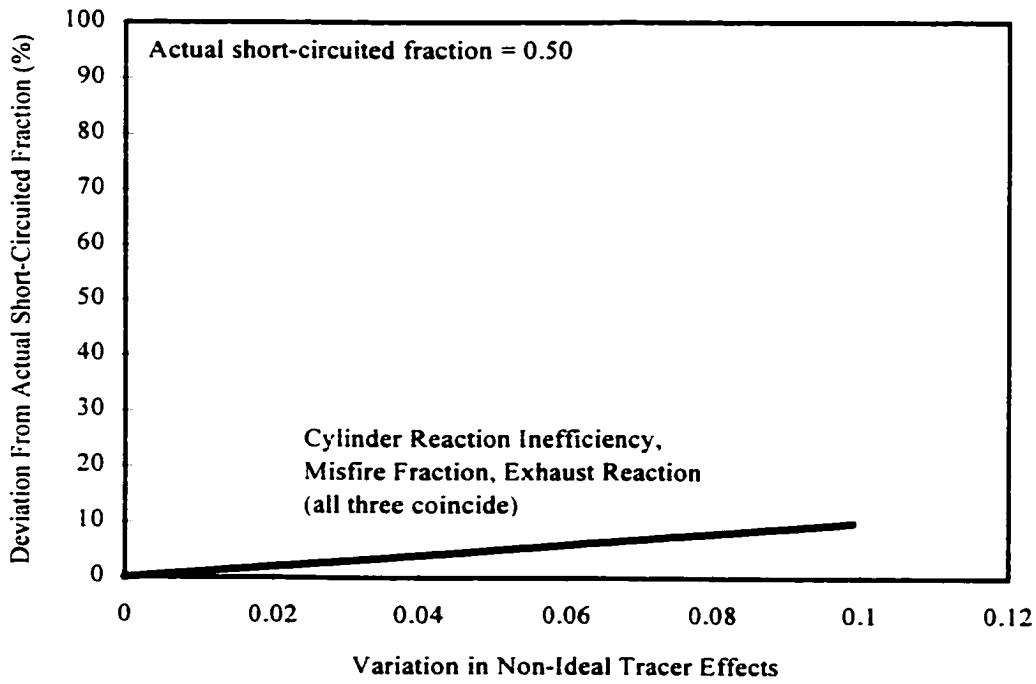

Figure 2.3 TGM Sensitivity to Non-Ideal Tracer Effects, Assuming f_{SC}=0.50

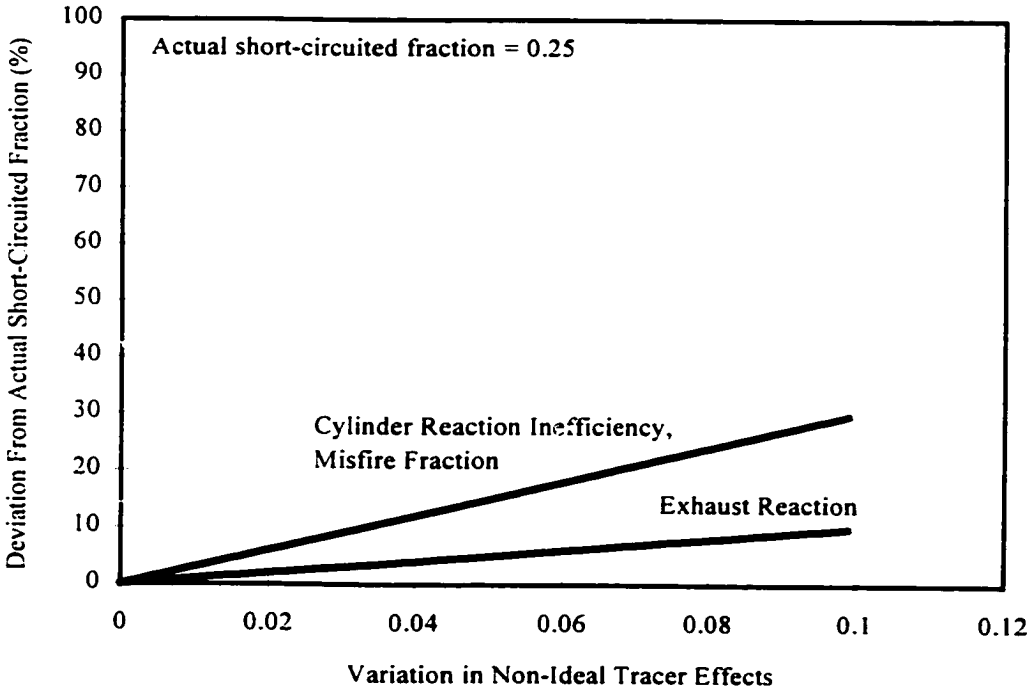

Figure 2.4 TGM Sensitivity to Non-Ideal Tracer Effects, Assuming f_{SC}=0.25

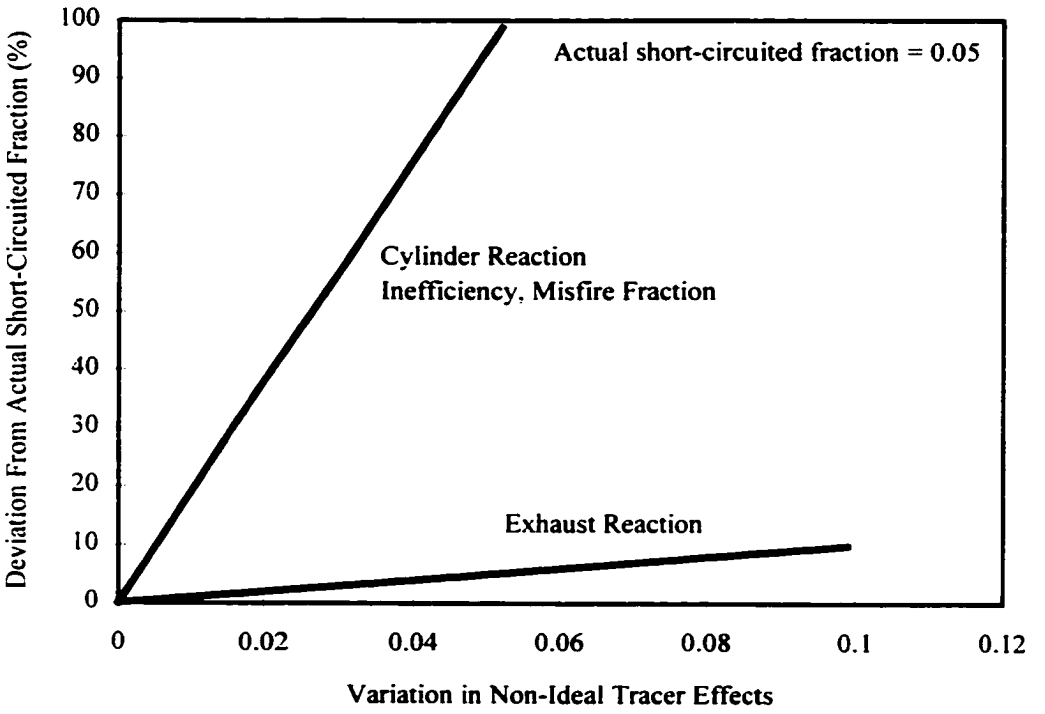

Figure 2.5 TGM Sensitivity to Non-Ideal Tracer Effects, Assuming f_{SC}=0.05

short-circuited fraction. The overall method error is very sensitive to cylinder reaction inefficiency and the misfire fraction at small short-circuited fractions. Blower scavenged 2-stroke cycle engines most likely have higher short-circuited fractions than 4-stroke cycle and crankcase scavenged 2-stroke cycle engines. Thus, blower scavenged engines are well suited for this technique. Nevertheless, if the corrections are accurately known then they can be accounted for using Equation 2.14. It is certainly easy to correct for the misfire fraction given that the cylinder is instrumented with a pressure transducer. Preliminary testing to quantify the cylinder reaction efficiency allows accurate compensation for this non-ideal tracer effect as well.

Perhaps a more direct way to illustrate the sensitivity of the quantifiable corrections to the tracer gas measurement is to evaluate the partial derivative of the short-circuited fraction with respect to ε_r, $(1-\eta_{cr})$, and f_{mf}. The partial derivatives are

$$\frac{\partial f_{sc}}{\partial \varepsilon_r} = \frac{\left\{1 + \left(F/A\right)_{ov}\right\} X_{t,e}}{(1-\varepsilon_r)^2 (\eta_{cr} - f_{mf}) SG_e X_{t,i}} \tag{2.15}$$

$$\frac{\partial f_{sc}}{\partial \xi} = \frac{\left\{1 + \left(F/A\right)_{ov}\right\} X_{t,e}}{(1-\varepsilon_r)(1-\xi-f_{mf})^2 SG_e X_{t,i}} + \frac{1}{(1-\xi-f_{mf})^2} \tag{2.16}$$

where

$\xi = 1-\eta_{cr}$ = cylinder reaction inefficiency

$$\frac{\partial f_{sc}}{\partial f_{mf}} = \frac{\left\{1 + \left(F/A\right)_{ov}\right\} X_{t,e}}{(1-\varepsilon_r)(\eta_{cr}-f_{mf})^2 SG_e X_{t,i}} + \frac{1}{(\eta_{cr}-f_{mf})^2} \tag{2.17}.$$

These partial derivatives form sensitivity coefficients for the short-circuited fraction with respect to each of the correction factors. Table 2.1 presents sensitivity coefficient calculation results for four different cases. These calculations further illustrate that the short-circuited fraction measurement is more sensitive to ξ and f_{mf} than it is to ε_r for equal variations in each parameter.

Correction Factors	$\partial f_{sc}/\partial \varepsilon_r$	Correction Factors	$\partial f_{sc}/\partial \xi$	Correction Factors	$\partial f_{sc}/\partial f_{mf}$
$\varepsilon_r = 0$ $\xi = f_{mf} = 0$	0.526	$\xi = 0$ $\varepsilon_r = f_{mf} = 0$	1.53	$f_{mf} = 0$ $\varepsilon_r = \xi = 0$	1.53
$\varepsilon_r = 0.1$ $\xi = f_{mf} = 0$	0.649	$\xi = 0.1$ $\varepsilon_r = f_{mf} = 0$	1.88	$f_{mf} = 0.1$ $\varepsilon_r = \xi = 0$	1.88
$\varepsilon_r = 0.2$ $\xi = f_{mf} = 0$	0.822	$\xi = 0.2$ $\varepsilon_r = f_{mf} = 0$	2.38	$f_{mf} = 0.2$ $\varepsilon_r = \xi = 0$	2.38
$\varepsilon_r = 0.3$ $\xi = f_{mf} = 0$	1.07	$\xi = 0.3$ $\varepsilon_r = f_{mf} = 0$	3.11	$f_{mf} = 0.3$ $\varepsilon_r = \xi = 0$	3.11

Table 2.1 Short-Circuited Fraction Sensitivity Coefficients, Assuming $(F/A)_{ov}=0.02$, $X_{l,e}=0.0005$, $SG_e=0.97$, and $X_{l,i}=0.001$.

2.6 Analytical Evaluation of Scavenging in 2-Stroke Cycle Engines Assuming Perfect Mixing

A scavenging model that provides reasonable estimates for trapping and scavenging efficiencies in 2-stroke cycle engines is perfect mixing. When the scavenging air or mixture enters the cylinder it is assumed to instantaneously mix with the cylinder contents. The mass that leaves the cylinder is then a mixture of the gas that flowed into the cylinder and the gas that initially resided in the cylinder. This assumption neglects direct short-circuiting and perfect displacement effects. Direct short-circuiting occurs when the intake gas is shunted directly from the intake ports through the cylinder and out the exhaust ports without mixing with the cylinder contents. This is likely to happen for

high delivery ratios toward the end of the scavenging process. Perfect displacement results when the scavenging air or mixture behaves like a piston and pushes the exhaust products out the exhaust ports. This happens early in the scavenging process when the ports are initially opened. The effects of direct short-circuiting and perfect displacement tend to offset each other, providing a reasonable baseline to compare with experimental data. The perfect mixing equations for trapping and scavenging efficiency, developed in Heywood[1], are

$$\eta_{sc} = 1 - e^{-\Lambda} \tag{2.18}$$

$$\eta_{tr} = \frac{1}{\Lambda}\left(1 - e^{-\Lambda}\right) \tag{2.19}.$$

Note that in the perfect mixing model the scavenging and trapping efficiencies are dependent on only one parameter, the delivery ratio. Though the perfect mixing model significantly simplifies a complex process, it highlights the importance of the delivery ratio on scavenging. Scavenging efficiencies increase with delivery ratio, and approach unity as the delivery ratio goes to infinity. The trapping efficiency decreases with increasing delivery ratio, and goes to zero as delivery ratio goes to infinity. The perfect mixing model is compared with the 2-stroke cycle engine test data in Chapter 6.

CHAPTER 3

TRACER GAS SELECTION

Correct tracer gas selection for the particular application involved is essential. Gases that have been investigated as tracers for IC engine analysis are ammonia, carbon monoxide, carbureted water gas, butane, oxygen, monomethylamine, and dimethylamine. In most of the published work on the tracer gas method monomethylamine is used as the tracer gas. The desirable characteristics of a tracer gas, adapted from Schweitzer and DeLuca[6], are

- Easy and safe to handle
- Readily detectable by common gas analyzers
- Completely destroyed when exposed to combustion temperatures in the cylinder
- Stable in the intake, exhaust, and sample systems
- Not present in significant quantities in the combustion products.

3.1 Monomethylamine

Monomethylamine occurs in herring brine, in urine of dogs after eating meat, in certain plants such as *Mentha aquatica*, and in crude methanol together with di- and trimethylamine[18]. It is a flammable gas at standard temperature and pressure.

Monomethylamine is irritating to the eyes, skin, and respiratory tract. It has an odor similar to ammonia. Monomethylamine is sold in liquefied form as a 33% aqueous solution; it is a good solvent for many organic substances. Some physical properties of monomethylamine as a function of temperature are given in Table 3.1.

The monomethylamine reaction rate has a strong dependence on temperature. This makes it possible for the last third and fourth characteristics given above to be satisfied. Monomethylamine is measurable by Fourier Transform Infra-Red (FTIR) analyzers. The vapor pressure is low enough so that it can be conveniently stored as a liquid at room temperature, but high enough to be used for direct injection into the intake air stream. It is not a normal constituent in the exhaust or intake gas for engines running on common fuels (i.e. gasoline, natural gas, propane, diesel, etc.). Because of these characteristics and the fact that it has been the most widely used, monomethylamine is one of the tracers studied in this research.

3.2 Nitrous Oxide

Nitrous oxide is a constituent of the earth's atmosphere, about 0.00005% by volume[18]. It is a colorless gas with a slightly sweetish odor. It is very stable and rather inert chemically at room temperatures. Nitrous oxide is sold as a compressed liquid with a vapor pressure of about 5600 kPa at room temperature. It is used to oxidize organic compounds at temperatures above 570 K, to make nitrites from alkali metals at their boiling points, in rocket fuel formulations, and in preparing of whipped cream. Nitrous oxide is a narcotic in high concentrations. It is less irritating to the skin than other oxides

Temperature (K)	Vapor Pressure (kPa)	Specific Gravity, Liquid	Latent Heat, Vap. (kJ/kg)
283	205	0.675	842
294	311	0.661	830
305	454	0.647	814
316	647	0.633	798
328	886	0.619	789
339	1196	0.604	761
350	1567	0.589	737
361	2013	0.574	714

Table 3.1 Physical Properties of Monomethylamine

of nitrogen. Some thermal properties of nitrous oxide as a function of temperature are given in Table 3.2.

Nitrous oxide is well known for its power enhancement in high-performance racing engines. It is safe to handle, stable at room temperature, and, because of its regular use for high-performance applications, is readily available. The role of nitrous oxide in power enhancement has generally been attributed to its oxygen content, which is 50% higher than air by weight, and its low inlet temperature caused by high throttling pressure drops. In fact, the limited literature available on nitrous oxide behavior shows that its decomposition is exothermic at high temperature, thereby providing a power-enhancement mechanism in addition to the increased oxygen concentration. This exothermic reaction suggests equilibrium behavior favoring products of decomposition. The combination of the exothermic reaction and the stability of nitrous oxide at room temperature suggest a high activation energy for the decomposition reaction. These are

Temperature (K)	Vapor Pressure (kPa)	Specific Gravity, Liquid	Latent Heat, Vap. (kJ/kg)
266	2659	0.948	264
273	3161	0.913	248
278	3573	0.876	236
283	4054	0.838	218
289	4638	0.788	201
294	5222	0.745	181
300	5943	0.641	161
309	7345	0.425	0

Table 3.2 Physical Properties of Nitrous Oxide

favorable characteristics for a tracer gas, since it will not decompose until high temperatures are reached and will not spontaneously form at lower temperature. Less than 5 ppm of nitrous oxide is found in most product gases from combustion systems. Fluidized bed coal combustors are the exception, yielding nitrous oxide levels of around 50 ppm[19]. The higher nitrous oxide level is due to lower combustion temperatures and fuel bound nitrogen. The dramatic power increases resulting from nitrous oxide enhancement suggest it at least partially decomposes within the cylinder, while its presence in the exhaust, presumably from scavenge short-circuiting, indicates it could be stable at exhaust temperatures. Nitrous oxide, although never used before as a tracer gas, looks favorable and is investigated in this work.

3.3 Oxygen

Oxygen has been used in the past for measuring trapping efficiency of 4-stroke cycle engines and will provide a good reference for comparison with the other tracers.

The oxygen content in the intake air is typically between 20 and 21%. The procedure is similar to the other tracers, except oxygen does not have to be injected into the intake air. It is preferable to run the engine at a stoichiometric or rich air-fuel ratio so that, ideally, all the oxygen reacts in the cylinder.

3.4 Chemical Kinetics

Understanding the chemical kinetics of a particular tracer gas helps predict its suitability for the technique and establish potential non-ideal tracer effects. Kinetics which are too slow at combustion temperatures or too fast at exhaust temperatures could impose the need to evaluate corrections for non-ideal tracer effects. A discussion of specific tracer gas kinetics follows.

3.4.1 Monomethylamine Kinetics. Much of the work on CH_3NH_2 kinetics was performed between 1930 and 1955[20,21,22,23]. In the work by Cullis *et al.*[21] the oxidation and pyrolysis temperatures of monomethylamine were examined. The temperatures were on the order of exhaust temperatures in most IC engines, so it is likely that oxidation will occur to some extent in the exhaust. The global oxidation reaction is second order and can be represented as

$$CH_3NH_2 + O_2 \Leftrightarrow \text{Products.}$$

When the temperature is high enough combustion, or high temperature oxidation, predominates with the first step being monomethylamine pyrolysis

$$CH_3NH_2 \Leftrightarrow HCN + 2H_2.$$

It has been suggested by Hill *et al.*[24] that this is followed by hydrogen combustion, which can be represented by the global reaction

$$2H_2 + O_2 \Leftrightarrow 2H_2O.$$

The measured laminar burning speed at standard conditions of monomethylamine in nitrogen, 23.2 cm/s, is approximately one tenth that of Hydrogen, 215 cm/s[24]. This indicates that the initiating dissociation step is likely to be important in determining the overall reaction rate. In the cylinder the tracer is only present in small concentrations, which will not propagate a flame. When monomethylamine is exposed to flame temperatures, on the order of 3000 K, it will dissociate. At this point the monomethylamine is effectively consumed, and what happens next is unimportant to the tracer gas method. The statements above regarding the dissociation step indicate that it is the key reaction in the cylinder. The dissociation reaction may also be important in the exhaust where the temperature is high enough for pyrolysis to occur, such as near the port.

Another mechanism for monomethylamine destruction is photolysis, which is when the excitation energy for a reaction is provided via electromagnetic radiation. The primary reaction for the photolysis of monomethylamine proceeds as follows

$$CH_3NH_2 + h\nu \rightarrow CH_3NH + H.$$

The first absorption band is around 220 nm[25], which is in the ultraviolet (UV) range. Most flame emission spectra are in the infra-red and visible range. Thus, photolysis is not likely to play an important role in the destruction of monomethylamine.

The above discussion of global reaction mechanisms is informative, however for quantitative calculations a more detailed mechanisms is recommended. In work by Hwang *et al.*[26] a 141 step mechanism was developed to model monomethylamine oxidation. The oxidation was studied using a rectangular shock tube to obtain temperatures from 1260 to 1600 K and IR laser absorption spectroscopy for mole fraction measurements. This mechanism is utilized in Chapter 4 for detailed chemical kinetic computations.

3.4.2 Nitrous Oxide Kinetics. One of the first investigations of the thermal decomposition of N_2O was by Hinshelwood and Burk[27]. The thermal decomposition of pure N_2O was studied from 840 to 1125 K. An important conclusion from this work was that the nature of the dissociation was second order. The dissociation of N_2O can be represented by the overall reaction

$$2N_2O \Leftrightarrow 2N_2 + O_2.$$

Hinshelwood's work was carried out at low pressures. Hunter[28] showed that nitrous oxide decomposition shows first order behavior at high pressures (above 6 atm)

$$N_2O \Leftrightarrow N_2 + O.$$

With regard to the tracer gas application this implies that nitrous oxide will display bimolecular behavior in the exhaust and unimolecular kinetics in the cylinder. Johnsson *et al.*[29] studied the decomposition of N_2O at small mole fractions (approximately 100 ppmv). The dissociation reaction is

$$N_2O + M \Leftrightarrow N2 + O + M$$

where M represents a third-body. The reaction rate varies depending on the composition of M. For this application, M is mostly diatomic nitrogen. In follow-on work by Glarborg[30] the effect of different diluent gases on N_2O decomposition was evaluated, using a quartz flow reactor designed for obtaining plug flow. Collision efficiencies were determined for Ar, O_2, CO_2, N_2, and H_2O as diluents. The results showed that the diluent gas had a significant impact on the N_2O reaction rate. In that work, a six-step reaction mechanism for N_2O consumption was developed which includes free radical reactions. This mechanism is implemented in Chapter 4 for chemical kinetic modeling of nitrous oxide destruction. Another potential path for nitrous oxide destruction is photochemical decomposition, discussed by Hayhurst and Lawrence[19]

$$N_2O + h\nu \rightarrow N_2 + O.$$

The wavelength of the electromagnetic radiation involved in this reaction was not given, which makes it difficult to assess the importance of this mechanism. Hence, the destruction of N_2O by way of photolysis can not be ruled out.

3.4.3 Oxygen Kinetics. Oxygen reacts primarily with the fuel and, late in the combustion process and in the exhaust, carbon monoxide. The overall reaction with an equivalence ratio of one for octane is

$$C_8H_{18} + 12.5O_2 \Leftrightarrow 8CO_2 + 9H2O.$$

Typically when oxygen is used as a tracer the engine is run rich which results in high levels of CO in the exhaust providing two mechanisms for oxygen consumption in the exhaust, reaction with CO and with unburned hydrocarbons.

3.4.4 Global Kinetics Comparison. To get an idea for how the reaction rates for these tracers compare with each other, an Arrhenius plot can be utilized with simplified kinetic mechanisms. For a second order reaction of

$$B + C \Leftrightarrow \text{Products},$$

the consumption of B can be represented by the rate expression

$$\frac{d[B]}{dt} = k[B][C], \tag{3.1}$$

where the brackets represent a concentration in moles per unit volume and t is time. The order with respect to each of the reactants is assumed to be unity. The rate constant, k, is defined by the Arrhenius equation

$$k = AT^n e^{-E_a/RT} \tag{3.2}$$

where T is temperature, E_a is the activation energy, A is the frequency factor, n is the temperature coefficient, and R is the universal gas constant. Figure 3.1 shows a comparison of the natural log of k vs. inverse temperature for the tracers being considered. The sources for the activation energy and frequency factor are given on the plot. The order of reaction with respect to the reactants was assumed to be unity for all cases, as shown in Equation 3.1. The temperature coefficient, n, was assumed to be zero. The plot does not take into account variations in concentrations, however this effect will be small compared to the influence of temperature. The desired behavior is to have a steep, temperature sensitive curve, sloping downward to the right, and positioned so that the tracer is reactive at combustion temperatures and stable at exhaust temperatures. Nitrous oxide and monomethylamine both have relatively steep curves, whereas the

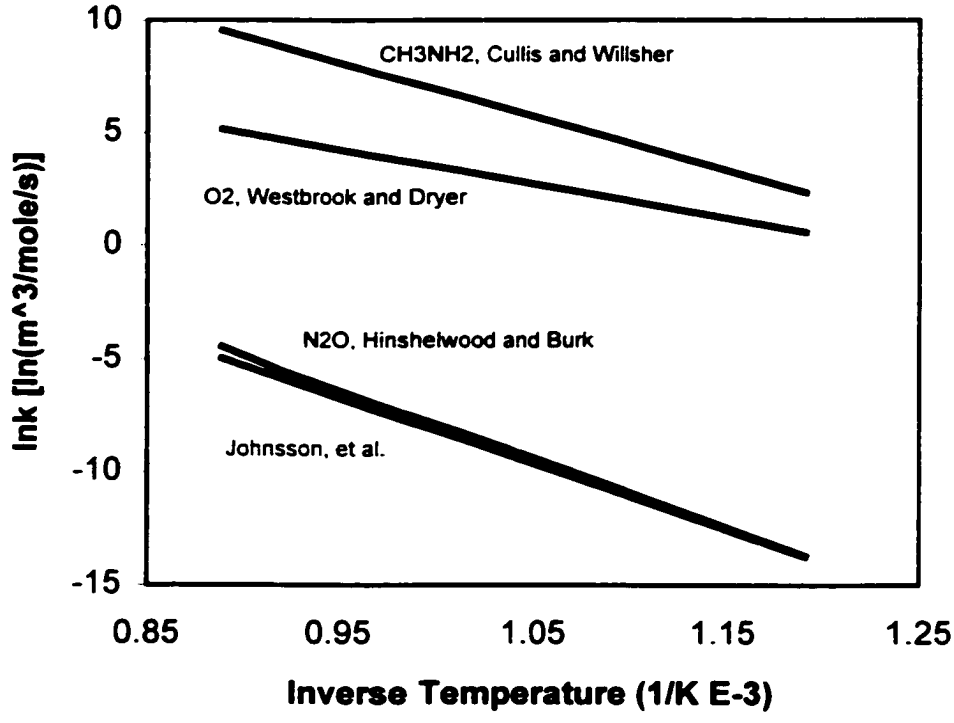

Figure 3.1 Arrhenius Plot Comparison of Tracer Gases

oxygen curve is more gradual. The purpose of this plot is qualitative rather than quantitative. Simplified mechanisms are, in general, not very accurate unless the concentration, temperature, and pressure ranges are the same as those for the original data. It is interesting to note that the curves for N_2O taken from the work of Johnsson *et al.* and Hinshelwood and Burk, almost 7 decades earlier, are nearly identical.

CHAPTER 4

TRACER GAS CHEMICAL KINETIC MODELING

The extent of tracer reaction in the cylinder and the degree of tracer consumption in the exhaust are identified as key factors in implementing the tracer gas method. In an effort to better characterize these effects a computer model is used for predicting tracer gas reaction in the cylinder and exhaust. Figure 4.1 shows a flow chart of the overall model. The temperature, pressure, and composition at any point in time are assumed to be uniform, which characterizes the model as zero-dimensional (i.e. no spatial dependence). The model inputs, temperature and pressure, are critical to making accurate predictions.

The model involves both an equilibrium and a chemical kinetics code. In general both possess an exponential dependence on temperature. Pressure impacts both codes as well. For equilibrium reactions a pressure dependence exists when the number of moles of reactants is different than that of the products, based on the stoichiometric coefficients for the set of reactions considered. Increasing pressure drives equilibrium reactions toward the side that has fewer moles. Chemical kinetic reaction rates are proportional to pressure raised to the overall order of reaction. However, in these calculations temperature is generally the dominant variable. A relatively small change in temperature can dramatically influence the results.

The exponential temperature relationship of tracer chemical kinetics warrants the development of a sophisticated model to track temperature both spatially and temporally.

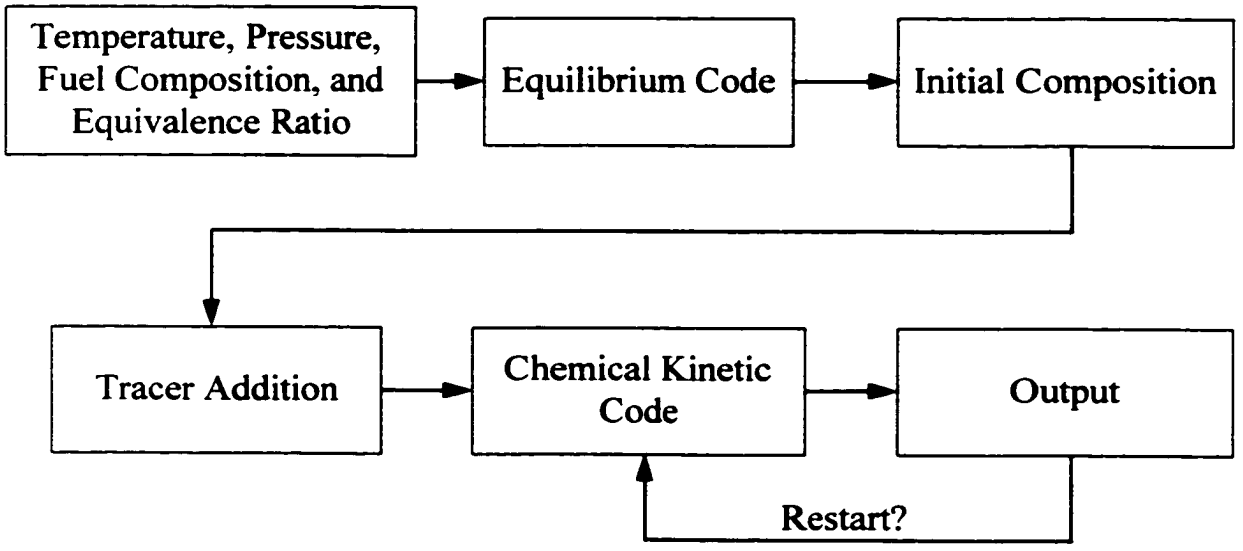

Figure 4.1 Overall Computer Model for Predicting Tracer Gas Consumption

This by itself is a formidable project. Rather than attempting to accurately model the temperature in the cylinder and in the exhaust, the temperature is bracketed. Evaluations of the lowest and highest expected temperature cases are carried out. Once the evaluations are performed, the temperature and pressure information along with the fuel composition and equivalence ratio are used by the equilibrium code to determine combustion product composition (Figure 4.1). The combustion product composition includes the primary free radical mole fractions O, OH, and H, which are critical inputs to the chemical kinetics code. At this point tracer is added at the appropriate mole fraction. Combustion is, in effect, modeled by the equilibrium code; therefore, tracer destruction in the cylinder is assumed to take place in the post combustion gases. This assumption neglects any tracer destruction that may occur during compression; however, this is likely to be unimportant when compared with the tracer consumption occurring in the

combustion products. The combustion products are typically near adiabatic flame temperatures just after being processed by the flame, and contain significant mole fractions of free radicals. The chemical kinetic code is run with initial conditions from temperature and pressure evaluations, equilibrium code output, and tracer addition. This model is likely to be conservative with regard to tracer destruction, since free radical mole fractions in flames typically exceed equilibrium values. Figure 4.1 shows a restart option. This is used when the temperature and pressure assumptions are changed in the middle of a run, yet the composition remains continuous. The restart option will become clearer during the discussion of specific cases.

The modeling consists of looking at the tracer reaction in the cylinder and in the exhaust for two very different engines at nominal operating conditions. The nominal operating conditions are consistent with test results described in Chapters 5 and 6. Table 4.1 illustrates the differences between the two engines considered. Average fuel compositions for natural gas and gasoline are utilized to approximate the actual compositions, taken from Heywood[1]. Where possible, test data are incorporated into the modeling process to more accurately define temperatures and pressures.

4.1 Equilibrium Code

The equilibrium code is included with a textbook by Turns[31], and originally developed by Olikara and Borman[32]. The program input parameters are temperature, pressure, fuel composition, and equivalence ratio. The output data are mixture enthalpy, mixture specific heat at constant pressure, mixture ratio of specific heats, mixture

Cooper-Bessemer 2-Stroke GMV-4TF	General Motors 4-Stroke V8
141 liter displacement	5.7 liter displacement
fuel: natural gas ($C_{1.4}H_{4.2}$)	fuel: gasoline ($C_{8.3}H_{15.5}$)
trapped equivalence ratio: 0.77	trapped equivalence ratio: 1.23
300 rpm	3000 rpm
fuel-injected	carbureted

Table 4.1 Engines and Operating Conditions Used for Chemical Kinetic Modeling.

molecular weight, moles of fuel per mole of products, and the mole fractions of eleven different combustion product species. The eleven species are H, H_2, NO, CO_2, O, OH, O_2, N_2, N, CO, and H_2O. The code considers seven different hypothetical equilibrium reactions, which are

$$1/2\ H_2 \Leftrightarrow H$$

$$1/2\ O_2 \Leftrightarrow O$$

$$1/2\ N_2 \Leftrightarrow N$$

$$1/2\ H_2 + 1/2\ O_2 \Leftrightarrow OH$$

$$1/2\ O_2 + 1/2\ N_2 \Leftrightarrow NO$$

$$H_2 + 1/2\ O_2 \Leftrightarrow H_2O$$

$$CO + 1/2\ O_2 \Leftrightarrow CO_2.$$

Curve fits for the equilibrium constants based on data from the JANAF Thermochemical Tables[33] are built into the program. A variety of numerical methods are implemented to obtain solutions that include Gaussian elimination, Newton Raphson iteration, and Newton's method. This program includes the primary constituents found in combustion products of real engines, with the exception being THC's. THC emissions depend on physical mechanisms such as incomplete mixing and flame quenching inside the cylinder, and are not predicted as combustion products based on chemical equilibrium considerations. The model assumes that the mixture is uniform, so the presence of THC emissions is not considered.

4.2 Chemical Kinetics Code

The Chemkin-II chemical kinetics package[34] is used to model tracer gas chemical kinetics in the cylinder and in the exhaust. The Chemkin package, written in Fortran 77, consists of two major software components, which are an interpreter and a gas-phase subroutine library. The interpreter is a program that reads a symbolic description of a user-specified reaction mechanism and, based on the species in the mechanism, extracts the needed thermodynamic data from a thermodynamic database. Only the Arrhenius coefficients for the forward rate constants are necessary in the mechanism, since Chemkin calculates the reverse rate constants from the forward rate constants and the thermodynamic data. The interpreter output is a binary file that is linked to the gas-phase subroutine library. The program from the gas-phase subroutine library implemented in this work is SENKIN[35]. The file structure of the kinetics model is given in the flowchart in Figure 4.2. SENKIN is a program that computes the time evolution of a homogeneous

reacting gas mixture in a closed system. The model accounts for finite-rate elementary chemical reactions, and performs kinetic sensitivity analysis with respect to the reaction rates. The sensitivity analysis is used primarily for developing chemical kinetic mechanisms, and was not employed in this modeling effort. The program considers five problem types

a. an adiabatic system with constant pressure,

b. an adiabatic system with constant volume,

c. an adiabatic system with the volume a specified function of time,

d. a system where the pressure and temperature are constant, and

e. a system where the pressure is constant and the temperature is a specified function of time.

The reaction mechanism consists mainly of the actual reactions, and the associated Arrhenius coefficients. The reactions and the coefficients are used by SENKIN to formulate a set of chemical kinetic rate equations, similar to Equations 3.1 and 3.2. The rate equations constitute a large portion of the differential equation set to be solved by SENKIN. SENKIN uses DASAC software, which was written by Caracotsios and Stewart[36], to arrive at the computational solution. DASAC handles the solution of the governing differential equations together with an efficient simultaneous computation of the first-order sensitivity coefficients. The numerical method is based on backwards

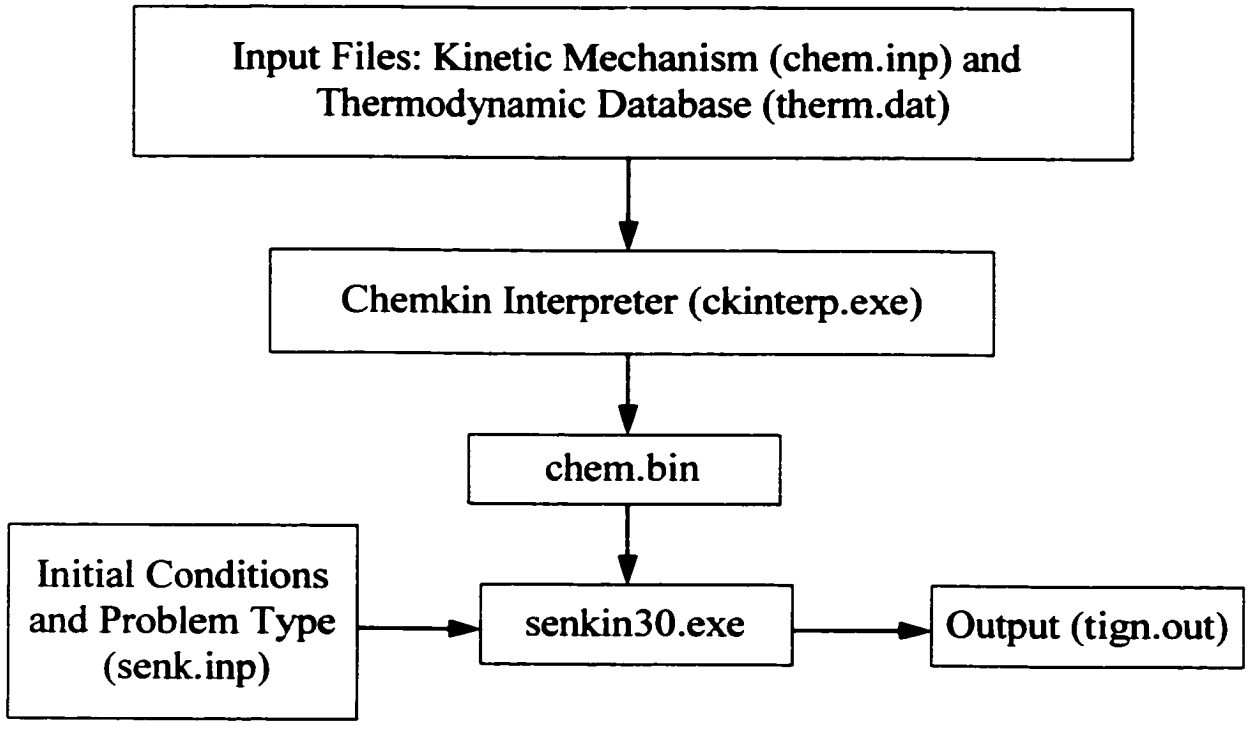

Figure 4.2 File Structure for the Chemical Kinetics Model

differentiation formulas and is especially well suited for solving the "stiff" differential equations that are common in chemical kinetics applications.

4.3 Chemical Kinetic Mechanisms

4.3.1 Nitrous Oxide. The foundation of the chemical kinetic mechanism for the destruction of nitrous oxide is from work by Glarborg *et al.*[30]. The mechanism developed by Glarborg contains 8 reactions, two of which are duplicates, and 11 species. Duplicate reactions in kinetic mechanisms have different Arrhenius coefficients. Therefore, it is a way of modeling reaction rates using the sum of two exponential functions. The

development was carried out using a quartz plug flow reactor in the temperature range of 1000-1400 K at 1 atm. The reactor was housed by a three zone electrically heated oven, allowing a uniform temperature profile within ±5 K throughout the reaction zone. Of the eight reactions in the mechanism, only the Arrhenius coefficients for the third-body reaction were developed in the work by Glarborg *et al.* The third-body reaction, discussed earlier, is

$$N_2O + M \Leftrightarrow N_2 + O + M,$$

where M represents a third-body, and passes from the reactants to the products unchanged. The rate constants for the other reactions were taken from the results of other work. This reaction was evaluated in four different carrier gases, Ar, N_2, O_2, and CO_2, and with various concentrations of H_2O. The initial N_2O concentration was 200 ppmv. Third-body efficiencies were calculated for the four carrier gases and H_2O. These (excluding Ar) are the primary constituents in the products of combustion. The third-body reaction is entered in the mechanism as four separate reactions, applying the corresponding third-body efficiency to each. A reaction involving NH was omitted early in the modeling effort because thermodynamic data had not been obtained yet. After the modeling was complete and the thermodynamic data acquired, numerous cases were rerun with the NH reaction incorporated into the mechanism to see if it played an important role. The cases that were rerun represented the range of conditions modeled. None of the cases showed any change in the consumption of N_2O with the additional reaction. The mechanism presented by Glarborg *et al.*, only contains an upper bound for the rate constant corresponding to the reaction of N_2O with OH. The Arrhenius

coefficients for this reaction were taken from a paper by Mebel *et al*[37]. The reaction, also from this work, of N_2O with NO was added to the mechanism[38]. Mebel *et al.* used both the transition state theory (TST) and the Rice-Ramsperger-Kassel-Marcus (RRKM) theories to evaluate the Arrhenius coefficients. The N_2O consumption mechanism, including the NH reaction, the Mebel *et al.* reactions and incorporating the third-body efficiencies from Glarborg *et al.* as four separate reactions, is given in Appendix A. The nomenclature for the Arrhenius coefficients is the same as is shown in Equation 3.2, and the order of reaction with respect to the reactants takes on the value of their respective stoichiometric coefficients.

4.3.2 Monomethylamine. The monomethylamine mechanism utilized is taken directly from work by Hwang *et al*[26]. In this research a 141 step monomethylamine oxidation mechanism was developed, based on previous work. Although it is an oxidation mechanism, monomethylamine dissociation, which was discussed in Chapter 3, is a chain initiation step. Monomethylamine oxidation was studied experimentally with a shock tube in the temperature range 1260-1600 K, at near atmospheric pressures. The initial gas compositions tested were 2.5% CH_3NH_2 with 2.5% O_2, 2.5% CH_3NH_2 with 10.3% O_2, and 1% CH_3NH_2 with 5% O_2 in Ar. Concentration vs. time profiles of CH_3NH_2 in the shock tube were measured using infrared laser kinetic absorption spectroscopy. The absorption profiles were satisfactorily modeled with the 141 step mechanism. The monomethylamine chemical kinetic mechanism is given in Appendix B. Nomenclature and order of reaction is consistent with that which was described for Appendix A.

4.4 In-Cylinder Tracer Reaction

The approach taken to characterize the tracer consumption in the cylinder is, as described earlier, to calculate high and low temperature cases that bracket the actual temperature in the cylinder. In both cases the reaction is assumed to take place in the post combustion gases. Both temperature cases begin at spark, which is assumed to occur at TDC. For the high temperature case SENKIN is run at constant volume (case b) beginning at the adiabatic flame temperature and pressure. It is run for a time duration from the time of spark to the location of peak pressure (LOPP), which constitutes a reaction duration of about 10 ms. The adiabatic flame temperature and pressure are determined by running the equilibrium code with the input data corresponding to the conditions at spark. At LOPP a new SENKIN run begins where an adiabatic volumetric expansion (case c) takes place, which corresponds to the piston movement from LOPP (18° ATC) to exhaust port opening (EPO, 108° ATC). The volumetric expansion between TDC and LOPP is neglected in the high temperature case. The SENKIN restart mode is utilized at the transition from constant volume to volumetric expansion. The SENKIN problem type changes, but the species mole fractions are continuous. The low temperature case is similar to the high temperature case, except the constant volume portion of the run is performed at the bulk temperature corresponding to peak pressure. It is worth noting that the bulk temperature is not the lowest temperature in the cylinder. Temperatures in and behind the flame are near adiabatic flame temperatures. Since the bulk temperature is an average cylinder temperature there must be zones in the cylinder below bulk temperature, at least within the timeframe of flame propagation.

4.4.1 Nitrous Oxide. The nitrous oxide reaction in the cylinder of the GMV-4TF for two different temperature cases is shown in Figure 4.3. The input concentration of nitrous oxide is only 1000 ppm, so the temperature does not change significantly during this part of the run even though nitrous oxide destruction is exothermic. In both temperature cases nitrous oxide consumption occurs quickly, relative to the duration of the power stroke. In the high temperature case nitrous oxide consumption occurs in about 2 ms, and in the low temperature case it occurs in about 9 ms. In the high temperature case, 99.7% of the tracer is consumed and for the low temperature case, 99.5% of the nitrous oxide is destroyed. At t=0, when the nitrous oxide consumption rate is the greatest, it is dominated by third-body reactions for both temperature cases. For the low temperature case, 99.5% of the initial nitrous oxide destruction rate is from third-body reactions with the two most dominant being

$$N_2O + N_2 \Leftrightarrow 2N_2 + O$$

$$N_2O + H_2O \Leftrightarrow N_2 + O + H_2O$$

with the N_2 reaction contributing 38% to the overall rate and the H_2O reaction 53%. For the high temperature case, the third-body reactions amount to 88% of the overall nitrous oxide destruction rate. The same two third-body reactions dominate as in the low temperature case, with the N_2 reaction making up 34% of the overall rate and the H_2O reaction 47%. In this case two other reactions become important, which are

$$N_2O + H \Leftrightarrow N_2 + OH$$

$$N_2O + OH \Leftrightarrow N_2 + HO_2,$$

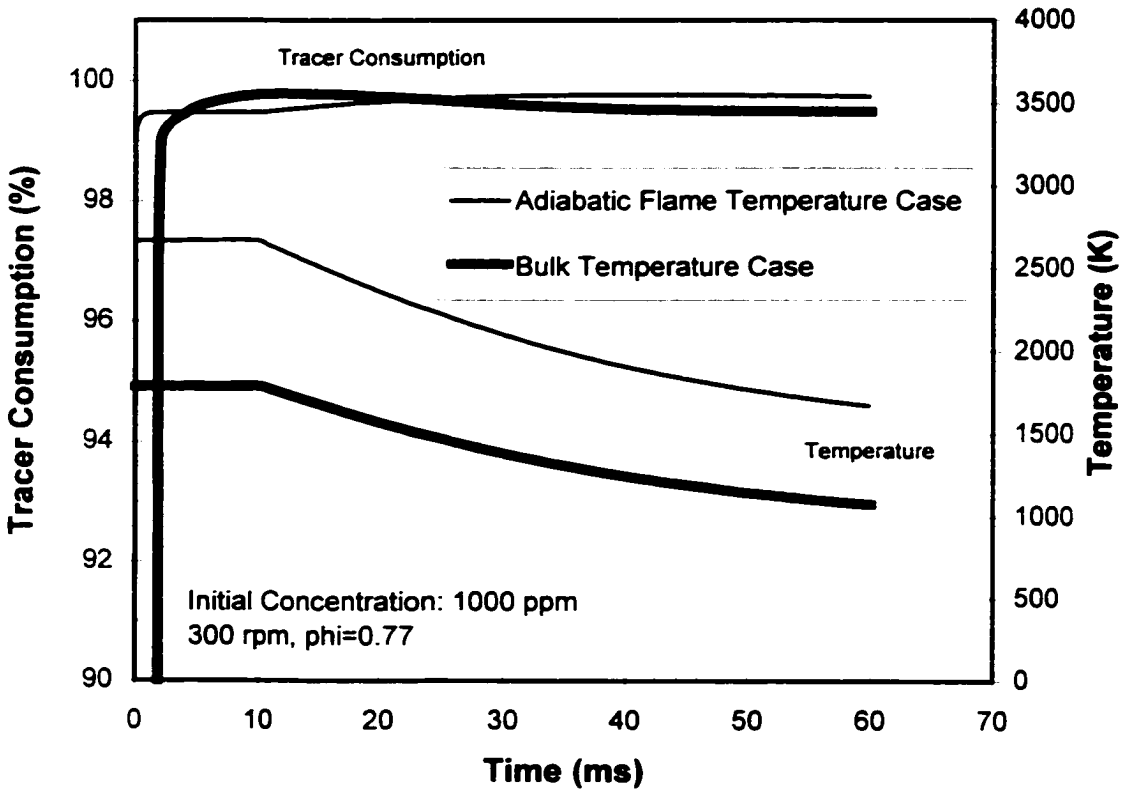

Figure 4.3 Nitrous Oxide Reaction in the Cylinder of the GMV-4TF Engine.

combining to add about 11% to the initial nitrous oxide destruction rate.

The expansion portion of the graph is interesting in that the nitrous oxide concentration changes as the piston expands. In the high temperature case nitrous oxide destruction continues as the piston expands, whereas in the low temperature case nitrous oxide is formed during expansion. The amount of nitrous oxide formed represents about 0.3% of the initial concentration, or 3 ppm. As mentioned in Chapter 3, with the exception of fluidized bed coal combustors the emissions of nitrous oxide from combustion sources are typically small (5 ppm or less). Measured nitrous oxide emissions from the GMV-4TF are typically around 6 ppm. Thus, the quantity of nitrous oxide

formation predicted by the model is in the right range. The low temperature case was rerun without any initial nitrous oxide concentration to see if any would form under these conditions. The result was that about 2.1 ppm was formed, so the amount of formation to a degree is related to the initial concentration of N_2O.

The ignition timing was assumed to be at TDC, however a more typical ignition timing for this engine would be 10° BTC. This does not have a significant impact on these calculations for two reasons. First the volume change between 10° BTC and TDC is only 3.8%. The second reason is that the reactions have nearly come to equilibrium between TDC and LOPP, so the additional reaction time is inconsequential. Additionally, any small effect the change in volume and additional reaction time have is partially negated because they are offsetting effects with regard to their impact on nitrous oxide reaction rate.

Figure 4.4 shows the predicted reaction of nitrous oxide in the cylinder of the GM 5.7 liter V8. The same procedure is followed to arrive at high and low temperature cases. The primary differences between the reaction in the cylinder of the GMV-4TF and the GM 5.7 l are the equivalence ratio, the fuel, and the engine speed. These differences lead to higher adiabatic flame temperatures, different combustion product composition, and a larger volumetric expansion rate. The runs begin at spark, 24° BTC, and end at exhaust valve opening (EVO), 108° ATC. The transition between the constant volume and adiabatic expansion parts of the runs occurs at 12.4° ATC, which is the LOPP. For the high temperature case 100% of the nitrous oxide is consumed and for the low

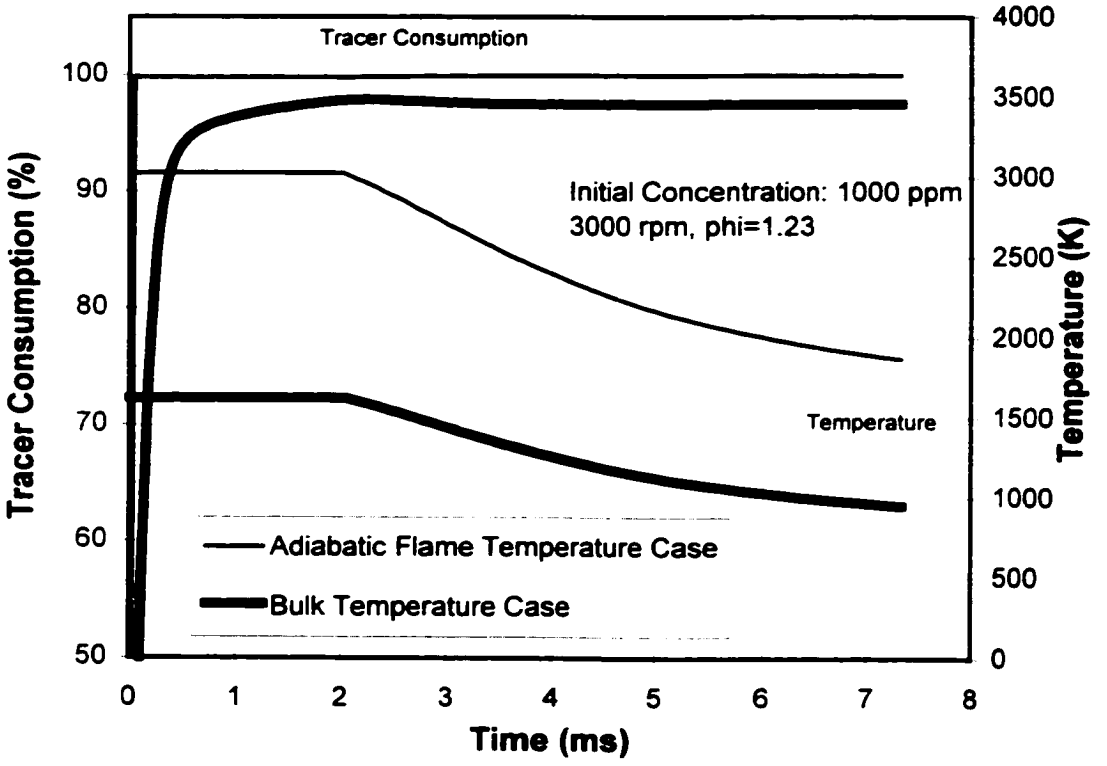

Figure 4.4 Nitrous Oxide Consumption in the Cylinder of the GM 5.7 Liter Engine.

temperature case 97.6%. In comparison to the GMV-4TF cylinder reaction, more nitrous oxide is destroyed for the high temperature case, but less is consumed in the low temperature case. This is most likely related to the differences in the two combustion events discussed above. Note that the adiabatic flame temperature for the GM 5.7 liter is higher than that for the GMV-4TF, while the bulk temperature at peak pressure is lower.

The GM 5.7 liter initial nitrous oxide reaction rate is dominated by third-body reactions, which contribute 93% to the overall destruction rate. The same two third-body reactions as in the GMV-4TF are predominant, N_2 and H_2O, which provide 38 and 46% of the initial overall N_2O consumption rate, respectively. The H reaction discussed above

is also important and makes up 7% of the initial total reaction rate. For the high temperature case third-body reactions are still important, but only make up 51% of the total nitrous oxide reaction rate. The reaction of nitrous oxide with the H (given above) contributes 44% to the initial overall rate. Higher H concentrations due to the rich equivalence ratio and the increased temperature are the main reasons for the shift in relative reaction rates. The OH reaction shown above is also important in the high temperature case.

During expansion, similar behavior to the GMV-4TF is seen. The y-axis scales in Figures 4.3 and 4.4 are different, so it is difficult to compare them by inspection. Roughly the same amount of nitrous oxide is formed during expansion for the low temperature case, 3 ppm. Typical measured exhaust nitrous oxide emissions from the GM 5.7 liter engine are around 3 ppm. An additional 0.26% of the initial nitrous oxide concentration is consumed during expansion for the high temperature case, slightly more than is seen in the GMV-4TF.

The nitrous oxide removal mechanism given in Appendix A does not contain a mechanism for NO formation and destruction. Nitric oxide formation generally becomes significant at high temperatures. To investigate the effects of high temperature NO chemistry the cylinder reaction cases were rerun with the extended Zeldovich mechanism added. The extended Zeldovich mechanism is given in Table 4.2, taken from Turns[31]. Adding the extended Zeldovich mechanism does not have a significant effect on the nitrous oxide consumption for the low temperature results for either engine, or the high temperature case for the GM 5.7 liter. The high temperature case for the GMV-4TF showed a significant difference. In that case 99.7% of the nitrous oxide was destroyed

Reaction	$A\left(\frac{cm^3}{mole \bullet s}\right)$	n	E_a (cal/mole)
$O + N_2 \Leftrightarrow NO + N$	1.8E+14	0	76,250
$N + O_2 \Leftrightarrow NO + O$	1.8E+10	1.0	9,300
$N + OH \Leftrightarrow NO + H$	7.1E+13	0	894

Table 4.2 The Extended Zeldovich Mechanism with Forward Rate Constants.

before the extended Zeldovich mechanism was added, whereas 99.9 % was consumed after the extended Zeldovich mechanism was added. This difference occurs during expansion, so it is likely to be related to NO being consumed by the extended Zeldovich mechanism reverse reactions. In the case without the extended Zeldovich mechanism the ending NO concentration is 13,000 ppm, while the NO concentration for the case with the extended Zeldovich mechanism is 8,290 ppm. These concentration values are much higher than typical engine-out emissions of NO. This is because with the high temperature case, the entire cylinder mass is held at the adiabatic flame temperature for longer than would be expected for a small element of volume that sees the temperature rise from a propagating flame. The reduction in the NO concentration tends to reduce the importance of the reverse reaction

$$NO + NO \Leftrightarrow N_2O + O$$

from the N_2O destruction mechanism in Appendix A, which is second order with respect to NO.

The nitrous oxide destruction in the cylinder is assumed to take place in the post combustion gases, so the issue of the effects of combustion arises. To model combustion, GRI-Mech Version 1.2 was added, which is a natural gas combustion mechanism developed by the Gas Research Institute (GRI)[39]. This mechanism is provided in Appendix C. Pure methane is assumed for the fuel at a trapped equivalence ratio of 0.77 for the GMV-4TF. The fresh charge is compressed to the point of spark, then SENKIN is run at constant volume until combustion occurs. The temperature, pressure, and composition just before combustion are used as initial conditions for a run that includes expansion. Figure 4.5 shows the results of this run, where 100% of the nitrous oxide is consumed. Therefore, running the combustion mechanism in parallel with the nitrous oxide removal mechanism yields a higher nitrous oxide consumption percentage. Also shown in Figure 4.5 are the motored temperature and pressure. Using the motored temperature and pressure profiles, a case is run to see if any nitrous oxide is consumed during a complete misfire. A combination of the nitrous oxide removal mechanism, the extended Zeldovich mechanism, and GRI-Mech where implemented for this case. This run resulted in no consumption of nitrous oxide, showing that the assumption of no nitrous oxide reaction during misfires is reasonable.

4.4.2 Monomethylamine. The cylinder reaction of monomethylamine is investigated utilizing the oxidation mechanism developed by Hwang *et al.* given in Appendix B. This mechanism already contains the three reactions in the extended Zeldovich mechanism. The same assumptions with regard to temperature, pressure, and initial tracer concentration for nitrous oxide are used with monomethylamine. The results are not

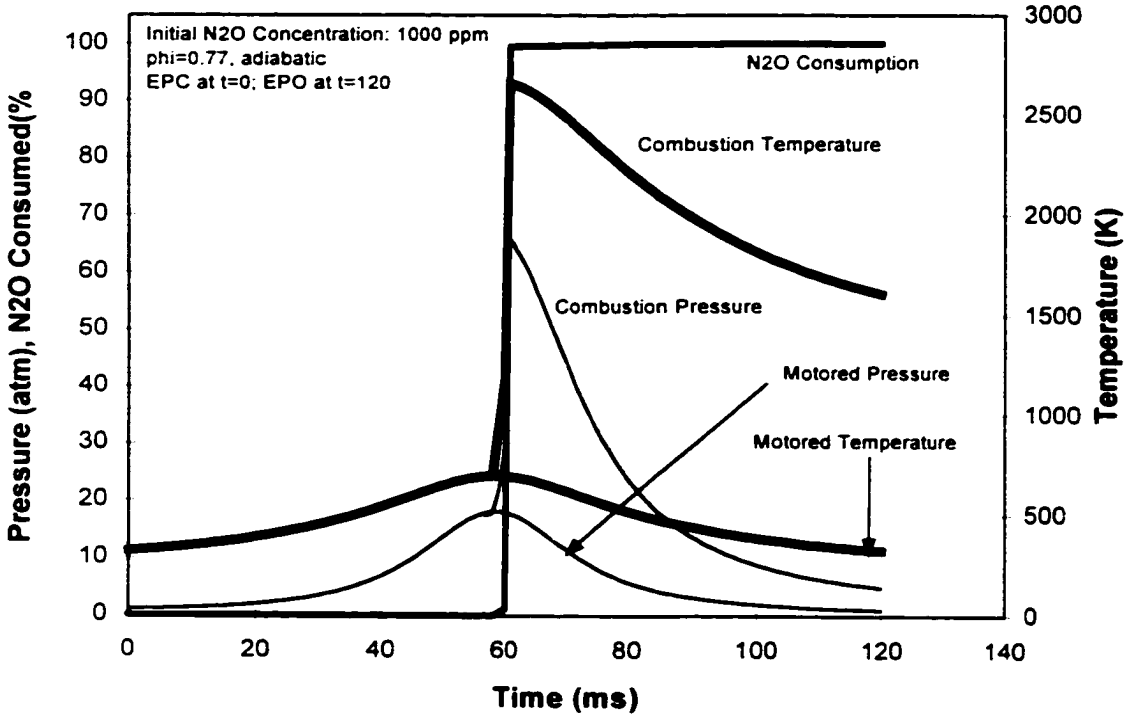

Figure 4.5 Nitrous Oxide GMV-4TF Cylinder Reaction with Combustion.

plotted, because in every case monomethylamine was consumed quickly and completely in the cylinder. This applies to both the GMV-4TF and the GM 5.7 l engines. For example, the low temperature case for the GMV-4TF begins with 1000 ppm. After 0.2 ms the concentration is down to 1.6E-9 ppm, and concentration after expansion is 2.2E-23. Similar degrees of tracer consumption are seen with the other cases, with the exception of the low temperature case for the GM 5.7 liter. In this case the remaining concentration was 0.015 ppm, which represents a consumption of 100.0%, to 4 significant figures. A motored case was also run to see if any monomethylamine was consumed during a misfire. The result was that no monomethylamine was consumed. Thus, the assumption

of no tracer reaction during a misfire is acceptable with monomethylamine as well as with nitrous oxide.

4.5 Exhaust Tracer Reaction

The reaction of the tracer in the exhaust system is modeled with the same kinetic mechanisms that are applied to the cylinder reaction. The equilibrium code in combination with an assumed initial tracer concentration are used to get the mixture composition at the entrance to the exhaust system. The reactions are carried out using SENKIN case e, where the pressure is held constant and the temperature is a specified function of time. Essentially the kinetics are run in a small volumetric element of gas, while it flows down the exhaust pipe at constant pressure, changing volume based on prescribed changes in temperature. Again, different temperature cases are developed to attempt to bound the tracer consumption. Presumably, the mass of tracer in the exhaust is from scavenge short-circuiting, so initial concentrations are lower than for the cylinder reaction. Assuming that the combustion products are thermally mixed at the time of exhaust port, or valve, opening, then the temperature has an upper bound in the exhaust system of the bulk cylinder temperature after it expands through the valve or port. There are several mechanisms that work to reduce the gas temperature very quickly. The last part of the cylinder gas to exit during blowdown has been expanded both from mass leaving the cylinder and the cylinder volume continuing to increase during blowdown. The gas that exits the cylinder during blowdown does so through the port, or valve, primarily via a sonic jet. Therefore, an expansion with an accompanying temperature and pressure drop occurs. Heat transfer plays a significant role as well, especially when the

gas is at high temperature. Heat transfer takes place through the cylinder walls, exhaust manifold, and exhaust pipe. Finally, as the gas exits the cylinder it mixes with gas from the previous cycle, and in the case of a 2-stroke engine, with scavenging air. All these effects work to reduce the average gas temperature. Despite all the mechanisms working to bring the gas temperature down quickly as it flows into the exhaust system, there is a possibility that at least a small portion of short-circuited tracer sees temperatures near the upper bound.

4.5.1 Nitrous Oxide. There are two different temperature cases evaluated to predict N_2O reaction in the exhaust system. The high temperature case begins at the cylinder bulk temperature at exhaust port opening (EPO) after it has been expanded through the port. The low temperature case assumes that the gas expands through the port and instantaneously mixes with the scavenging air (at intake manifold temperature) from the previous cycle, with an assumed trapping efficiency of 0.50. The exhaust manifold for this engine has a large volume, so the gas resides about half of the time in the exhaust manifold and the other half in the exhaust pipe.

Temperature measurements are only available downstream of the exhaust manifold. Hence, temperature measurements are not helpful in determining the shape of the temperature profile near the port. The temperature profiles are arrived at by using a simple finite volume/heat balance approach. The exhaust system is divided into small control volumes along the gas flow path. The first law of thermodynamics is applied by equating the heat transfer through the walls to ambient with the difference between the flow enthalpy entering the control volume and the flow enthalpy leaving. The control

volume exit temperature is then solved for. Carrying this out for each control volume, a temperature profile down the exhaust system is produced. The overall heat transfer coefficient is then scaled so that the ending temperature matches the measured stack temperature for both the high and low temperature cases.

Figure 4.6 shows a simple representation of the exhaust system on the GMV-4TF. The transition between the exhaust manifold and the exhaust pipe causes a bump in the temperature profile near the middle for the GMV-4TF exhaust flow. This is caused by higher heat transfer rates resulting from an increased exhaust flow Reynolds number as the cross-sectional area is reduced from the manifold to the pipe. The velocity vectors in the schematic scale approximately with average velocities for the low temperature case. The difference in average velocity vector length would be more pronounced for the high temperature case. As shown in the figure, the large flow area difference between the exhaust manifold and the exhaust pipe results in the gas spending about half of the time in the manifold. A few details should be pointed out that are not represented in the schematic. First, there is a divider in the exhaust manifold separating the flow through cylinders 1 and 3 from the flow through cylinders 2 and 4, which are on opposite sides of the engine. Additionally, two of the cylinders on each side are closer to the end of the manifold; the manifold length shown in Figure 4.6 is an average flow distance. Finally, bear in mind that the exiting cylinder gas not only mixes with the scavenging air from the previous cycle, but it can also mix with the exhaust from the neighboring cylinder.

Figure 4.7 shows the nitrous oxide reaction in the exhaust of the GMV-4TF. Nitrous oxide appears to be relatively stable in the exhaust. For the high temperature case about 2.5% is consumed, while no consumption is predicted for the low temperature case.

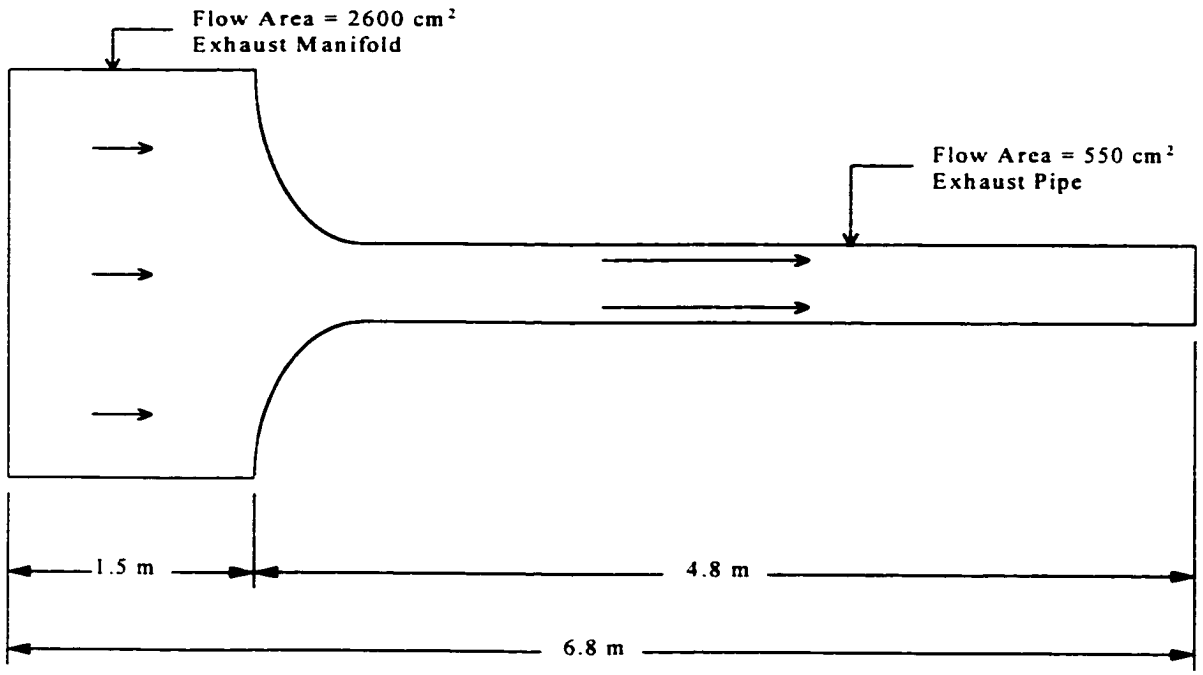

Figure 4.6 Schematic of Exhaust System on the GMV-4TF 2-Stroke Cycle Engine.

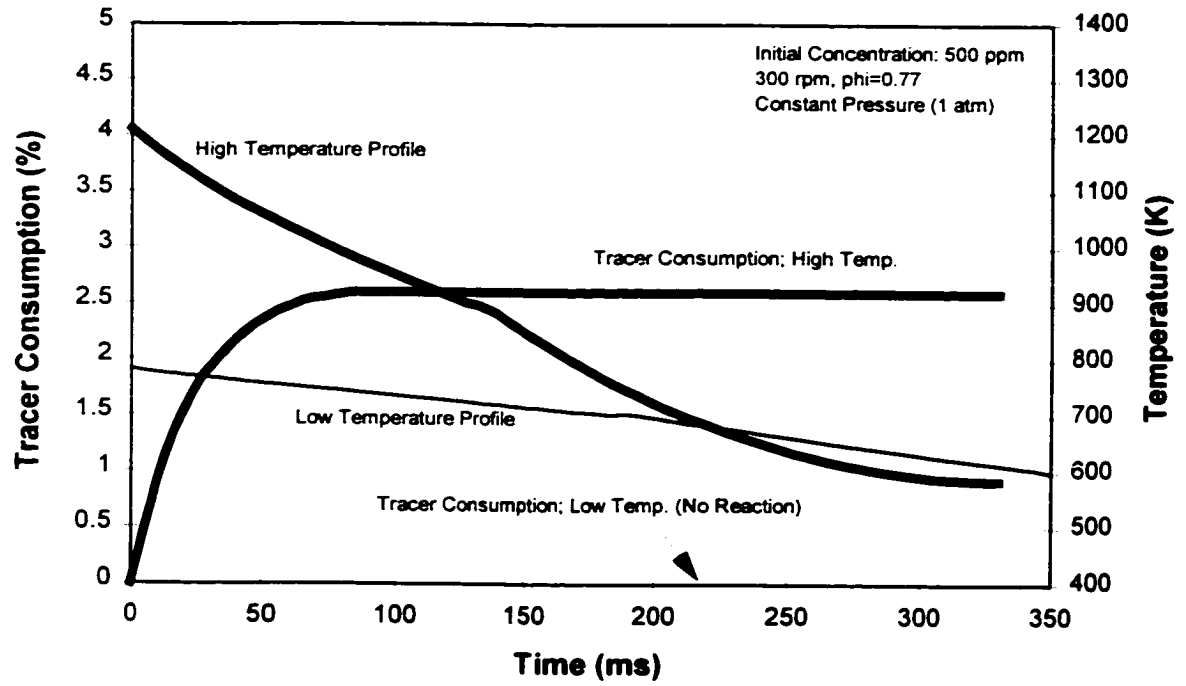

Figure 4.7 Nitrous Oxide Reaction in the Exhaust of the GMV-4TF Engine.

For the high temperature case the nitrous oxide consumption occurs in the exhaust manifold while the temperature is above 1000 K.

The nitrous oxide reaction in the GM 5.7 l engine exhaust is presented in Figure 4.8. The exhaust temperatures for this engine in general are considerably hotter. This is primarily because 4-stroke cycle engines have a much lower fraction of short-circuited gas. Also the temperature upper bound is higher, based on the same criterion as is used for the GMV-4TF. Although exhaust temperatures are generally higher for the GM 5.7 liter, the residence time in the exhaust is about 15% of the residence time for the GMV-4TF. The modeling is meant to approximate what goes on in the actual engine testing, presented in Chapter 5. The GM 5.7 liter engine uses an exhaust header where the flow from individual cylinders is kept separate, as opposed to an exhaust manifold where the flow from individual cylinders mix. The testing in Chapter 5 and the modeling in this chapter correspond to exhaust flow from a single cylinder through a header pipe, extended for the length of the exhaust system.

The temperature profiles in Figure 4.8 are arrived at differently than for the large bore natural gas engine. In this case, measured temperatures are available beginning approximately 7 ms downstream of the exhaust port followed by three more measurements spanning most of the length of the exhaust system. The measured temperature data are indicated on the plot. At those locations, the temperature is assumed to be constant. The area where analysis is needed is the length of pipe between the exhaust port (t=0) and the first temperature data point. For the low temperature case, the curve fit through the measured data is simply extrapolated to t=0. In the high temperature case, a point is added at t=0 that represents the high temperature bound. This temperature

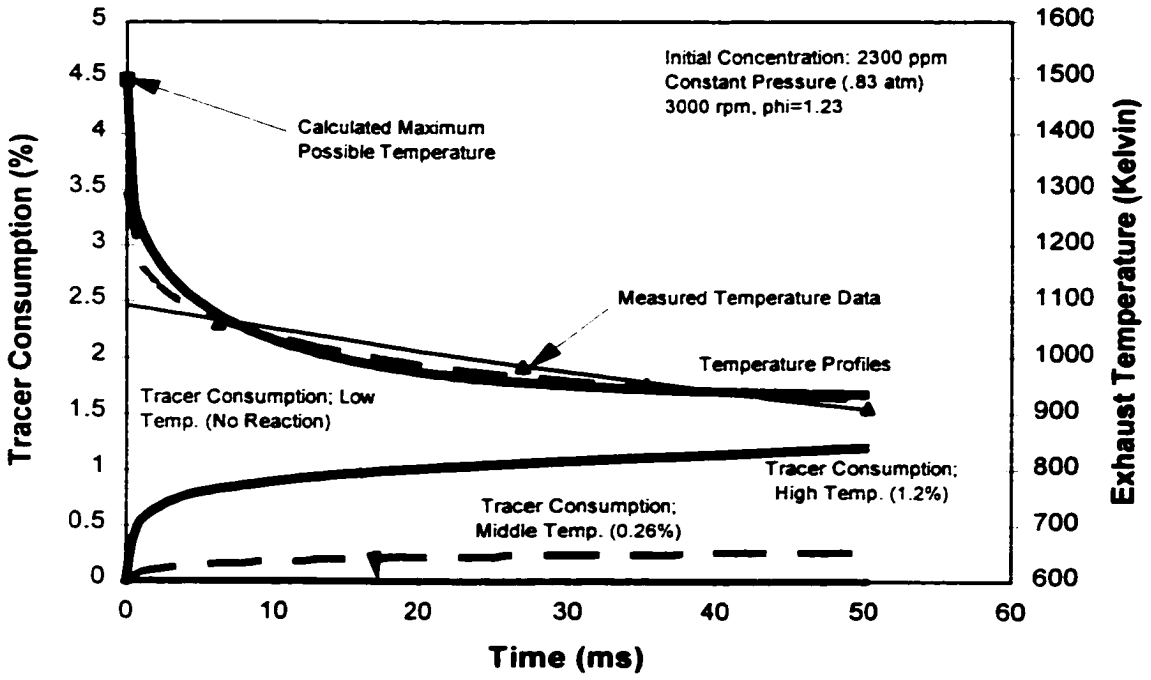

Figure 4.8 Nitrous Oxide Reaction in the Exhaust of the GM 5.7 l Engine.

bound is the bulk temperature in the cylinder just before exhaust valve opening, reduced by an expansion through the exhaust valve. A curve is then fit to those five points. Because there is such a large difference between the high and low temperature cases, a middle temperature case is analyzed. This is performed by adding a fifth point at t=0 equal to the average of the initial temperatures for the high and low temperatures cases, and fitting a curve to the resulting five points.

Figure 4.8 shows that the nitrous oxide consumption in the exhaust of the GM 5.7 liter engine is very low, 0, 0.26, and 1.2% for the low, middle, and high temperature cases, respectively. An initial concentration of 2300 ppm is used to reflect exhaust reaction testing in Chapter 5. A comparison of tracer consumption in the

GM 5.7 liter exhaust with 500 ppm (used for GMV-4TF exhaust reaction modeling) and 2300 ppm initial concentrations was made and the difference was insignificant. In the high temperature case, most of the nitrous oxide destruction takes place in the first 10 ms. As discussed earlier, only a small percentage of the gas volume in the exhaust is likely to see temperatures close to the upper bound. This combined with the small percent consumption for the high temperature cases, 2.5% for the GMV-4TF and 1.2% for the GM 5.7 liter, leads to the conclusion that nitrous oxide exhaust reaction is inconsequential for the conditions that have been modeled. The high temperature cases for each engine were rerun with the extended Zeldovich mechanism added to the nitrous oxide destruction mechanism. No significant differences in nitrous oxide consumption resulted.

4.5.2 Monomethylamine. The mechanism by Hwang *et al.* is used for modeling monomethylamine consumption in the exhaust, which is the same mechanism utilized for the cylinder reaction. The same methodology and temperature cases are used for monomethylamine as for nitrous oxide destruction in the exhaust. The only exception is the measured temperature data for the GM 5.7 l engine exhaust. The monomethylamine temperature data was collected on a different day with subtle changes in the hardware configuration (discussed in Chapter 5). The resulting temperature profiles are within 25 K of the nitrous oxide profiles at any point in time.

Figure 4.9 gives the results of the monomethylamine kinetic modeling in the exhaust of the GMV-4TF. The plot shows that 100% of the monomethylamine is consumed for the high temperature case and none of the tracer is destroyed in the low

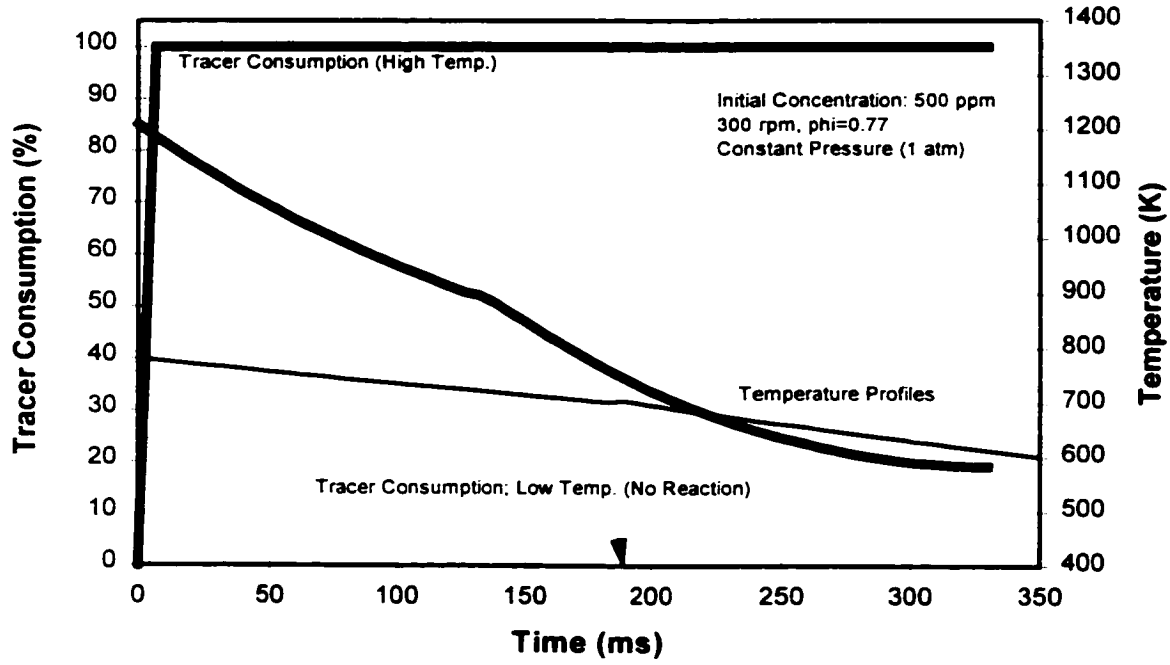

Figure 4.9 Monomethylamine Reaction in the Exhaust of the GMV-4TF Engine.

temperature case. This suggests that during the initial stages of blowdown it is possible for significant levels of monomethylamine to be destroyed. When exhaust gases near the upper temperature bound exit the cylinder during initial stages of blowdown, they can entrain scavenged short-circuited gas containing tracer. Later in the blowdown process and downstream of the port after mixing has occurred, very little monomethylamine is consumed. The implication is that the physical mechanisms of mixing and jet penetration could be as important as chemical kinetics. Monomethylamine consumption in the GM 5.7 l exhaust is presented in Figure 4.10. The modeling predicts that 1.8, 11, and 57% of the tracer is destroyed in the exhaust for the low, middle, and high temperature cases, respectively. In each case most of the consumption occurs within 5 ms, also

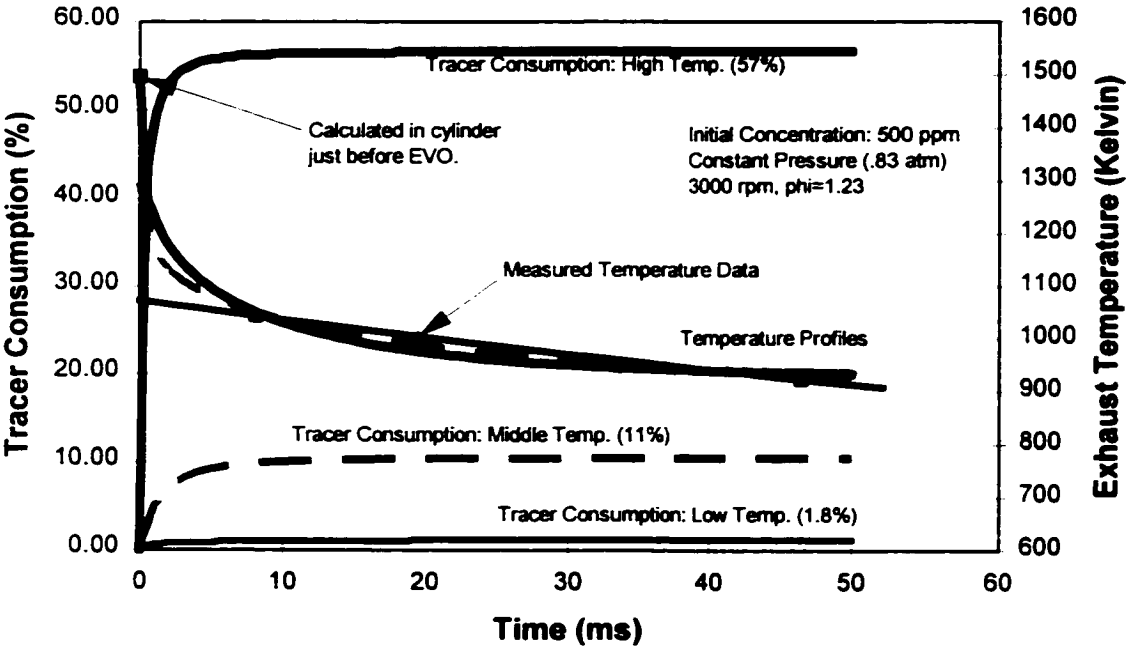

Figure 4.10 Monomethylamine Reaction in the Exhaust of the GM 5.7 l Engine.

indicating that a significant portion of short-circuited monomethylamine that mixes with the initial jet of exhaust products could be destroyed.

4.5.3 Exhaust Temperature Sensitivity. To gain more insight into the influence of exhaust temperature on the exhaust reaction, a temperature sensitivity analysis is performed. A constant volume adiabatic reaction is carried out for 5 ms for various temperatures. The calculations are performed for both the GMV-4TF and the GM 5.7 l engines. The results are given in Figures 4.11 and 4.12 for the GMV-4TF and the GM 5.7 l engines, respectively. The tracer consumption in the GMV-4TF exhaust becomes significant (5%) for monomethylamine and nitrous oxide at about 1100 K and

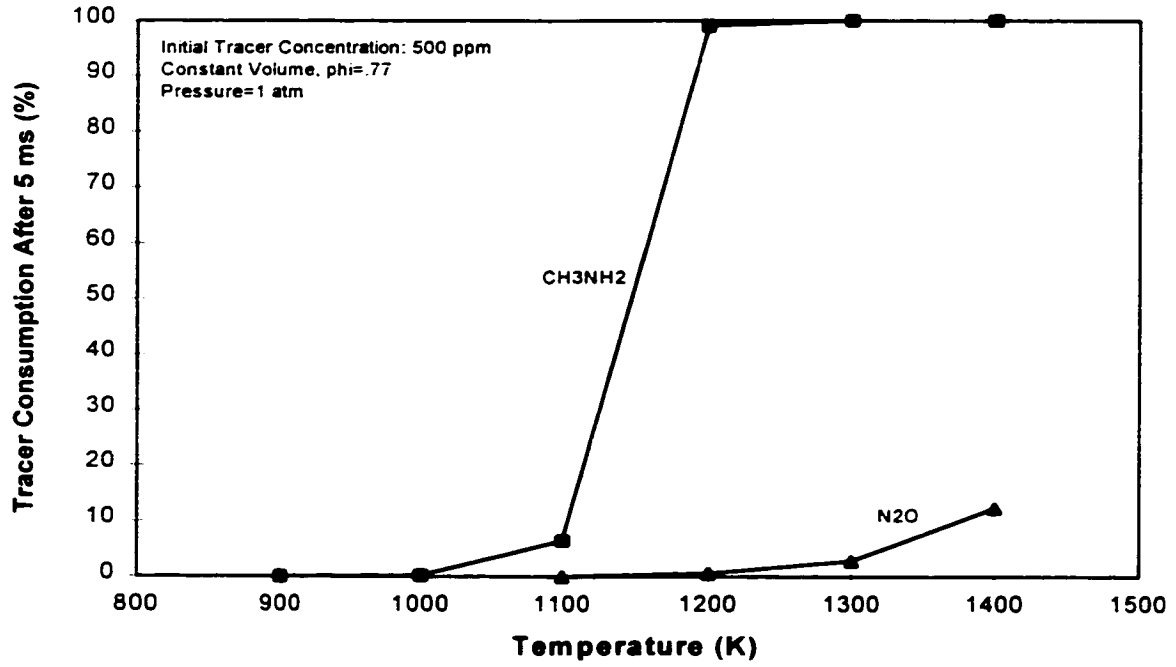

Figure 4.11 Temperature Sensitivity Analysis for the Exhaust Reaction in the GMV-4TF.

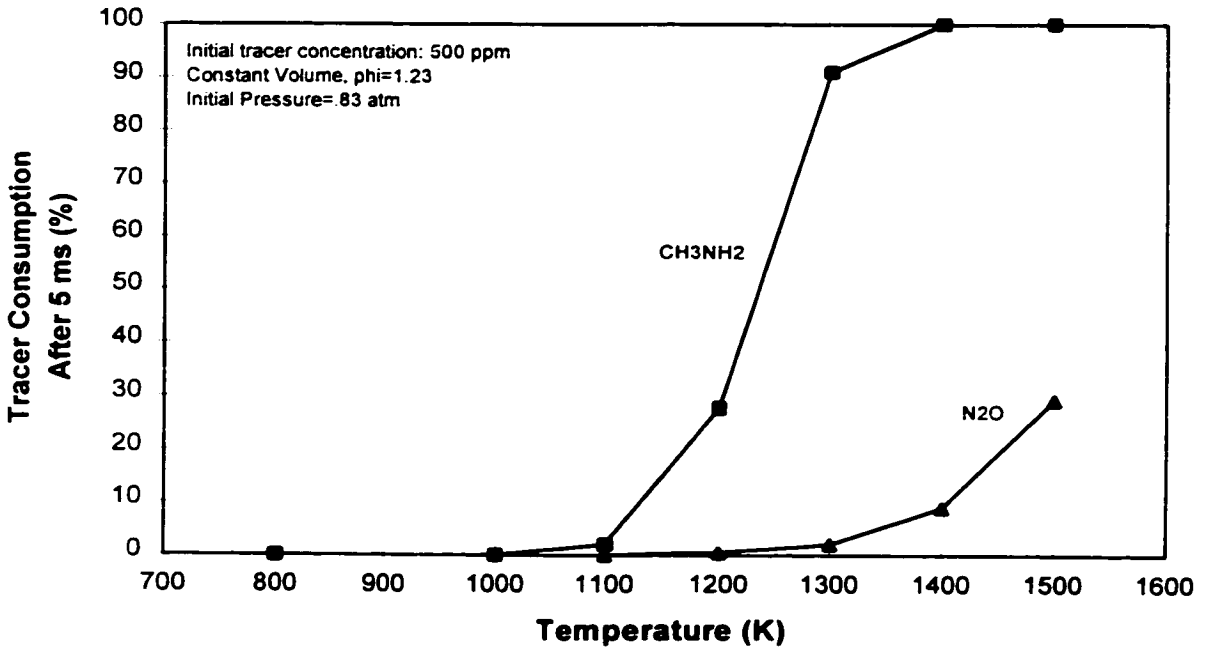

Figure 4.12 Temperature Sensitivity Analysis for the Exhaust Reaction in the GM 5.7 Liter Engine.

1350 K, respectively. The tracer reaction in the GM 5.7 liter exhaust becomes significant at roughly 1125 K and 1375 K for monomethylamine and nitrous oxide, respectively. For both scenarios the difference in temperature where the exhaust tracer reaction becomes significant is about 250K, with nitrous oxide being more stable. Additionally, once the tracer reaction becomes significant the nitrous oxide curves display a more gradual increase in slope, which is desirable when the goal is to limit the reaction in the exhaust.

CHAPTER 5

FOUR-STROKE CYCLE ENGINE TESTING

In this chapter the tracer gas method is applied to a 4-stroke cycle, automotive size, internal combustion engine. Measurements are presented for the cylinder reaction efficiency, exhaust reaction, and trapping efficiency. The TGM correction factors are characterized for monomethylamine, nitrous oxide, and oxygen. Based on the reviewed literature, the tracer gas method with an externally injected tracer had not been applied yet to a 4-stroke cycle engine at the beginning of this test program. Therefore, the results are representative of a technique in the initial phase of development. Consequently, suggestions are made for improvements to the method for future continued development.

5.1 Test Plan and Apparatus

The testing focused on three areas. They were (1) cylinder reaction efficiency, (2) exhaust reaction and (3) measuring the short-circuited fraction. The testing was performed at the CSU EECL on a GM 5.7 l 4-stroke cycle engine. Some characteristics of this engine are given in Table 1. A Nicolet REGA 7000 FTIR Exhaust Gas Analyzer was used to detect both CH_3NH_2 and N_2O. O_2 was detected using a paramagnetic analyzer housed in a Rosemount NGA-2000 5-Gas Emissions Bench. The focus of the emissions measurements was on the tracers, but other exhaust constituents such as CO_2, H_2O, NO_X,

Fuel	gasoline
Bore	10.2 cm
Stroke	8.84 cm
Displacement	5.78 l (5.7 l nominal)
Compression Ratio	10.4/1
No. Cylinders	8
Fuel Delivery	Carburetor
Ignition	Spark

Table 5.1 Engine Characteristics, GM 5.7 Liter.

THC, and CO were measured as well. An ECM AFRecorder 2400A was used for F/A ratio measurements. The test cell was equipped with a Superflow SF-730 computer data acquisition system and a Superflow SF-801 stepper valve controlled water brake dynamometer. The speed was controlled with a Woodward Governor TQ125 speed governor. A Superflow Engine Cycle Analyzer was employed to measure cylinder pressure and detect combustion misfire.

The manufacturers material safety data sheets for CH_3NH_2 and N_2O were reviewed carefully during test apparatus design to ensure good material compatibility as well as safe operation. Monomethylamine and nitrous oxide can be harmful if they are inhaled or come in contact with the skin. The monomethylamine reaction is more serious. Monomethylamine and nitrous oxide can react with each other to form potent carcinogens (N-Nitrosamines). Monomethylamine slowly corrodes copper, aluminum, zinc and galvanized surfaces. Stainless steel and Teflon are recommended wetted materials for both gases.

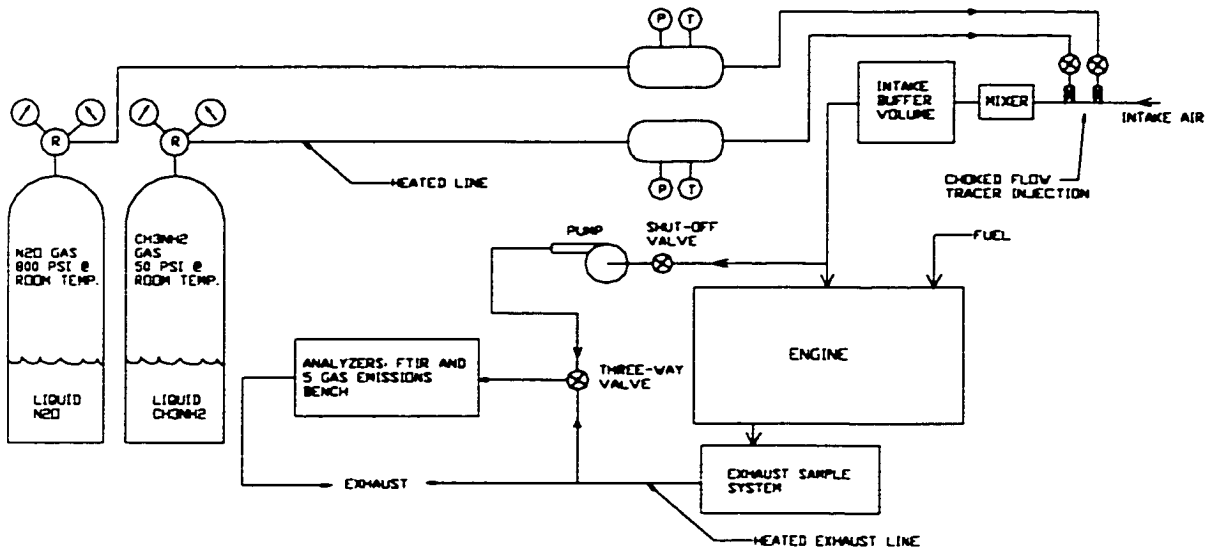

Figure 5.1 Tracer Gas Method Test Schematic.

The overall test schematic is shown in Figure 5.1. The tracer injection system accommodated both nitrous oxide and monomethylamine, although they were not tested simultaneously. The two smaller buffer volumes were for measuring stagnation pressure and temperature prior to injection. The tracer flow into the intake was choked so that the mass flow was dependent only on upstream stagnation pressure and temperature. If the flow is subsonic, the mass flow depends on downstream pressure as well and would be affected by inlet pressure fluctuations. The monomethylamine bottle and injection system was heated and insulated to prevent condensation on interior walls. Only the regulator in the nitrous oxide injection system was heated. The nitrous oxide vapor pressure is approximately 5510 kPa at room temperature. Condensation was only a concern in the regulator, downstream of the regulator orifice where the temperature drops due to throttling. An 85 liter surge tank was installed in the intake system between the tracer injection point and the carburetor to decrease intake pressure fluctuations. A mixer was

installed just downstream of the tracer injection point to insure a uniform mixture entering the carburetor. A three-way valve was located between the engine and the analyzers to facilitate measurement of both intake and exhaust tracer concentrations.

5.2 Sampling

Exhaust gas sampling close to the exhaust manifold proved to be difficult to perform accurately. A considerable amount of effort was put into resolving what was interpreted as sampling errors. The sampling error experienced was most likely caused by a combination of gas stratification and exhaust pressure fluctuations. When short-circuited gas flows past the exhaust valve and into the exhaust system, it resides just down stream of the port for approximately 3/4 of a cycle. The pulse of combustion products resides just down stream of the port for about 1/4 of a cycle before the next short-circuited pulse comes through the exhaust valve. Thus, the sample pump pulls from the short-circuited pulse 75% of the time. It is possible that the measured composition may not be a true mass average of the exhaust constituents when sampling is carried out near the exhaust port. This effect is described in Chapter 2, and shown schematically in Figure 2.1. The problem is further complicated when exhaust pressure fluctuations are considered.

Figure 5.2 shows the exhaust sample system. There were four sample taps with corresponding thermocouples for measuring sample temperatures. The sample taps consisted of 6.4 mm tubes, which enter the exhaust pipe through Swagelok fittings,

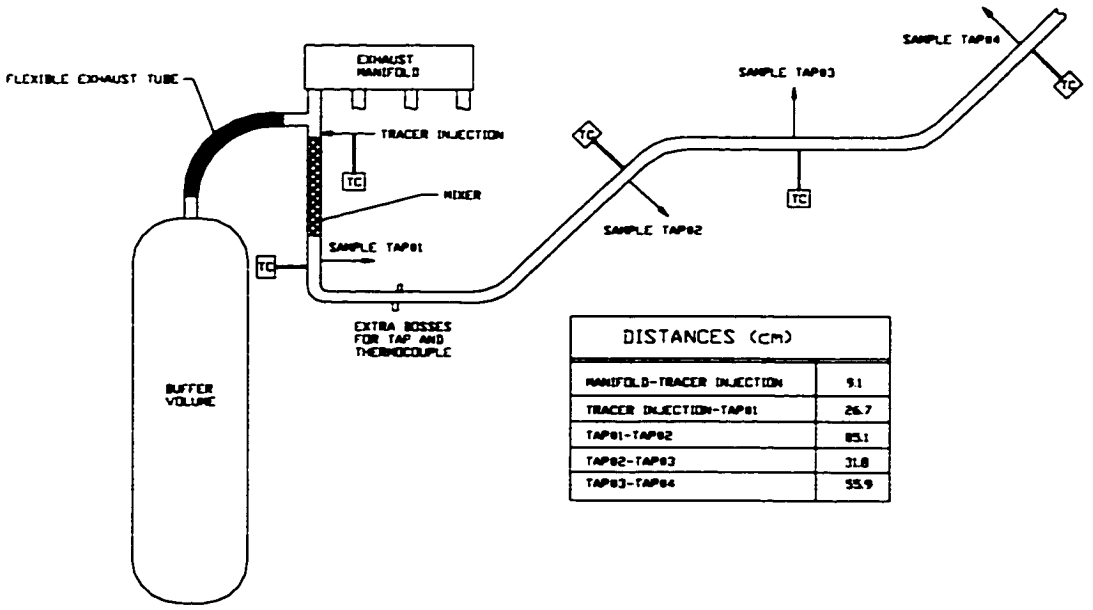

Figure 5.2 Exhaust Sampling Configuration.

terminating at the center of the pipe with a 45° angle, open side facing upstream. The thermocouples read the temperature near the center of the exhaust pipe, axially offset by about 1.3 cm from the sample tap. The sample lines were heated to between 390 and 420 K between the tap and the analyzers to prevent water condensation. A mixer and 25 liter buffer volume were added for the exhaust reaction and short-circuiting measurements just downstream of the exhaust port, placing the first sample tap about 36 cm from the port. The mixer and buffer volume were added to increase mixing and reduce pressure pulsations. Pressure measurements were made before and after the mixer and buffer volume were installed at 3000 rpm and 108, 163, and 203 N-m. The result was that peak pressure fluctuations were reduced by approximately 50% for all three cases. The most significant reduction was at about 25 Hz, which corresponds to the exhaust valve opening frequency or half the engine frequency, 1500 rpm. The zero overlap testing

was performed with no mixer or buffer volume and the sample tap about 3 cm downstream of the exhaust port. With the zero overlap cam, scavenge short-circuiting does not occur, so errors due to exhaust stratification were not expected.

5.3 Results and Discussion

5.3.1 Cylinder Reaction Efficiency: Zero Overlap Cam Tests. A zero overlap cam donated by Competition Cams was installed in the engine for measuring the cylinder reaction efficiency. The zero overlap cam ensures that there is no short-circuiting, assuming negligible valve leakage. The resulting tracer concentration in the exhaust is used to calculate the cylinder reaction efficiency. In this case, sampling error concerns are alleviated because there is no stratification. The only gas entering the exhaust manifold is the post combustion gas from the cylinder, presumably well mixed. Regardless of the exhaust pressure, the composition of the gas entering the sample tap is constant. The exhaust was sampled as close to the port as possible (3.3 cm) to avoid errors due to exhaust reaction. The results from the cylinder reaction efficiency tests are plotted in Figures 5.3 to 5.5. Equation 2.8 was used to calculate cylinder reaction efficiencies. The plots show the cylinder reaction efficiency dependency on load at two different speeds and on speed at 108 N-m. In general the measured efficiencies for oxygen were slightly lower than those measured by Huber[9] (98.5 to 99.5%).

At 1500 rpm, the anticipated effects of load (Figure 5.3) were seen with oxygen and to a lesser degree with monomethylamine. That is, cylinder temperatures in general increase with load, so the cylinder reaction efficiency was expected to be higher at larger loads. It is unclear why the drop in cylinder reaction efficiency in moving from 163 to

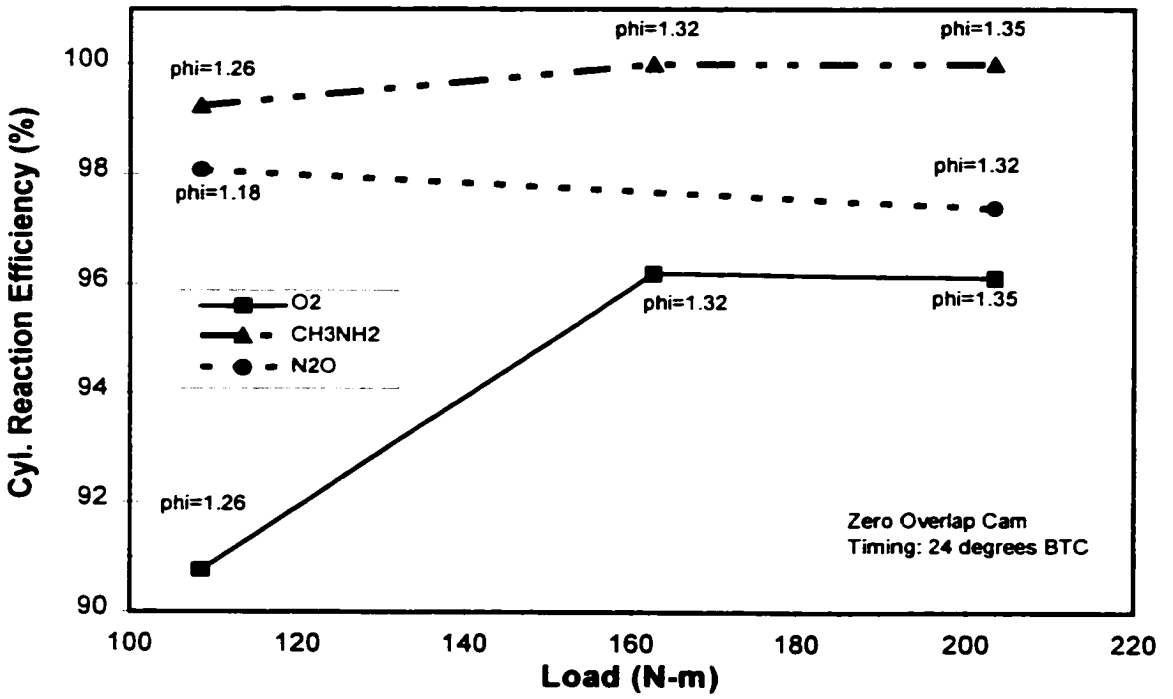

Figure 5.3 Cylinder Reaction Efficiency vs. Load at 1500 rpm.

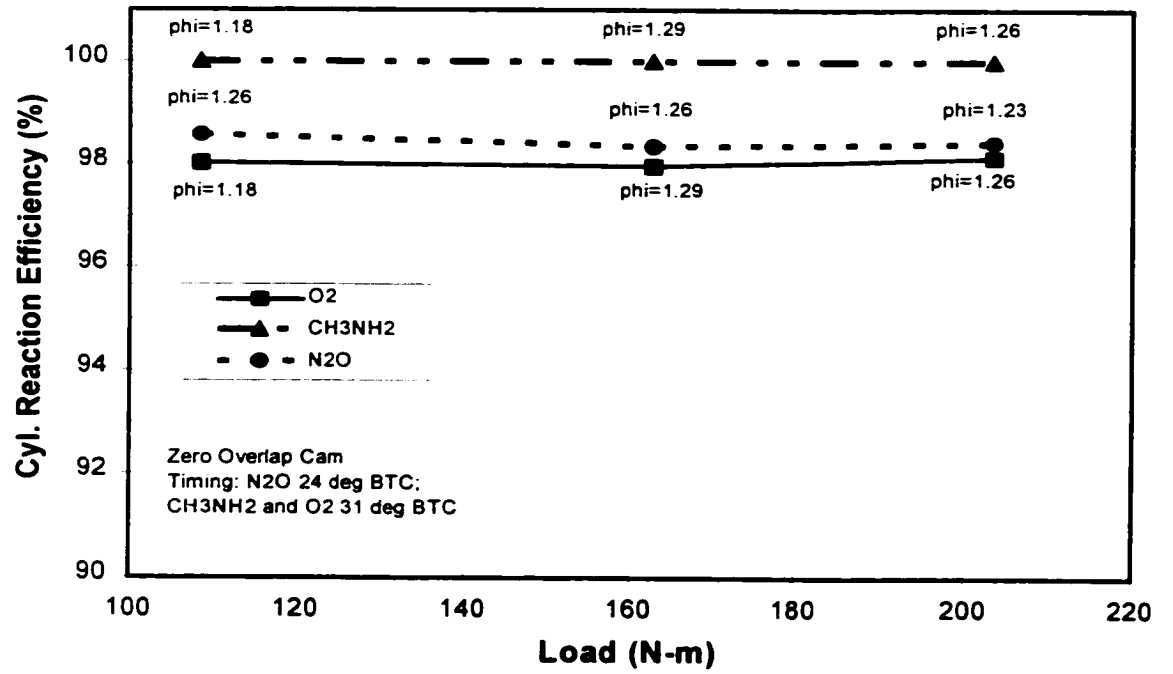

Figure 5.4 Cylinder Reaction Efficiency vs. Load at 3000 rpm.

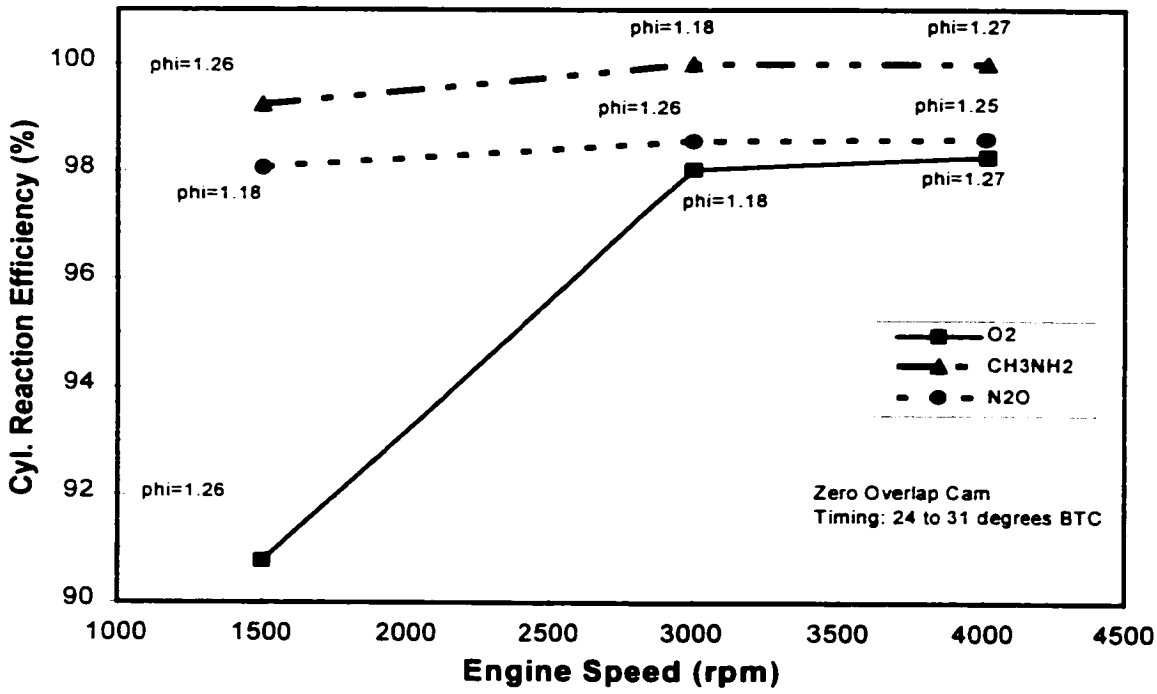

Figure 5.5 Cylinder Reaction Efficiency vs. Speed at 108 N-m.

108 N-m is so large for oxygen; however, examination of emissions and cylinder pressure statistics indicate that the 108 N-m O_2 data point is valid. The nitrous oxide data show a slight decrease in efficiency with an increase in load. One possible explanation is that the increase in load was accompanied by an increase in equivalence ratio, which by itself decreases in-cylinder temperatures. However, it is unlikely that the drop in temperature due to the increase in equivalence ratio would offset the increase in temperature associated with the load increase. The equivalence ratios were inconsistent through much of the testing. This was primarily due to difficulties in controlling A/F ratio in a carbureted engine at different operating conditions. At 3000 rpm (Figure 5.4), the cylinder reaction efficiency appears to be nearly independent of load. This is

counterintuitive, based on the cylinder temperature argument made above. One possible explanation is that the tracer kinetics in the cylinder are not changing under these operating conditions. Because of the stiff nature of tracer chemical kinetic differential equations, observable changes are only present in a narrow temperature range, above which the tracer is completely destroyed and below which the tracer is stable. Under these operating conditions, the tracer gas in the bulk charge could be getting completely consumed when the flame propagates across the cylinder. Perhaps the mechanisms by which the tracer is escaping combustion temperatures are related to the THC mechanisms discussed earlier, namely crevice volumes, organic deposit adsorption/desorption, wall quenching, quenching from local regions in mixture being too rich or too lean (oxygen only), and exhaust valve leakage. In comparison to the tracer cylinder reaction efficiencies, typical fuel combustion efficiencies were around 99% for stoichiometric conditions. The potential relationship of tracer gas cylinder reaction efficiency to THC mechanisms suggests that tracer cylinder reaction efficiency may be dependent on combustion chamber design.

5.3.2 Exhaust reaction. The test results for the exhaust reaction testing are plotted in Figures 5.6 and 5.7. The hardware configuration is described above (Figure 5.2). Tracer remaining in percent is on the y-axis and residence time in exhaust is on the x-axis. The sample tap temperature is plotted on the second y-axis. The tracer remaining is calculated by taking one minus the exhaust destruction fraction (Equation 2.10), relative to exhaust sample tap#1. The residence time is calculated from the average gas velocities and the

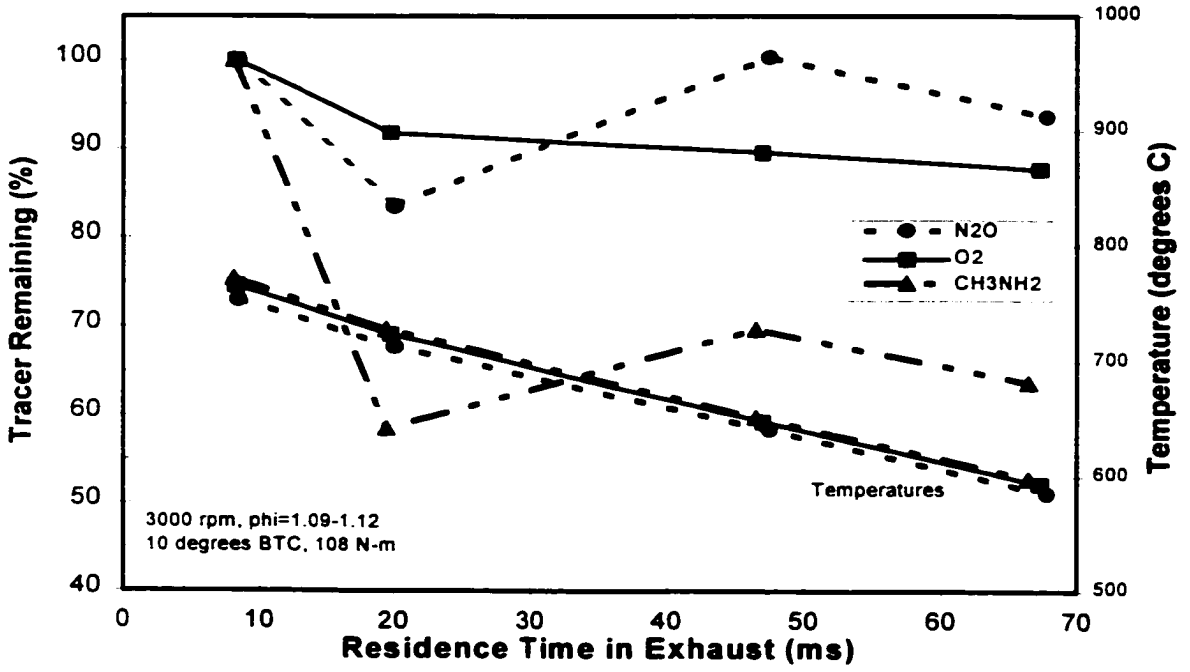

Figure 5.6 Exhaust Reaction with an Engine Load of 108 N-m.

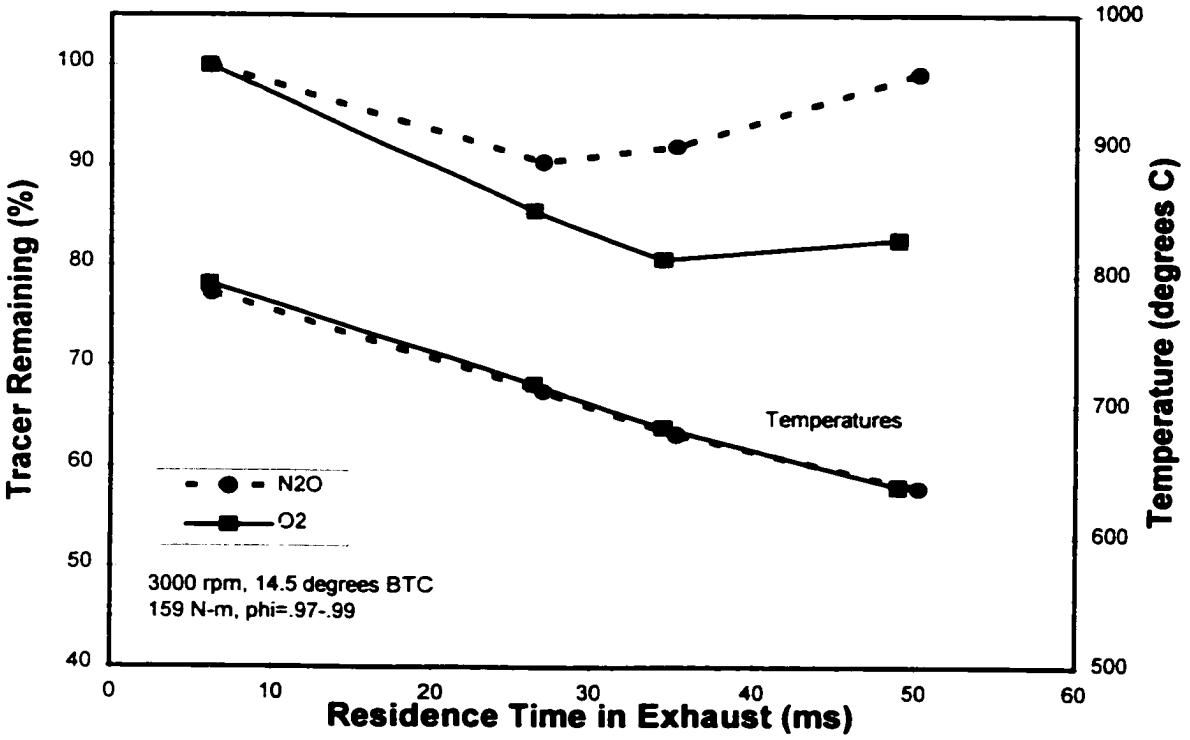

Figure 5.7 Exhaust Reaction with an Engine Load of 159 N-m.

distance down the exhaust pipe. The test data presented were taken with two layers of fiberglass header insulation wrapped around the exhaust pipe in an attempt to decrease the temperature drop down the pipe. The temperature drop was reduced to less than 20% from 50% without insulation. Initial exhaust reaction testing (not presented) was performed by injecting approximately 3000 ppm of tracer into the intake and looking at the tracer concentrations in the exhaust from a combination of short-circuiting and cylinder reaction inefficiency. The problem with this technique was that the exhaust concentrations of tracer were small and the stratification of combustion products and short-circuited gas was present. For monomethylamine there was only 6 ppm measured at the first sample tap and no monomethylamine was detected at the second tap.

The exhaust reaction test data presented are from tests carried out by injecting tracer directly into the exhaust system just downstream of the manifold. This eliminates the problems of the previous technique, but the mixing of the tracer and exhaust flow now becomes important. There are several differences between the test data presented in Figures 5.6 and 5.7. In the second test (Figure 5.7) the location of sample tap #2 was moved further downstream, away from a 90 degree bend just upstream of the original location. Monomethylamine was not evaluated in the second test because it was evident from the first test (Figure 5.6) that the stability in the exhaust was poor. Finally the engine operating conditions, given on the plots, are different.

In Figure 5.6, monomethylamine appears to still be reacting at the last sample tap where the temperature is about 630°C. Although this does not determine the maximum permissible exhaust temperature, it is consistent with Schweitzer's[6] conclusion that the

exhaust temperature should be below 425°C when using monomethylamine. At the exhaust temperatures tested, the exhaust reaction is at least 35% for monomethylamine. An important point about the data for the exhaust reaction tests is that the percent remaining is relative to sample tap#1. The exhaust reaction is likely to be higher because the reaction from the tracer injection point to tap#1 is not taken into account. When the exhaust temperature is around 750°C the data indicate that the monomethylamine reaction rate is large, so the reaction between the tracer injection point and the first sample tap is likely to be significant. Oxygen, too, has a high reaction rate at maximum exhaust temperatures; therefore, its exhaust reaction is probably higher than measured. The sampling errors which have been discussed are most apparent near the port. Ideally the sampling should be performed as far down stream as possible to allow the gases to mix thoroughly and for the pressure pulsations to dissipate. Sampling after all cylinders have come together would minimize error due to pressure pulsations and exhaust stratification, although this technique would only provide an overall engine average short-circuiting measurement. If there is significant exhaust reaction then a trade-off must be made between the tracer exhaust reaction and the proximity of the sample tap to the exhaust port.

The measured exhaust reaction of nitrous oxide appears to be the lowest, though the sampling effects seemed to affect nitrous oxide the most. The average mole fraction of nitrous oxide measured at the sample taps fluctuated up and down with the distance down the exhaust pipe. It is extremely improbable that nitrous oxide is being created in the exhaust. To illustrate this point an equilibrium calculation was carried out at the

maximum and the minimum exhaust temperatures. The equilibrium relation for the nitrous oxide dissociation reaction discussed in Chapter 3 is

$$X_{N_2O} = \frac{X_{N_2}{}^2 X_{O_2}\left(P/P^0\right)}{e^{\frac{-\Delta G^0}{RT}}}$$

where the X's are mole fractions, P is the exhaust pressure, P^0 is a reference pressure (1 atm), and ΔG^0 is the change in Gibbs free energy for the reaction. Typical exhaust mole fractions for oxygen and nitrogen of .003 and .71, respectively, were used. The pressure was assumed to be one atmosphere. The change in Gibbs free energy was calculated using data from the JANAF tables. The nitrous oxide mole fraction was evaluated at 700 and 1100 Kelvin. The results were that the amount of nitrous oxide present at equilibrium for these conditions is negligible (0.14 parts per trillion for 700 K and 25 parts per trillion for 1100 K). Therefore, thermodynamically the formation of nitrous oxide in the exhaust is not favored.

As improvements were made to the sample system after initial testing, the fluctuations in nitrous oxide concentration were reduced but not eliminated. These improvements included reducing pressure fluctuations, improving sample probe design and location, and increasing concentration levels. Referring to Figure 5.7, the nitrous oxide level dips down to about 90% at sample tap#2 and then comes back up to 99.2% at the end of the pipe. Based on the above equilibrium argument, the dip in nitrous oxide is most likely from an unresolved sampling error. The data show the concentration at sample tap#4 returning to a value within 1% of the starting value at tap#1. The data

certainly do not indicate a large reaction error in the exhaust for nitrous oxide. It is suspected that the exhaust reaction is very low, within 1%.

5.3.3 Measurement of Short-Circuited Fraction. Measurements were made of the short-circuited fraction after both the exhaust reaction and cylinder reaction efficiency were characterized. The valve overlap on the engine that was tested was not large, so a high short-circuited fraction was not expected. The valve lift profiles are shown in Figure 5.8. The short-circuited gas measurements are plotted in Figures 5.9 and 5.10. The measurements were made with the buffer volume and mixer in place, at the sample tap furthest down the exhaust pipe. Nitrous oxide was utilized since it was the most stable in the exhaust and had a high cylinder reaction efficiency that did not vary significantly with engine operating conditions. The short-circuited fractions expressed as percentages in Figure 5.9 were calculated using Equations 2.1 and 2.6. Equation 2.6 was derived assuming that there is 100% consumption in the cylinder, no misfires, and no reaction error in the exhaust. The short-circuited fractions in Figure 5.10 were calculated using Equation 2.13, which takes into account non-ideal tracer effects. Average values of $\eta_{cr} = .984$ and $\varepsilon_r = .036$ were used and the misfire fraction was assumed to be zero. Misfires are typically not significant for rich or stoichiometric engine operation. The exhaust reaction is very conservative. The cylinder reaction efficiency did not vary much with engine operating parameters for nitrous oxide so using average values introduces very little uncertainty. The equivalence ratios were slightly less than one, but since the

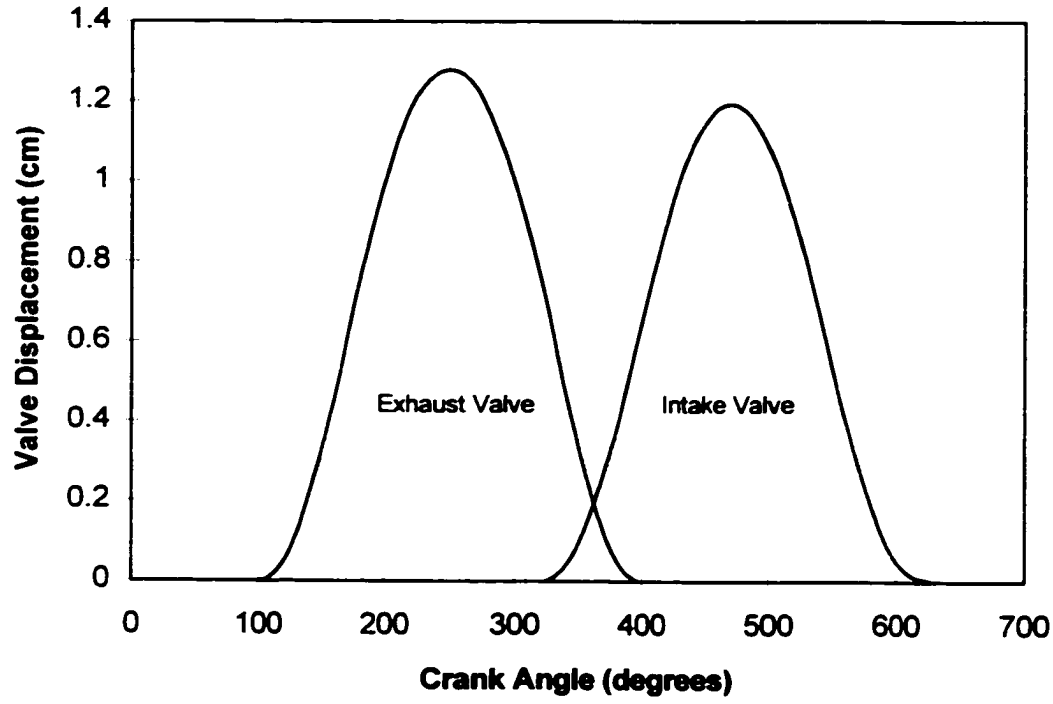

Figure 5.8 Valve Lift Profiles.

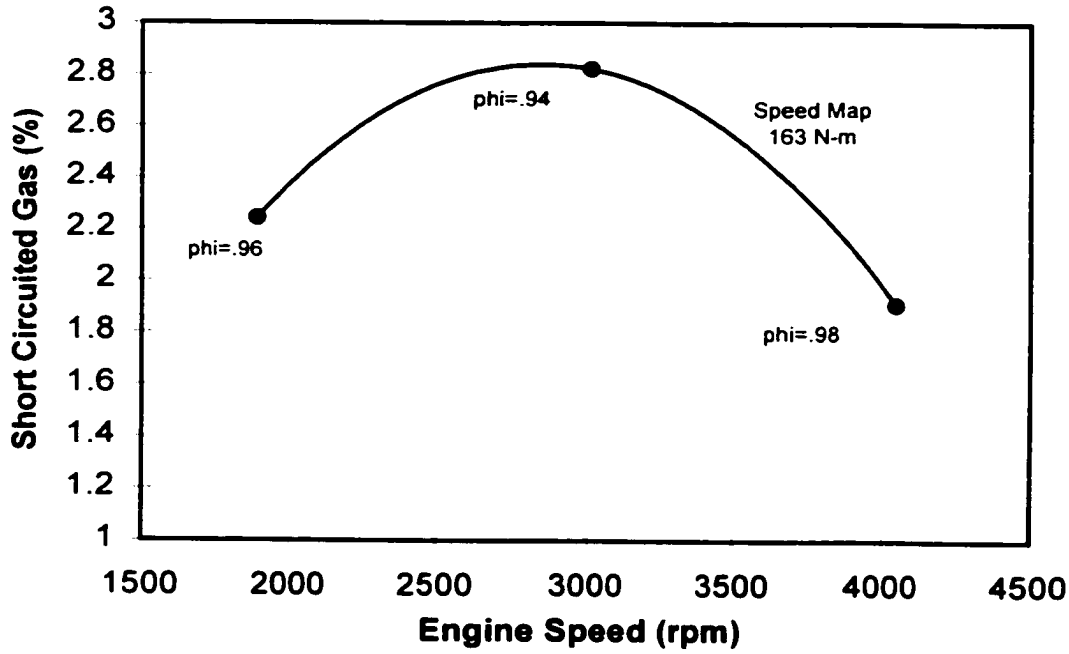

Figure 5.9 Short-Circuited Gas Measurements Using N_2O Without Non-Ideal Tracer Corrections.

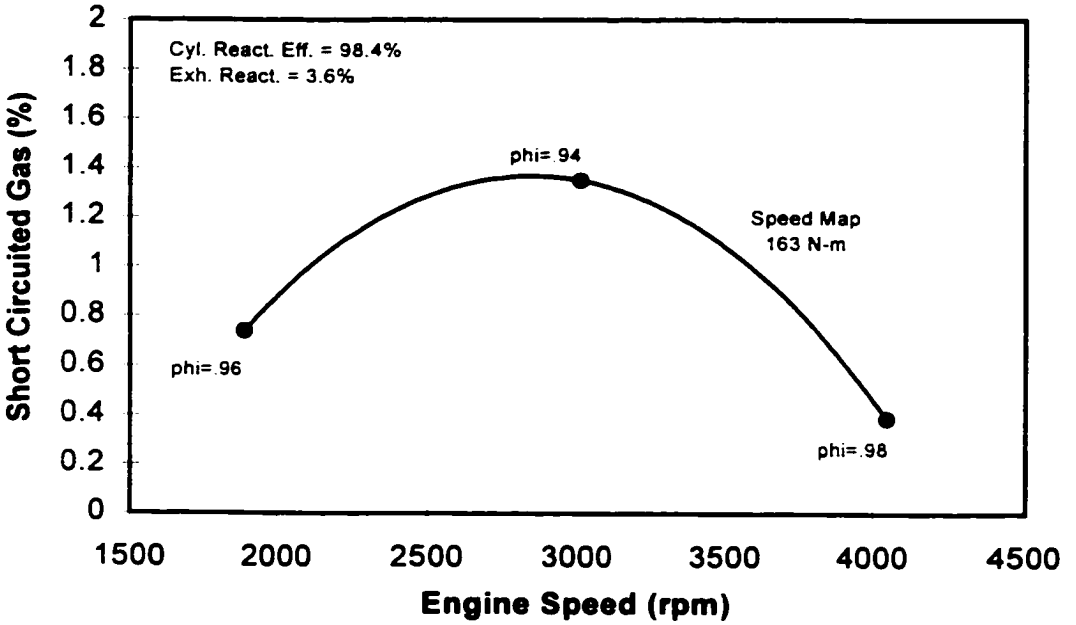

Figure 5.10 Short-Circuited Gas Measurements Using N_2O, Corrected for Non-Ideal Tracer Effects.

oxygen method was not being used it did not matter. The trapping efficiency can be calculated simply by taking one minus the short-circuited fraction (Equation 2.1). For the conditions tested it averaged a little better than 99%.

The quantity of short-circuited gas as expected was low, around one percent. The amount of short-circuited gas depends heavily on cam and exhaust system design (exhaust tuning). The pressure wave from exhaust valve opening travels to the end of the pipe at the local speed of sound and returns as a rarefaction wave. Exhaust systems are normally sized so that the rarefaction wave arrives at the exhaust manifold during valve overlap and draws more of the cylinder contents into the exhaust, enhancing scavenging, while at the same time pulling intake air into the cylinder to initiate filling[40]. It is at this

time when a portion of the intake charge can pass directly into the exhaust system; therefore, the speed at which the maximum short-circuiting occurs will most likely correspond to that for optimal scavenging. The scavenging characteristics of the test engine are not expected to be reflective of the original engine design because of the drastic off-design modifications to the exhaust system. Based on Figure 5.10 it appears that the instrumented header pipe is tuned for maximum scavenging at around 2800 rpm at 163 N-m. Bear in mind that this is based on a curve fitted to three data points. More data is needed to be able to measure the tuned speed more accurately. A tuning phenomenon, similar to that which takes place in the exhaust, occurs in the intake manifold. The measurement of the optimal scavenging speed with the tracer gas method includes both effects.

The speed for optimal scavenging can be estimated by looking at tuning in the exhaust only. In this calculation the exhaust pressure and rarefaction waves were assumed to propagate at the local speed of sound. The speed of sound is dependent on temperature, composition, and ratio of specific heats, all of which change as the wave propagates down the pipe. The composition does not change significantly, yet temperature and the ratio of specific heats do. These variations were taken into account. The end of the pipe was assumed to be at the point where the 4 cm instrumented header pipe joins the 8 cm pipe containing the gas from the other 7 cylinders. Pressure wave dissipation and interactions with pressure waves from other cylinders were neglected. With these assumptions, the speed for optimal scavenging was calculated to be 3180 rpm. The gas dynamics in the exhaust are complex; the accuracy of this calculation is not expected to be better than

±25%. When compared to the measured value of 2800 rpm the calculated value of 3180 rpm is within the expected accuracy and, thus, supports the test data.

The procedure used to measure the short-circuited fraction had inherent difficulties with exhaust sampling. These sampling difficulties were not fully resolved. The reason for sampling individual cylinder header pipes was to allow for future cylinder to cylinder resolution. For future applications, some modifications need to be made to the current procedure to eliminate the difficulties with exhaust sampling. These modifications are

- For quantitative measurement of trapping efficiency the exhaust sampling should be performed after the exhaust from all cylinders has been mixed. Sampling the exhaust near the port gives rise to significant sampling error.
- To resolve relative differences in trapping efficiency between individual cylinders, the exhaust can be sampled near the port at equal distances away for each cylinder. Differences in exhaust tuning as well as faulty valves can resulting in relative differences between cylinders.

5.3.4 Effect of Equivalence Ratio Variations. The test results in this work are from a carbureted engine. It is difficult to control equivalence ratio on carbureted engines when operating parameters vary significantly. The equivalence ratios are indicated on the graphs presented. The effects of this on the tracer gas testing are not known quantitatively, but are expected to be small overall. The equivalence ratio throughout testing varied from 0.94 to 1.35 (i.e. always near stoichiometric or rich). In the cylinder

nitrous oxide and monomethylamine are consumed by dissociation, making temperature the most important parameter. The relative effect that equivalence ratio has on in-cylinder temperatures can be seen by calculating the adiabatic flame temperature for various equivalence ratios. The constant volume adiabatic flame temperature changes by about 6% when equivalence ratio varies from 0.94 to 1.35. The peak in constant volume adiabatic flame temperature occurs at about 3020 K at an equivalence ratio near 1.2. A 6% change in temperature at near adiabatic flame temperatures is probably inconsequential to tracer dissociation in the bulk charge; nevertheless, more data is needed to be certain. The cylinder reaction efficiency for oxygen is more likely to be sensitive to equivalence ratio, although the equivalence ratios for these test results were always rich. The equivalence ratio throughout oxygen cylinder reaction efficiency testing varied from 1.18 to 1.35, so there was always an abundance of fuel for oxygen consumption.

Two exhaust reaction tests are presented, one at approximately phi=1.1 and the other at about phi=0.98. Monomethylamine was not tested at phi=0.98 and was excluded from final short-circuited gas tests due to its exhaust instability. The equivalence ratio is not likely to affect nitrous oxide consumption in the exhaust because the primary mechanism is dissociation rather than oxidation. However, the exhaust reaction of oxygen could be affected by equivalence ratio variations. The primary overall reaction for oxygen exhaust consumption is with unburned hydrocarbons (THC). For equivalence ratios of 1.1 and 0.98 the oxygen and THC concentrations were O_2=1600 ppm, THC=1870 ppm and O_2=2040 ppm, THC=1690 ppm, respectively. Oxygen destruction goes roughly as the product of O_2 and THC if the order of reaction with respect to each is assumed to be one.

Therefore, these changes tend to offset each other to a degree with regard to oxygen destruction. As equivalence ratio gets richer from 1.1 initial exhaust oxygen concentration does not change very much while THC emissions increase significantly. In this case the reaction rate of oxygen can be expected to increase significantly.

CHAPTER 6

TWO STROKE ENGINE TESTING

The natural gas industry uses over 8,000 large bore (bore diameter ≥ 14 inches), slow speed (speed < 300 rpm) natural gas engines for compression and power generation in the United States[41]. These engines typically operate at high utilization factors, and produce more than 110 billion kW-hours of motive power annually. The annual fuel consumption is more than 28 trillion standard liters of natural gas and they produce approximately 10% of the total NO_x emissions in the United States from stationary sources. As extensive as the large bore natural gas stationary engine population is, there is no standardized technique for measuring the trapped A/F ratio. It was established in Chapter 1 that the trapped A/F ratio has a dramatic effect on emissions. The measurement of trapping efficiency with the tracer gas method can be used directly to calculate trapped A/F ratio. The test results presented and the test procedure outlined show that the tracer gas method is an accurate, field adaptable technique for evaluating trapped A/F ratio.

In this chapter the tracer gas method is implemented on a stationary 2-stroke cycle, 4-cylinder, large bore natural gas engine. The engine is manufactured by Cooper-Bessemer, model number GMV-4TF, shown in Figure 1. It is representative of the large bore natural gas stationary engine fleet currently in use by the natural gas

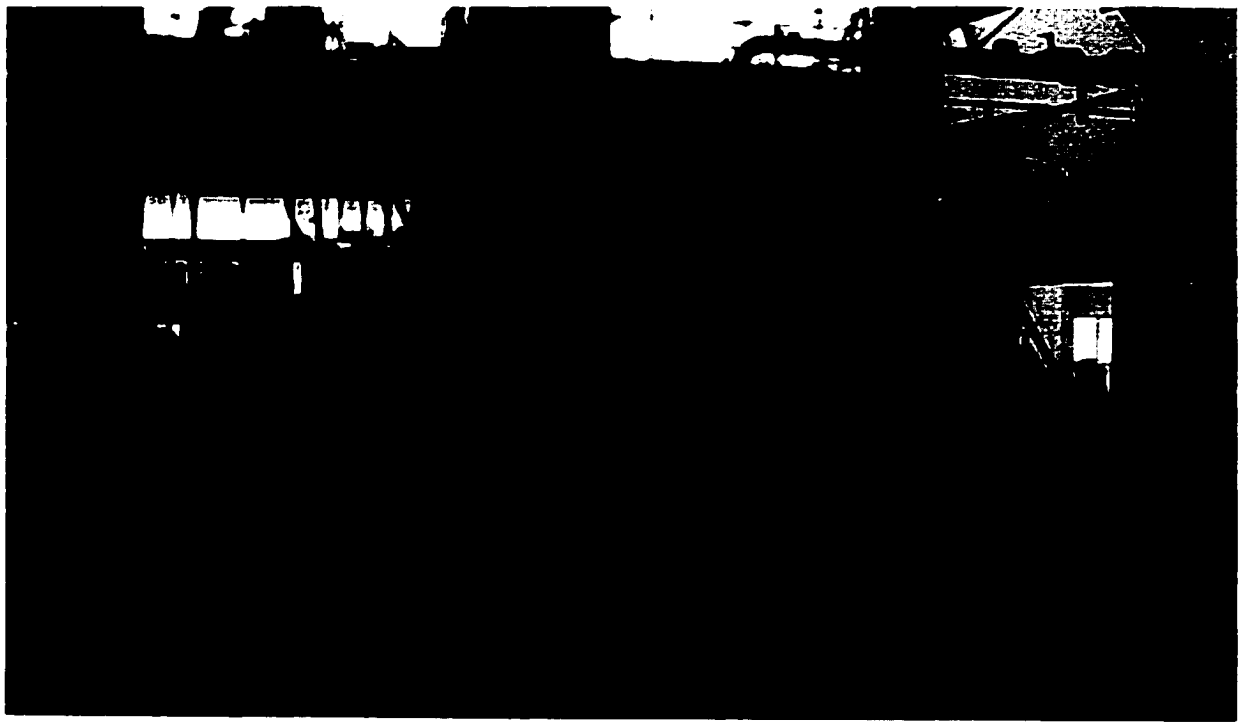

Figure 6.1 The Cooper-Bessemer GMV-4TF Large Bore Natural Gas 2-Stroke Cycle Engine.

industry. Trapping efficiency measurements are carried out with the tracer gas method at various engine operating conditions. These measurements are compared with the results from other techniques, both experimental and analytical. Non-ideal tracer effects are evaluated through the use of in-cylinder and exhaust port sampling and sampling at various locations along the exhaust pipe. Engine operating conditions are altered through variations in boost pressure, speed, back pressure, and intake port restriction.

6.1 Trapped A/F Ratio

If the trapping efficiency can be measured accurately using the tracer gas method, the trapped A/F ratio can be evaluated based on the overall A/F ratio and the measured trapping efficiency (Equation 1.3). The overall A/F ratio is typically calculated in large bore 2-stroke cycle engines using an exhaust composition analysis technique, described by Fanick *et al.*[42], commonly referred to as the carbon balance method. Evaluating the overall A/F ratio from independent measurements of airflow and fuel flow is another option, and may seem like the most direct method. However, airflow measurements at flowrates characteristic of large bore engines are difficult to carry out and error prone[43]. Since modern engine testing is seldom performed without emissions measurements, exhaust gas analysis has emerged as the standard method for overall A/F ratio evaluation in this engine class. Because the overall A/F ratio calculation is key to obtaining the trapped A/F ratio from trapping efficiency, the carbon balance method is discussed in detail.

The carbon balance method assumes that all the carbon in the measured exhaust constituents, CO, CO_2, and THC, with the exception of a small amount in the form of CO_2 in the intake air, comes from the fuel. The following combustion reaction for lean A/F ratios is assumed

$$1[(1\text{-}j\text{-}k\text{-}l)CxHy + jCO2 + kN2 + lO2] + a[O2 + 3.76N2 + bH2O] \rightarrow$$

$$cH2O + dCO2 + eCO + fNOr + gO2 + hN2 + iCHz.$$

The stoichiometric coefficients *j*, *k*, and *l* and the fuel composition coefficients *x* and *y* are evaluated from fuel composition analysis. The test apparatus for the GMV-4TF is equipped with humidity control. The coefficient *b* in this case is calculated directly from a relative humidity measurement in the intake air duct just upstream of the engine intake manifold. The coefficient *r* is based on the composition of NO_X (i.e. the relative percentages of NO, NO_2, and N_2O_5). Based on FTIR measurements at typical engine operating conditions, a value of 1.1 is assumed for *r*. The composition of THC emissions, shown as CH_z in the combustion reaction above, is assumed to be the same as the fuel. Hence, the coefficient *z* is simply equal to the ratio *y*/*x*. The remaining eight unknowns *a*, *c*, *d*, *e*, *f*, *g*, *h*, and *i* are evaluated from four dry emission measurements, CO, CO_2, NO_X, and THC, and four atom balance equations for carbon, hydrogen, oxygen, and nitrogen. The overall A/F ratio is calculated from the stoichiometric coefficient *a* according to the equation

$$\left(A/F\right)_{ov} = \frac{a}{SG_f} \tag{6.1}$$

where SG_f is the specific gravity of the fuel. More details of the analysis can be seen in the computer code given in Appendix D. Two versions of the program are provided, one for dry emissions data (from a 5-Gas emissions bench) and another for wet emissions data (from an FTIR). The computer code is written in Engineering Equation Solver (EES).

This development of the carbon balance method appears quite different then that of Fanick *et al.*, though the basic assumptions are the same. The method is heavily dependent on an accurate CO_2 measurement, because most of the carbon present in the emission constituents exists as CO_2. High CO_2 and low CO in the exhaust is characteristic

of engines that burn lean A/F ratios, which is the case for most large bore natural gas engines. Even the sub-class of large bore natural gas engines called "rich-burn" engines, operate with equivalence ratios near stoichiometric. Thus, they operate at rich equivalence ratios in comparison to other large bore natural gas engines, not in the general sense of the word.

6.2 Test Plan

The test plan is designed to evaluate the tracer gas method as a means for measuring trapping efficiency, and subsequently determining scavenging efficiency and the trapped A/F ratio. The trapped A/F ratio in this work is normally expressed as the trapped equivalence ratio, or simply equivalence ratio. The definition of trapped equivalence ratio in terms of A/F ratios was presented as Equation 1.1. Expressing the data in terms of trapped equivalence ratios rather than trapped A/F ratios makes the data applicable to different natural gas compositions and, to a certain extent, different fuels. The testing focuses on three areas, which are

(1) Quantification of non-ideal tracer effects for this application,

(2) Evaluation of trapped equivalence ratio with tracer gas method and comparison to the perfect mixing model and in-cylinder and port sampling techniques, and

(3) Tracer gas measurements for engine parameter variations.

The non-ideal tracer effects are discussed in detail in Chapter 2, all of which are addressed in this investigation. Evaluations of the tracer exhaust reaction and cylinder

reaction efficiency are carried out differently than in the 4-stroke cycle engine testing. Since the 2-stroke cycle engine uses intake and exhaust ports rather than valves, the use of a zero overlap cam to determine cylinder reaction efficiency is not possible. Additionally, the exhaust reaction can not be evaluated by taking samples along the exhaust pipe. The residence time in the exhaust manifold is so large (see Figure 4.6) that the exhaust gases cool considerably by the time they enter the exhaust pipe. Therefore, any tracer exhaust reaction that takes place is most likely to occur in the exhaust manifold. The GMV-4TF is not configured for exhaust sampling from the manifold. Tracer exhaust reaction and cylinder reaction efficiency for the GMV-4TF are determined through a combination of in-cylinder, exhaust port, and stack sampling, which is discussed in more detail later. In the 4-stroke cycle engine testing in Chapter 5 the correction for engine misfire was not significant. This was because the engine was operated with rich trapped equivalence ratios. It is not uncommon for large bore natural gas engines to operate near the lean limit, where the misfire fraction can be significant. Misfire fraction is resolved from engine cylinder pressure traces as discussed in Chapter 2. and is accounted for during data reduction.

Data are taken via three data acquisition computers. One computer is dedicated to the FTIR. It contains infrared absorption spectra for the various species being detected, and uses that information in combination with the infrared absorption spectrum of the sample gas to determine gas composition. The second computer records data from the 5-Gas Rosemount Emission Bench, combustion analysis system, tachometer, dynamometer, supercharger, humidity control system, and numerous thermocouples and pressure transducers. The combustion analysis system is produced by DSP Technology,

Inc., Version ACAP3.0e. It consists primarily of piezoelectric pressure transducers in each cylinder, a high speed data acquisition system (including the third data acquisition computer), and analysis software. For each cylinder it provides, among other things, pressure vs. crank angle profiles, heat release information, and location and magnitude of peak pressure. The general procedure for taking data is as follows: (1) allow engine to stabilize by observing time-based trends of engine emissions, speed, load, intake manifold pressure (boost), block and exhaust temperatures, and amplitude and location of peak pressure, (2) begin injecting tracer and wait for the concentration to stabilize, and (3) acquire data with data acquisition computers. The FTIR computer takes data for 3 minutes and records average values in a data file every 30 seconds. The data acquisition computer that records data from the 5-gas emissions bench scans for 5.5 minutes, and writes the average, minimum, and maximum values to a data file.

6.3 Delivery Ratio

The quantity that affects scavenging the most is the delivery ratio. For example, in the perfect mixing model (Equations 2.18 and 2.19) the trapping and scavenging efficiencies depend solely on the delivery ratio. Recall that the delivery ratio is defined as the delivered mass per cycle over a reference mass. The reference mass is defined as the trapped cylinder mass at exhaust port closure. In terms of measured quantities, the definition becomes

$$\Lambda = \frac{dm_{del}/dt}{V_{pc}\rho_{pc}N_{cyl}\omega} \tag{6.2}$$

where

dm_{del}/dt = measured air mass flow through engine
V_{pc} = cylinder volume at exhaust port closing
ρ_{pc} = calculated charge density at exhaust port closing using exhaust manifold pressure and intake manifold temperature
N_{cyl} = number of cylinders
ω = engine speed in revolutions per second.

Delivery ratio is proportional to the gas flowrate through the engine, and it is inversely proportional to the charge density at port closure and the engine speed. Parameters that can significantly change delivery ratio are the speed, intake manifold, and exhaust manifold pressure (exhaust back pressure).

To calculate the charge density in Equation 6.2 the ideal gas law is applied, which requires the cylinder volume and pressure, temperature, and molecular weight of the charge at port closure. Although the intake manifold pressure is the parameter that is typically controlled during a boost map, it is the pressure in the cylinder just after port closure that affects delivery ratio and engine performance most directly. Since the exhaust ports close after the intake ports, the exhaust manifold pressure gives the best approximation of cylinder pressure at port closure[44]. Although intake manifold pressure is the parameter controlled during a boost map, the exhaust manifold pressure is used in the calculation of delivery ratio. The charge temperature at port closure is taken as the intake manifold temperature. The intake charge molecular weight is assumed to be that of air for delivery ratio calculations.

The effect of speed on delivery ratio is fairly intuitive. Speed directly affects the reference mass flow in the denominator of Equation 6.2, with minimal influence on the

average mass flow of air through the engine for a constant intake manifold pressure. As speed changes, the pressure drop across the engine remains relatively constant because the effective area of the ports does not change. Thus, at constant intake manifold pressure the delivery ratio decreases with increasing speed.

The effect of engine boost and exhaust back pressure on delivery ratio is more complex than the effect of speed. A brief description of how engine boost and exhaust back pressure are controlled is warranted. Exhaust back pressure is typically about 8.5 kPa lower than the intake air pressure in the GMV-4TF engine, which is the pressure drop through the engine. The total pressure drop through the engine and exhaust system combined is about 25 kPa at nominal engine operating conditions. The exhaust back pressure valve is responsible for the 16.5 kPa of additional pressure drop. An electric circuit analogy, shown in Figure 6.2, is a simple way to visualize the system. The exhaust back pressure valve is a 25 cm butterfly valve located several meters downstream of the exhaust manifold. The function of the back pressure valve is to simulate the pressure drop across a turbocharger exhaust turbine. To obtain precise control over engine boost the intake air is pressurized with a supercharger, driven independently by an electric motor. Turbochargers are typical in field engines, which necessitates the simulation of turbocharger back pressure via the exhaust back pressure valve. The pressures shown in Figure 6.2 from left to right are for the intake manifold, exhaust manifold, and atmosphere. The engine and exhaust back pressure valve are shown as flow resistors. As the valve resistance is reduced, or the valve is opened further, the total resistance across the system decreases. Assuming constant intake manifold pressure, the flow through the engine increases and results in a corresponding increase in delivery ratio. The back

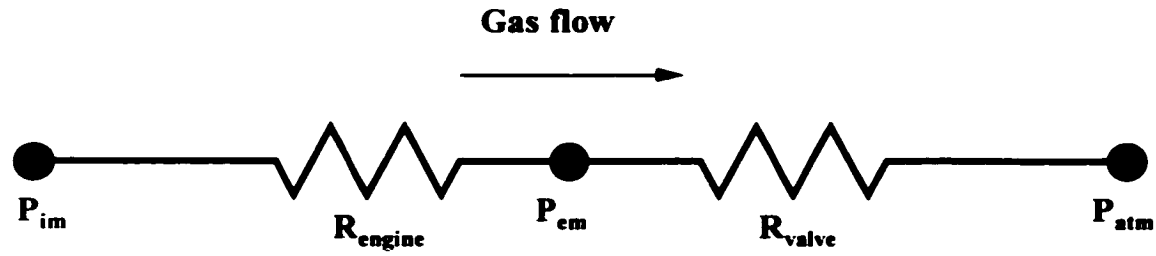

Figure 6.2 Electric Circuit Analogy of Gas Flow Through Engine

pressure valve is electronically actuated, and the valve position is the main parameter in the control system that controls the pressure drop across the engine. Typically the pressure drop across the engine is maintained at 8.5 kPa at various engine operating conditions by adjusting the exhaust back pressure valve setting. For higher boosts the back pressure valve closes to create more resistance through the valve to maintain constant engine pressure drop. For lower boost the back pressure valve opens to reduce the resistance through the valve to maintain constant engine pressure drop. This is similar to the behavior of exhaust turbines in turbochargers. More details on the turbocharger simulation package are given in a CSU Masters Thesis by Schoonover[45].

When intake manifold pressure is increased, the driving pressure differential across the engine and exhaust system is increased. Consequently the mass flow of air through the engine increases, which tends to increase delivery ratio. At the same time the exhaust manifold pressure increases, while the pressure drop across the engine is maintained constant. The increase in exhaust manifold pressure results in a larger reference mass flow, which tends to decrease delivery ratio. Therefore, two competing effects with regard to delivery ratio exist. A simple relationship between intake manifold

pressure and delivery ratio can not be determined without further analysis and/or engine testing.

When exhaust manifold pressure is reduced by opening the back pressure valve further, the total flow resistance across the engine and exhaust system decreases. For constant intake manifold pressure this increases the mass flow of air through the engine, thereby increasing delivery ratio. Simultaneously the reference mass decreases due to decreases in exhaust manifold pressure, which tends to increase delivery ratio. These two effects combine and have a dramatic effect on delivery ratio, and a consequent large impact on scavenging. Though this parametric variation results in an interesting test, it is not representative of turbocharger operation. In an engine equipped with a turbocharger, a drop in exhaust manifold pressure would be accompanied by a drop in intake manifold pressure. Varying the exhaust manifold pressure independently should be viewed as a means of validating the tracer gas method at a wider range of trapping efficiencies, and not as a scenario representative of field operation.

6.4 Test Apparatus

6.4.1 Tracer Injection System. The apparatus employed to inject tracer into the intake air of the engine is similar to that used for the 4-stroke cycle engine tests. A test schematic including the main components is shown in Figure 6.3, and some of the actual hardware is shown in Figure 6.4. The tracer gas injection system accommodates both tracers, monomethylamine and nitrous oxide. Both tracers are purchased in liquid form and the liquid vapor pressure is utilized as the source pressure for injection. Monomethylamine has a vapor pressure of about 400 kPa at room temperature and

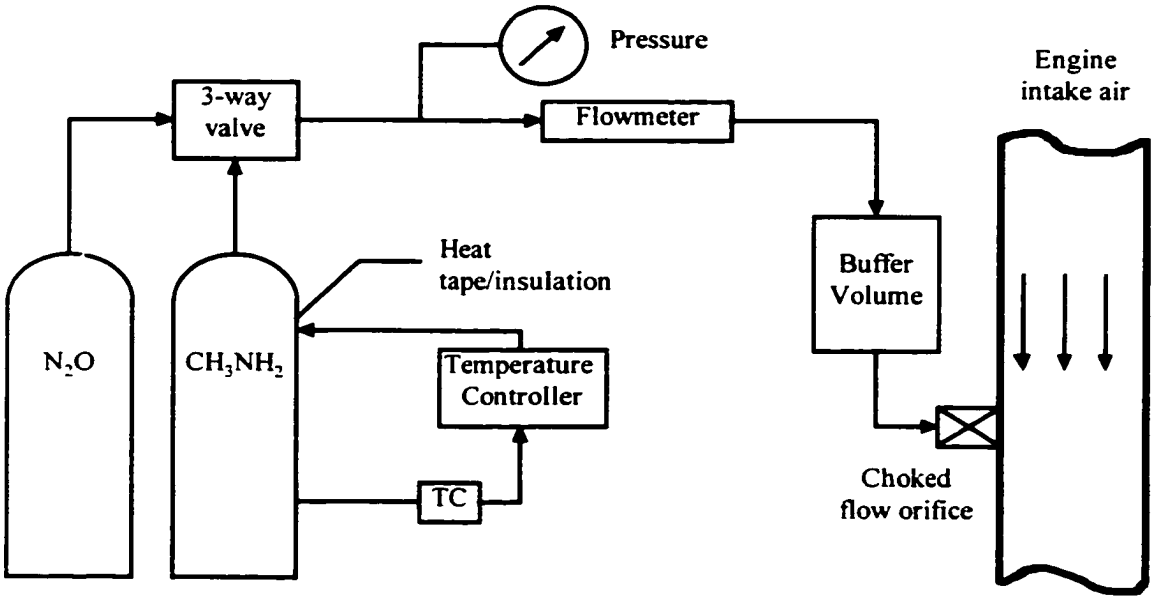

Figure 6.3 Test Schematic for 2-Stroke Cycle Engine Testing

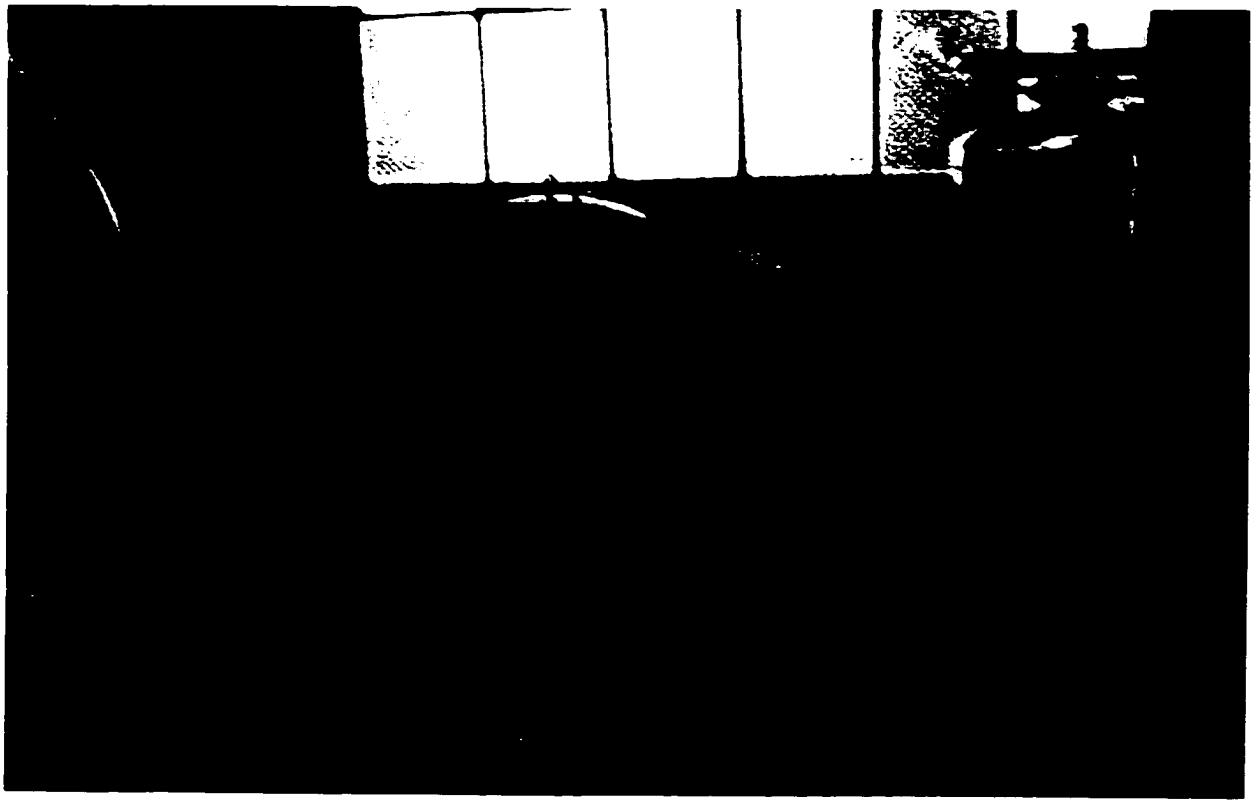

Figure 6.4 Tracer Gas Injection System for the GMV-4TF.

nitrous oxide has a vapor pressure of about 5600 kPa at room temperature. The monomethylamine bottle is wrapped with heat tape and insulation and instrumented with a thermocouple and a temperature controller. This provides the ability to control monomethylamine source pressure by controlling the temperature of the bottle. The nitrous oxide vapor pressure at room temperature is high enough so that temperature control is not necessary. The test set-up includes a three-way ball valve to switch between tracers. The tracer regulators and injection lines are heated to prevent tracer condensation due to throttling temperature drops through the regulator or other restrictions. Both gases can be corrosive, and liquid condensation accelerates the corrosion process. The tracer injection pressure and flowrate are measured, primarily to make it easier to duplicate data points. The tracer intake mole fraction is recorded with the FTIR. A buffer volume is installed near the tracer injection orifice to attenuate any pressure fluctuations in the system. The tracer enters the intake air stream via a choked flow orifice. When the flow is choked, the mass flow rate depends only on upstream stagnation pressure and temperature. The tracer injection orifice is sized so that the jet centerline velocity is reduced to a value approximately equal to the average intake air velocity before it reaches the opposite side of the intake air pipe. This analysis is performed using axisymmetric turbulent jet equations developed in Turns.[31] For the 20 cm I.D. intake air pipe, this results in an orifice diameter of about 1.6 mm. The tracer injection orifice is located 10 to 12 meters upstream of the intake manifold. A characteristic mixing time is evaluated to ensure that the distance between the location of the tracer injection orifice and the intake manifold is sufficient for uniform mixing to occur. This analysis follows the work of Abraham *et al.*[46] Based on the characteristic mixing time and the average air velocity in

nitrous oxide has a vapor pressure of about 6000 kPa at room temperature. The monomethylamine bottle is wrapped with heat tape and insulation and instrumented with a thermocouple and a temperature controller. This provides the ability to control monomethylamine source pressure by controlling the temperature of the bottle. The nitrous oxide vapor pressure at room temperature is high enough so that temperature control is not necessary. The test set-up includes a three-way ball valve to switch between tracers. The tracer regulators and injection lines are heated to prevent tracer condensation due to throttling temperature drops through the regulator or other restrictions. Both gases can be corrosive, and liquid condensation accelerates the corrosion process. The tracer injection pressure and flowrate are measured, primarily to make it easier to duplicate data points. The tracer intake mole fraction is recorded with the FTIR. A buffer volume is installed near the tracer injection orifice to attenuate any pressure fluctuations in the system. The tracer enters the intake air stream via a choked flow orifice. When the flow is choked, the mass flow rate depends only on upstream stagnation pressure and temperature. The tracer injection orifice is sized so that the jet centerline velocity is reduced to a value approximately equal to the average intake air velocity before it reaches the opposite side of the intake air pipe. This analysis is performed using axisymmetric turbulent jet equations developed in Turns.[31] For the 20 cm I.D. intake air pipe, this results in an orifice diameter of about 1.6 mm. The tracer injection orifice is located 10 to 12 meters upstream of the intake manifold. A characteristic mixing time is evaluated to ensure that the distance between the location of the tracer injection orifice and the intake manifold is sufficient for uniform mixing to occur. This analysis follows the work of Abraham *et al.*[46] Based on the characteristic mixing time and the average air velocity in

the pipe, the tracer is well mixed in less than 1 m of pipe length. Thus, the length of pipe allotted for the tracer to mix with the intake air is more than adequate.

6.4.2 Engine Description. The characteristics of the Cooper-Bessemer GMV-4TF engine are summarized in Table 6.1. A 10-cylinder version of this engine, the GMV-10TF, is also produced and is common in the field. It has identical cylinder, port, and manifold geometry. The GMV-4TF in the CSU EECL when new was crankcase scavenged. It is now supercharged, which allows for the variation of boost pressure. The nominal ignition source is spark, although the engine accommodates other ignition sources such as multi-strike and prechamber. The nominal engine configuration is emphasized in this test program. The fuel delivery is with electronic gas admission valves that operate at an injection pressure of about 280 kPa. Again, other fuel delivery configurations are possible but the nominal configuration is the one that is tested. Nominal operating conditions are given in Table 6.2.

6.4.3 Scavenging Configuration. The classification of the scavenging configuration of the GMV-4TF is not obvious. Generally scavenging arrangements on engines are lumped into three broad categories, which are cross, loop, and uniflow scavenging. An illustration of each is shown in Figure 6.5. The GMV-4TF scavenging port configuration has been labeled as loop scavenged by the engine manufacturer, Cooper-Bessemer[47], although the design contains features of both loop and cross scavenging. The subcategory of loop scavenged configurations that it falls under is the Curtis type. Ironically the Curtis type loop scavenging configuration evolved from a cross scavenged configuration.

Model	GMV-4TF
Manufacturer	Cooper-Bessemer
Displacement	141 liters
Bore	35.6 cm
Stroke	35.6 cm
Number of Cylinders	4
Scavenging	Curtis
Air Delivery	Supercharger
Ignition	Spark
Fuel Delivery	Electronic Injection
Fuel	Natural Gas

Table 6.1 GMV-4TF Engine Characteristics

In 1920 Schnürle discovered a method by which the use of the troublesome deflector piston in cross scavenged engines could be eliminated. Instead of the single scavenging (intake) port diametrically opposed to the exhaust port, a pair of ports were located symmetrically around the exhaust port and on the same level, as shown in Figure 6.6. The scavenging flow was directed upward and away from the exhaust port. Curtis developed this idea further by adding more scavenging ports opposite the exhaust port. The configuration has been classified as loop scavenged because the flow path, at least from the "Schnürle" ports, prescribes a loop rather than flowing across the cylinder. In the GMV-4TF there are eight scavenging ports and five exhaust ports located across from each other. The exhaust port length spans the bottom 29% of the stroke

Brake Power	330 kW
Torque	10 kN-m
Brake Mean Effective Pressure	1.9 MPa
Average Peak Cylinder Pressure	3.4 MPa
Average Location of Peak Pressure	19° ATC
Engine Speed	300 rpm
Brake Specific Fuel Consumption	220 g/kW-hr
Ignition Timing	10° BTC
Overall A/F Ratio (carbon balance)	43
Air Mass Flowrate	0.86 kg/s
Fuel Mass Flowrate	0.020 kg/s
Intake Manifold Pressure	25 kPag
Exhaust Manifold Pressure	17 kPag
Exhaust O_2	14%, dry
Exhaust THC	770 ppm, dry
Exhaust NO_x	800 ppm, dry
Exhaust CO	81 ppm, dry
Exhaust CO_2	4.2%, dry
Intake Manifold Temperature	320 K
Exhaust Stack Temperature	600 K
Average Cooling Water Temperature	340 K

Table 6.2 GMV-4TF Nominal Engine Operating Conditions

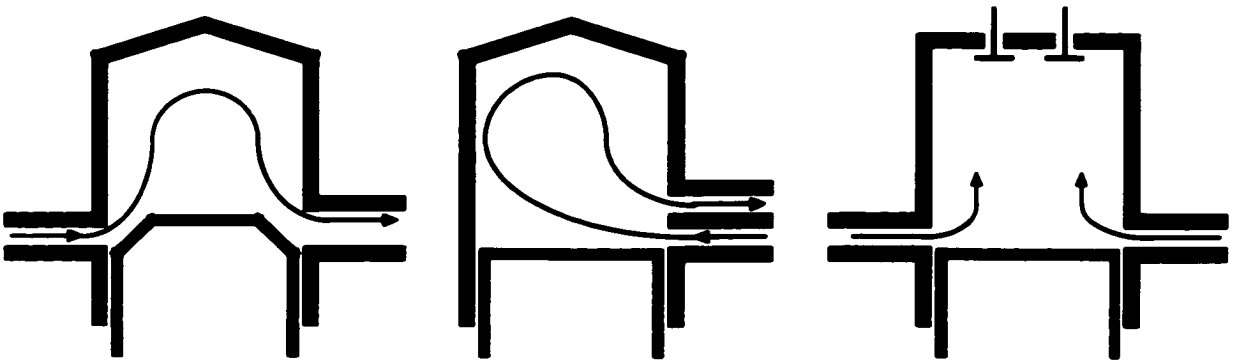

Figure 6.5 Methods of Scavenging 2-Stroke Engines

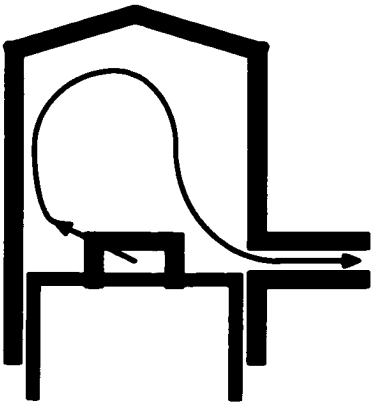

Loop Scavenge (Schnurle Type)

Figure 6.6 Schnurle Type Loop Scavenging: Intake Flow is Directed Upward and Away from the Exhaust Port.

(approximately 10 cm), and the intake port length covers the bottom 21% of the stroke (approximately 7.5 cm). The intake ports wrap around the cylinder, covering approximately 210°. The intake ports opposite the center exhaust port are directed upward and across the cylinder. The intake ports that wrap around the cylinder are "Schnürle" ports and are directed upward toward the opposite side of the cylinder from the center exhaust port. The exhaust ports wrap around the cylinder as well, covering approximately 120°. The piston cross section is M-shaped, so when the ports are partially covered it acts like a deflector piston. The deflector piston and the fact that some exhaust ports are opposite intake ports are characteristics of the cross scavenge configuration. The direction of the entering scavenging flow and the piston shape work to more effectively scavenge the upper portion of the cylinder.

The scavenging flow for this cylinder was studied with Schlieren photography by Boyer *et al.*[47] An interesting conclusion that was made was that the scavenging air enters the cylinder through the intake ports in turbulent jets. The flow penetrates the combustion products rather than entraining them, and initially resides near the cylinder head. Conversely, the gas flow that exits the cylinder is characterized by laminar flow streamlines. The authors describe this as a desirable situation for this port design, because the scavenging air tends to accumulate behind the combustion products and subsequently pushes them out like a laminar gas piston. Another important observation was that the injected fuel did not initially mix with the air. Instead, it penetrated the air in the form of a turbulent jet and struck the piston. The fuel was subsequently mixed with the air by the residual gas motion set up by the scavenging flow. Although the authors described the

level of mixing at spark as adequate, it seems likely that the lower portion of the cylinder near the piston would be richer than the upper portion because of the initial accumulation of fuel near the piston. This point is discussed more below in the context of in-cylinder sampling results.

6.4.4 Instrumentation. The exhaust composition and tracer concentrations were measured using the same emissions instrumentation as is described in Chapter 5. The inlet air and exhaust flowrates were measured using Dietrich Standard Diamond II Annubars. The Annubar™ is a differential pressure device that operates as a self-averaging Pitot tube. The natural gas fuel flowrate was measured with an AGA (American Gas Association) standard orifice flowmeter. Orifice flowmeters are generally more accurate than Annubar™ flowmeters, but come with the penalty of larger pressure losses. The engine and support hardware are instrumented with numerous pressure sensors and thermocouples. A comprehensive description of the engine test bed and instrumentation is given in two Masters Theses by Schoonover[45] and Potter[48].

6.5 Evaluation of Non-Ideal Tracer Effects

Potential difficulties with the tracer gas method that have been discussed are combustion misfire, inconsistent exhaust sampling, exhaust reaction, and incomplete cylinder destruction. Combustion misfires are detected with in-cylinder pressure measurements and accounted for in all the tracer gas calculations, where applicable.

6.5.1 Exhaust Tracer Destruction and Sampling. Exhaust sampling was carried out at various locations downstream of the exhaust manifold. It has been shown that the residence time in the exhaust manifold for the GMV-4TF is relatively large. As a result the exhaust constituents are well mixed and the gas temperature is significantly lower than cylinder exit temperature before they get to the first sample tap location. Therefore, any tracer exhaust reaction that takes place is expected to occur primarily in the manifold. Additionally, the gases are likely to be well mixed upon exiting the exhaust manifold so sampling errors are improbable downstream of the exhaust manifold. The distance between the exhaust manifold and the stack is approximately 5.2 meters. Tracer mole fraction measurements were taken along the exhaust pipe under nominal engine operating conditions. The results are shown in Figure 6.7. Short-circuited fraction values, calculated from Equation 2.13 assuming ε_r=0 and η_{cr}=1, are presented instead of raw mole fraction measurements. The short-circuited fraction is proportional to the tracer mole fraction in the exhaust pipe, yet the calculation accounts for variations in misfire fraction and intake tracer mole fraction variations between data points.

The data shows a large difference between the average short-circuited fractions measured with N_2O and with CH_3NH_2. This discrepancy will be discussed later in detail. If there is no tracer reaction in the exhaust and no sampling errors, the data should form horizontal straight lines. The data for both tracers is relatively smooth, with no large increases or decreases as was seen in the 4-stroke cycle engine testing. This indicates that for both tracers the exhaust gas sampling is consistent and the exhaust gases are well mixed.

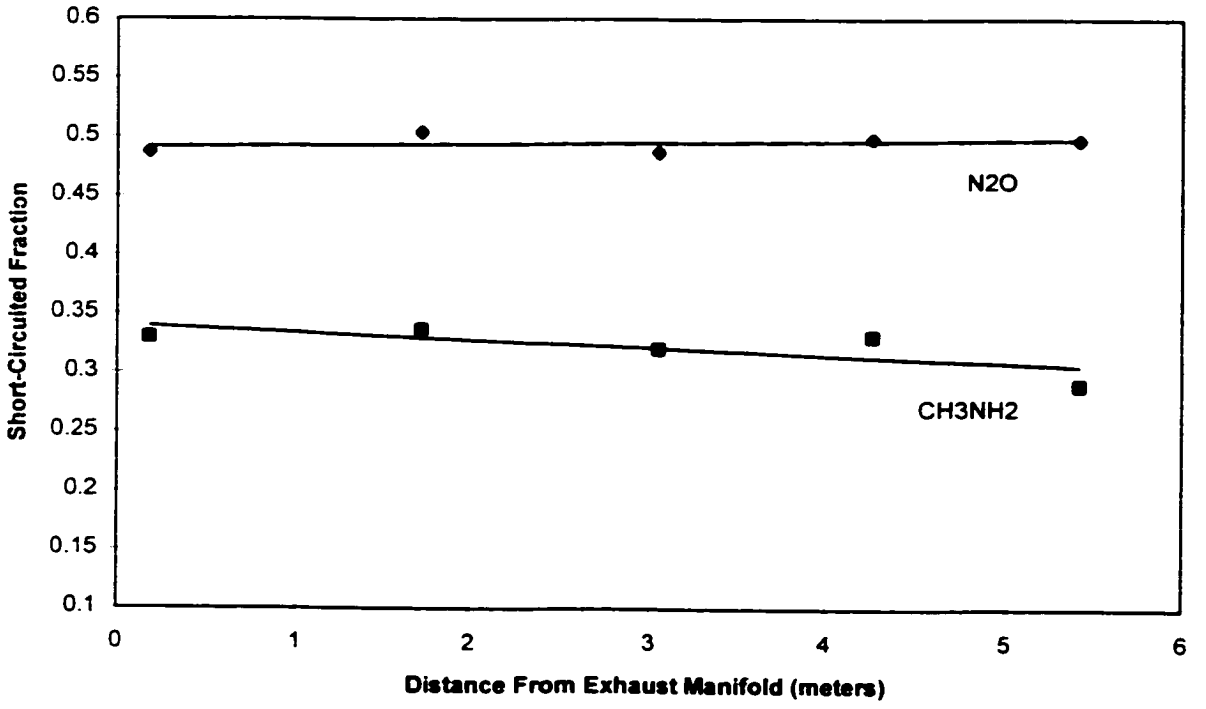

Figure 6.7 Tracer Short Circuited Fraction in Exhaust System.

Nitrous oxide appears to be very stable in the exhaust pipe, forming a fairly straight, horizontal line. Monomethylamine short-circuited fractions show a gradual decreasing trend as the distance down the exhaust pipe increases. The data indicates that approximately 6% of the monomethylamine is destroyed in this section of the exhaust system.

This test provides data on the exhaust stability of N_2O and CH_3NH_2 in the portion of the exhaust system downstream of the exhaust manifold. For CH_3NH_2 it suggests that the reaction in the exhaust manifold is probably substantial, because gas temperatures in

the exhaust manifold are significantly higher than those downstream in the exhaust pipe and the residence time in the exhaust manifold is large. Since there is some indication of CH_3NH_2 exhaust reaction downstream of the manifold, it is likely that significant destruction takes place in the exhaust manifold. The apparent large monomethylamine exhaust reaction could explain most of the difference between the nitrous oxide and monomethylamine average short-circuited fractions. However, there is no way to draw any definitive conclusions about the stability of the tracers in the exhaust manifold based on this data alone. Since the exhaust manifold is not equipped with sample taps, the exhaust reaction for the entire exhaust system can not be determined from direct exhaust sampling. Instead, the exhaust reaction will be calculated based on direct measurements of cylinder reaction efficiency and trapped A/F ratio through the use of in-cylinder and exhaust port sampling.

6.5.2 Cylinder Reaction Efficiency. The calculation of cylinder reaction efficiency from in-cylinder sampling valve and/or port checkvalve data was described in Chapter 2. The in-cylinder sampling valve is mounted in the air-start port in the cylinder head of cylinder #2 in the GMV-4TF. Cylinders 2 and 4 are located on the same side (referred to as the 2-4 bank) of the engine. The exhaust sample tap is located on the 2-4 bank side of the exhaust elbow just down stream of the exhaust manifold. The piston motions are slightly different between the 1-3 and 2-4 banks, probably because of an oversight in the original design of the piston linkages. The end result is that the exhaust and intake ports for cylinders 1 and 3 are open 3.9 and 4.4% longer, respectively, than cylinders 2 and 4.

This causes a significant difference in the scavenging between the two sides, consequently the 2-4 bank A/F mixture, both trapped and overall, is richer than for the 1-3 bank. Thus, the in-cylinder sampling results must be correlated to the exhaust measurements from the same side of the engine.

Figure 6.8 presents a cross-section of a cylinder and piston, which shows the location of the air-start port. The air-start port is not used for starting the engine in this test setup. An external air starter is coupled to the crankshaft between the engine and the dynamometer for starting the engine. This allows the cylinder head air-start port to be utilized for in-cylinder sampling and other diagnostic measurements. The sample valve is a 3.2 cm diameter poppet valve with a 0.97 cm lift, and is electro-hydraulically actuated. The valve, shown in Figure 6.9, was custom-designed for this application by Optimal Engineering, Inc. and manufactured by the Woodward Governor Company. The valve is connected to a 30 liter Teflon lined aluminum sample cylinder by a short section of pipe, approximately 30 cm long.

The in-cylinder sample valve has a relatively large effective flow area, which makes it possible to extract a significant portion of the mass in the engine cylinder each time it is actuated. Based on the literature that has been reviewed on in-cylinder sampling, a sample size of about 20% of the engine cylinder mass or greater is considered to be an accurate representation of the average cylinder composition. However, since different engine designs have varying levels of in-cylinder mixing the required sample size is expected to vary among different engine designs. The basic procedure for extracting in-cylinder samples was to (1) purge the sample cylinder three times with nitrogen by

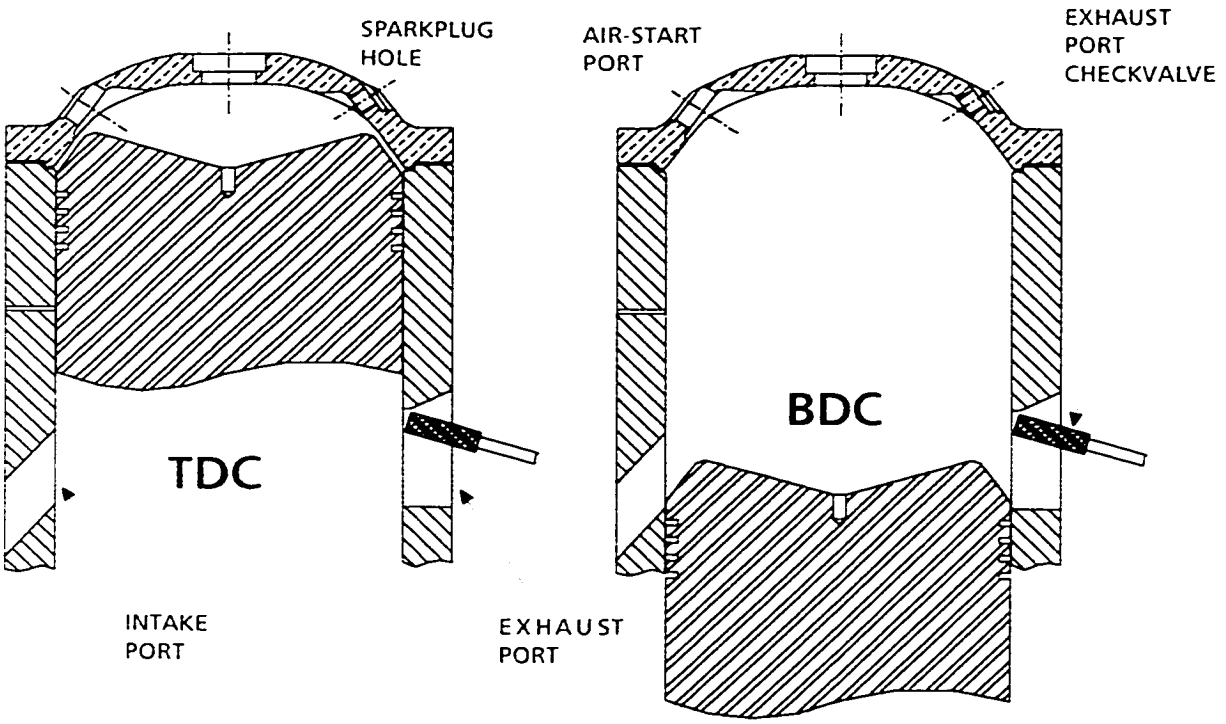

Figure 6.8 Piston and Cylinder for GMV-4TF Showing Spark Plug Hole and Air-Start and Scavenging Ports

pressurizing to about 630 kPa and venting to atmosphere, (2) evacuate the sample cylinder to an absolute pressure between 80 and 180 torr, (3) sample the engine cylinder contents with the sample valve multiple times, allowing the engine to stabilize between samples, until a pressure of about 300 kPa is obtained in the sample cylinder, and (4) after allowing roughly 10 minutes for the sample cylinder temperature to stabilize and the gases to mix, measure the composition of the sample cylinder contents with the gas analyzers. The sample cylinder and line to the gas analyzers were heated to 380 K to prevent moisture condensation.

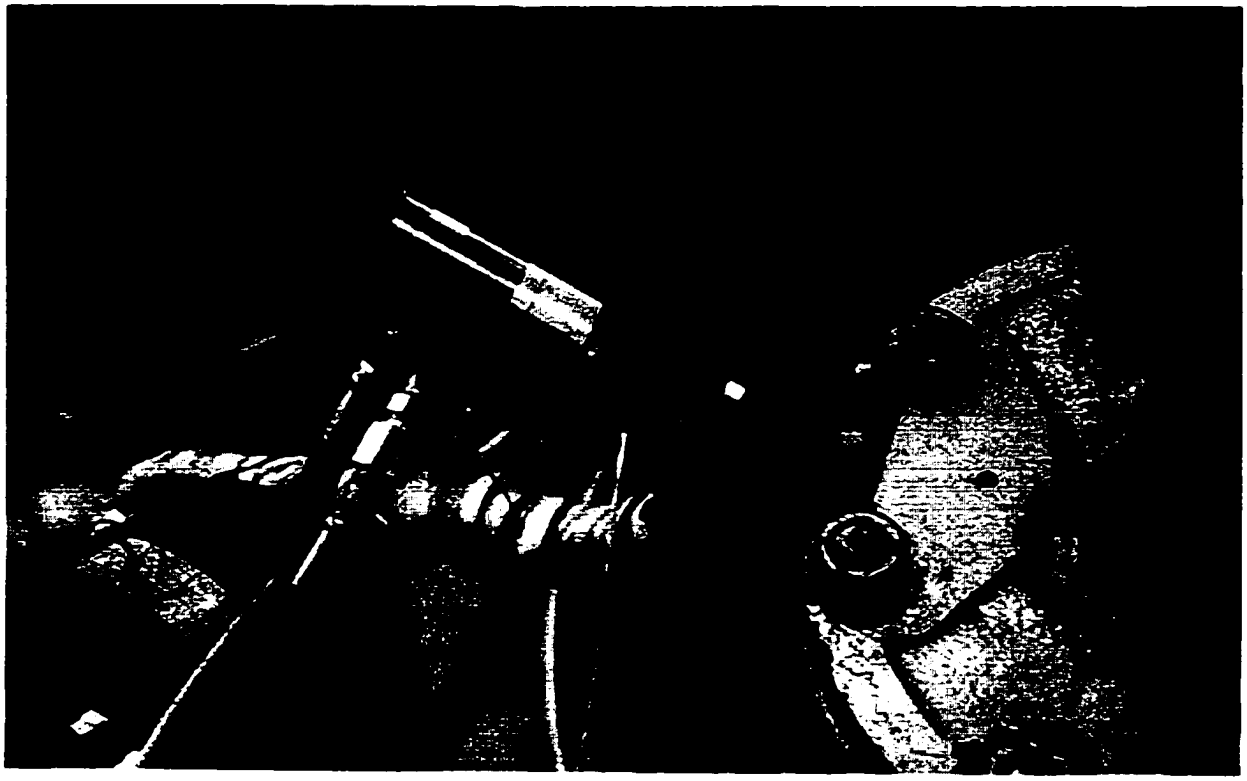

Figure 6.9 Electro-Hydraulically Actuated In-Cylinder Sample Valve Mounted in the Air-Start Port of Cylinder #2.

In-cylinder sample valve opening and closing times were adjustable. Samples extracted during compression were intended to represent the average composition of the trapped cylinder charge prior to combustion, whereas samples extracted during expansion were intended to represent the average composition of the trapped cylinder contents after combustion. A significant amount of preliminary experimentation was necessary to determine the best sample valve opening and closing times for extracting samples during compression and expansion. The resulting parameters that were implemented to acquire data are presented in Table 6.3. Note that the samples extracted during compression removed more than 40% of the cylinder mass, which is considered to give an accurate

PARAMETER	COMPRESSION	EXPANSION
Sample Valve Opening	83° BTC	30° ATC
Sample Valve Closing	3° BTC	90° ATC
Duration Open	80°	60°
Cylinder Mass Extracted Per Cycle	40 - 55%	10 – 20%

Table 6.3 In-cylinder Sample Valve Parameters for Extracting Samples During Compression and Expansion

representation of the average cylinder composition. In contrast, samples taken during expansion amounted to less than 20% of the cylinder mass. Thus, expansion samples may not represent the average composition of the cylinder. This will be discussed in more detail later.

A checkvalve (see Figure 6.8) was mounted in the center exhaust port to sample the exhaust blowdown pulse. It was oriented with the valve inlet facing into the flow and as close as possible to the cylindrical path traced by the outer diameter of the piston, thus recovering much of the dynamic pressure of the exhaust gas jet exiting the cylinder. The spring in the checkvalve that the valve inlet pressure acts against was selected so that the checkvalve opens just above the highest boost pressure tested, yet well below cylinder pressure at port opening. The checkvalve had a flow area of approximately 7 mm^2 when fully open. This cross sectional area was over two orders of magnitude smaller than the flow area of the in-cylinder sample valve (980 mm^2) and, therefore, did not have the capability to extract a large percentage of the cylinder mass. However, since it opens every cycle the average flowrate was sufficient for gas analysis.

Cylinder reaction efficiency evaluations based on in-cylinder sampling, applying Equation 2.9, are presented in Table 6.4. Cylinder reaction efficiency evaluations for monomethylamine are not given. It was presumed that monomethylamine reaction in the exhaust manifold would make it difficult to achieve repeatable trapping efficiency measurements. Thus, adequate testing time was not allotted for this evaluation. The average cylinder reaction efficiency for nitrous oxide is about 0.96. This is very good considering that it appears to be stable in the exhaust system.

The exhaust port checkvalve was also used to sample combustion products when tracer was flowing through the engine. No nitrous oxide was detected through the exhaust port checkvalve at any of the boost levels tested. This result can be interpreted two ways. Either the exhaust port checkvalve samples a region where tracer is completely consumed, or the tracer detected with the in-cylinder sample valve during expansion is consumed during the latter part of the expansion stroke. In light of this, the average nitrous oxide cylinder reaction efficiency of 0.96 should be viewed as a conservative value.

6.5.3 Comparison of Tracer Gas Method with In-Cylinder Sampling. In-cylinder sampling during compression and expansion and exhaust blowdown sampling with the checkvalve allowed the evaluation of the trapped equivalence ratio by several different techniques. One of the techniques has not been discussed explicitly, which involves the analysis of a tracer seeded in-cylinder compression sample to evaluate the scavenging

TRACER	EXH. MAN. PRESSURE, kPag	COMPRESSION SAMPLE, ppm	EXPANSION SAMPLE, ppm	CYLINDER REACTION EFFICIENCY, η_{cr}
N_2O	16.9	762	34.1	0.956
N_2O	35.6	756	20.5	0.973

Table 6.4 Evaluation of Cylinder Reaction Efficiency Through In-Cylinder Sampling at Nominal Speed and Load.

efficiency. The calculation of scavenging efficiency is adapted from the technique of Kannappan[14] to include an adjustment for incomplete tracer destruction in the cylinder. The resulting equation is

$$\eta_{sc} = \frac{X_{t,tr}\eta_{cr}}{X_{t,a}SG_{tr} - X_{t,tr}(1-\eta_{cr})} \tag{6.3}$$

where $X_{t,tr}$ is the mole fraction of tracer trapped in cylinder before fuel addition. The other terms have been previously defined. Any fuel present in the sample is mathematically removed before applying Equation 6.3. This removes the effects of incomplete fuel and air mixing, and only requires that the air delivered be well mixed with the residual gases at the time the sample is taken. The scavenging efficiency is multiplied by the trapped mass to get the mass of air delivered. The mass of fuel delivered to each cylinder per cycle is evaluated from the orifice flowmeter fuel flow measurement. It is assumed that the fuel delivered to each cylinder is the same, which is a good assumption based on the inspection of the input voltage profiles to the fuel injector

drivers. The air delivered is then divided by the fuel delivered to calculate the trapped A/F ratio.

The possibility of deriving an in-cylinder A/F ratio from the concentration of fuel in the cylinder was considered. To get a relatively large sample the valve had to be open for most of the compression stroke duration. Although the sample valve did not open until after the fuel injection event was finished, analysis of the samples revealed that the A/F ratio calculated in this manner was extremely lean, below the flammability limit. This indicated that the fuel was not well mixed with the air when the sample was extracted.

Figure 6.10 presents trapped equivalence ratio and delivery ratio vs. intake manifold pressure for the various techniques that have been discussed. The data show that as the intake manifold pressure increases the charge gets progressively leaner, with a slight leveling trend at the larger pressures. Note that the curve fit to the nitrous oxide tracer gas method (TGM) data passes through each group of data points with some occurring above and some below. The location of data from a particular technique with respect to the nitrous oxide TGM curve is fairly consistent. For example, all of the equivalence ratios from exhaust analysis of in-cylinder samples taken during expansion appear below the nitrous oxide TGM curve, at significantly leaner equivalence ratios. As discussed earlier, the in-cylinder samples during expansion extracted only 10 to 20% of the cylinder mass per cycle. It was asserted earlier that because the fuel jet initially strikes the piston, a region richer than the bulk charge is most likely created near the bottom of the cylinder, and consequently a leaner region near the top. This, in combination with the

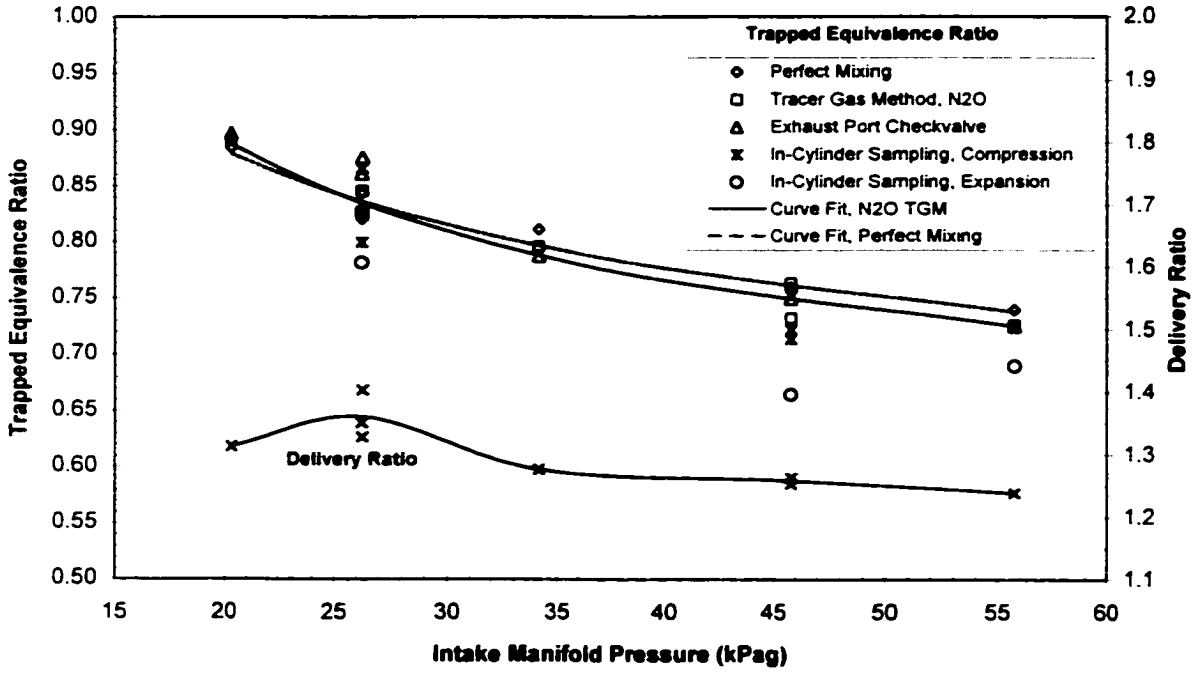

Figure 6.10 Trapped Equivalence Ratio and Delivery Ratio vs. Intake Manifold Pressure.

relatively small sample size, could explain the in-cylinder expansion data being leaner than the rest of the data.

The exhaust port checkvalve and the nitrous oxide TGM data are very close to each other for nearly all of the boost levels. The exhaust port checkvalve, as discussed earlier, extracts a relatively small sample each cycle because of the smaller flow area. However, with regard to mixing of trapped cylinder gases, the location of the exhaust port checkvalve is optimal. When the exhaust ports open the trapped cylinder gases are as uniform as they will ever get before being mixed with scavenging air, which occurs just

downstream of the exhaust ports. Thus, the increased level of mixing in the port checkvalve samples may help compensate for smaller sample sizes.

One monomethylamine TGM point (not shown) was taken at a boost of 46 kPag. The resulting trapped equivalence ratio is 0.57, approximately 24% leaner than the exhaust port checkvalve point at the same boost. The exhaust port checkvalve point is used for comparison because it is located near the center of the other data at the same boost. This monomethylamine TGM calculation assumes a cylinder reaction efficiency of 1. Excessive destruction of monomethylamine in the exhaust accounts for the discrepancy. To quantify the amount of monomethylamine destroyed in the exhaust the actual trapped equivalence ratio is assumed to be equal to the trapped equivalence ratio evaluated from the exhaust port checkvalve technique. The fraction destroyed in the exhaust is then solved for, which results in a value of ε_r=0.44. Hence, for this boost level, nearly 50% of the monomethylamine reacts in the exhaust. To accurately measure scavenging characteristics and trapped equivalence ratio with the monomethylamine TGM, the fraction destroyed in the exhaust would need to be characterized for each operating condition to be tested. The usefulness of monomethylamine as a tracer is severely limited for this application.

The trapped equivalence ratio is also evaluated using the perfect mixing model. The perfect mixing model predicts trapped equivalence ratio well for this engine design. Recall that the perfect mixing model assumes that no blowdown of pure combustion products or short-circuiting of scavenging air occurs. If the effects of these two assumptions offset, then the model can make accurate predictions. Apparently this is the

case in the GMV-4TF engine, but is not likely to be the case for other two-stroke cycle engine designs. For other engine designs, ideally, the perfect mixing model should be compared to other techniques before using it to predict scavenging characteristics.

The nitrous oxide TGM data is corrected for incomplete cylinder reaction using the average of the measured nitrous oxide cylinder reaction efficiencies given in Table 6.4, but the exhaust reaction is assumed to be negligible. In contrast to monomethylamine, nitrous oxide compares quite well with the other measurement techniques. Within the accuracy of the data, it appears that there is no significant consumption of nitrous oxide in the exhaust system. The other techniques for evaluating trapped equivalence ratio, in-cylinder sampling and exhaust port checkvalve sampling, have errors associated with them. However, they are often referred to in the literature as "direct measurements". The main error associated with in-cylinder sampling and exhaust port checkvalve sampling is the extraction of a sample that is not representative of the entire cylinder mass due to incomplete mixing. Actually, the TGM is the only one of the techniques presented that is a true bulk measurement. Based on the data it appears to be as accurate, if not more accurate, than the "direct measurement" techniques. The nitrous oxide TGM is used in the following sections to study scavenging characteristics of the GMV-4TF engine.

6.6 Tracer Gas Method Trapping Efficiency Measurements

Trapping efficiency measurements were carried out on the GMV-4TF engine using the tracer gas method with nitrous oxide. Data for boost and speed variations were acquired using both monomethylamine and nitrous oxide, but only the nitrous oxide data

are presented. This is because the monomethylamine tests gave unrealistic scavenging efficiencies (η_{sc}>1.0). This is caused by excessive destruction of monomethylamine in the exhaust. Exhaust reaction makes the short-circuited fraction appear small, yielding trapping and scavenging efficiencies that are too large. The maximum achievable scavenging efficiency corresponds to the idealized case called perfect displacement. With perfect displacement the maximum scavenging efficiency is equal to one for delivery ratios greater than one. With perfect displacement the incoming scavenging air behaves like a piston and pushes the combustion products out the exhaust ports. For this idealized case, excess air does not improve scavenging. An attempt could have been made to correct the data for exhaust reaction. Correcting for an error of this magnitude is not practical for field application and could be misleading. Additionally, monomethylamine was difficult to work with because of the corrosiveness and pungent odor. Monomethylamine is also more difficult to obtain then nitrous oxide. It is currently regulated by the US Government as a controlled substance because of its use in the illegal manufacturing of amphetamines.

The delivery ratio is calculated using Equation 6.2, where the mass flow of air through the engine is evaluated from the overall A/F ratio and the fuel flow measurement with the orifice flowmeter. For the scavenging measurements presented in this section, the misfire fraction and incomplete cylinder destruction were compensated for. The misfire fraction is evaluated by looking at the pressure-time histories for approximately 1000 cycles, and recording the number of cycles where the pressure did not rise higher than 110% of peak motored pressure.

6.6.1 Speed Variations. Large bore natural gas engines are in general constant speed engines. Therefore, the potential variations in speed were not large. However, the allowed speed variations did significantly change delivery ratio and consequently the scavenging characteristics. Figures 6.11 and 6.12 show how trapping and scavenging efficiency change with speed. Calculations based on perfect mixing are presented with the nitrous oxide TGM data for comparison. Recall that the perfect mixing model is not an ideal case. Actual scavenging can be better or worse than that predicted by perfect mixing. Delivery ratios are plotted on the second y-axis. Throughout the speed map the intake manifold pressure was held constant at 25 kPag. The torque was maintained constant at about 9 kN-m by reducing the fuel flow as speed decreased. The trapping efficiency is seen to increase nearly linearly with speed and the scavenging efficiency decreases with speed for both evaluation methods. As speed increases, the airflow through the engine remains approximately constant because the effective port flow area does not change. The decrease in scavenging efficiency with speed can be attributed to two factors, (1) the mass of combustion products per cycle to be scavenged increases with increasing speed and (2) the time for the scavenging air to remove combustion products from the cylinder per cycle decreases with increasing speed.

The nitrous oxide TGM scavenging efficiencies are generally higher than those evaluated with the perfect mixing model, but not by very much. In looking in the literature for data to compare with, recall that the scavenging configuration of the GMV-4TF possesses characteristics of both loop and cross scavenging. Data from large two-stroke diesel engines by Gyssler[49], delivery ratios from 1.2 to 1.4, show scavenging

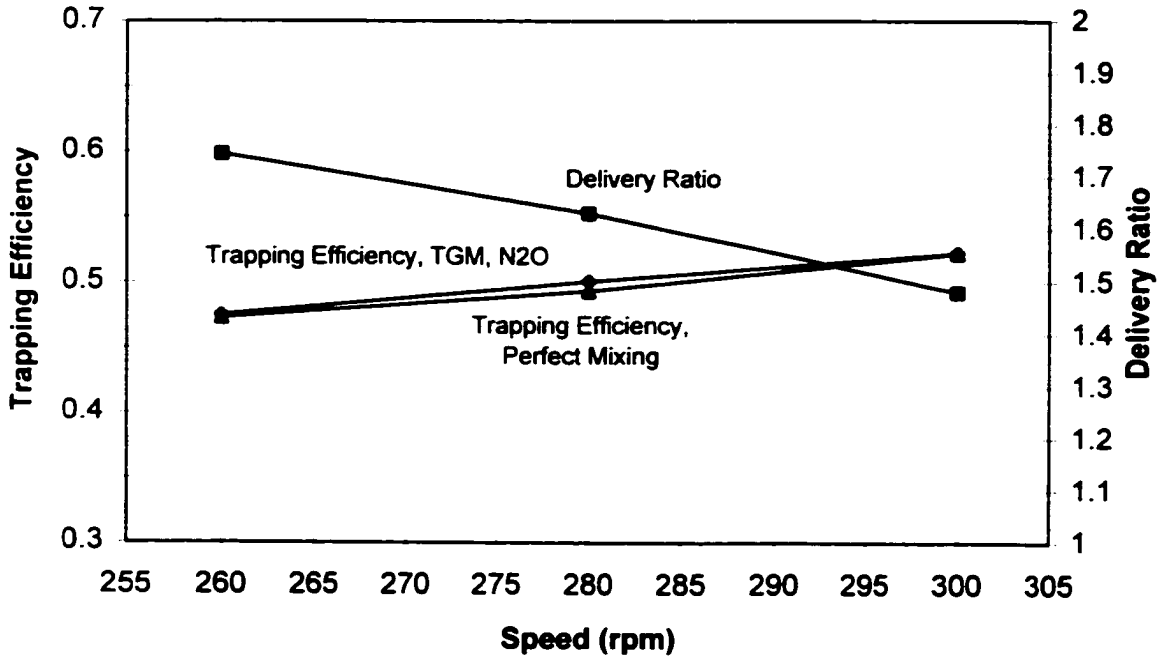

Figure 6.11 Trapping Efficiency vs. Speed

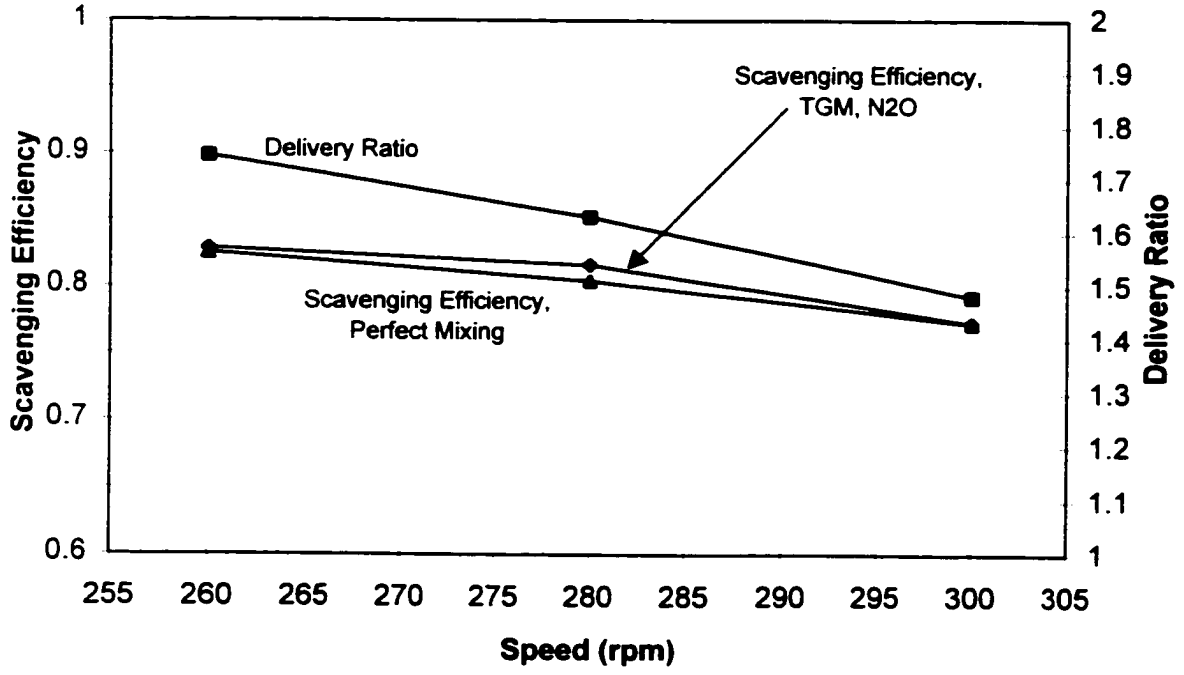

Figure 6.12 Scavenging Efficiency vs. Speed

efficiencies from loop scavenged engines slightly above perfect mixing (0.01 to 0.1 above) and cross scavenged engines slightly below perfect mixing (0.05 to 0.1 below). In other published data by Houtsma[16] scavenging efficiencies from loop scavenged engines are reported as being about 0.05 to 0.1 lower than perfect mixing for delivery ratios 0.8 to 1.4. The scavenging efficiencies measured with the nitrous oxide TGM for the speed map range from coincident to 0.03 above perfect mixing. Therefore, the nitrous oxide TGM data falls within boundaries defined by the range of the test data from these sources.

6.6.2 Intake Manifold Pressure (Boost) Variations. The trapping and scavenging efficiencies were measured using the TGM throughout a boost map. The trapping and scavenging efficiencies are plotted vs. intake manifold pressure in Figures 6.13 and 6.14. Recall that the intake manifold pressure is the parameter that is varied, but it is the exhaust manifold pressure that most directly affects engine performance. Delivery ratios are plotted on the second y-axis. In general the pressure drop across the engine is kept constant throughout the boost map, so increases in intake manifold pressure are accompanied by increases in exhaust manifold pressure. The intake manifold pressure more than tripled during the test, though the delivery ratio did not change proportionately. Therefore, only small changes in scavenging characteristics were seen. Based on the nitrous oxide TGM measurements, general trends of increasing trapping efficiency with intake manifold pressure and decreasing scavenging efficiency with intake manifold pressure are observed. The exception to both of these trends is at the lowest intake manifold pressure. It appears that a maximum in delivery ratio occurs at an intake

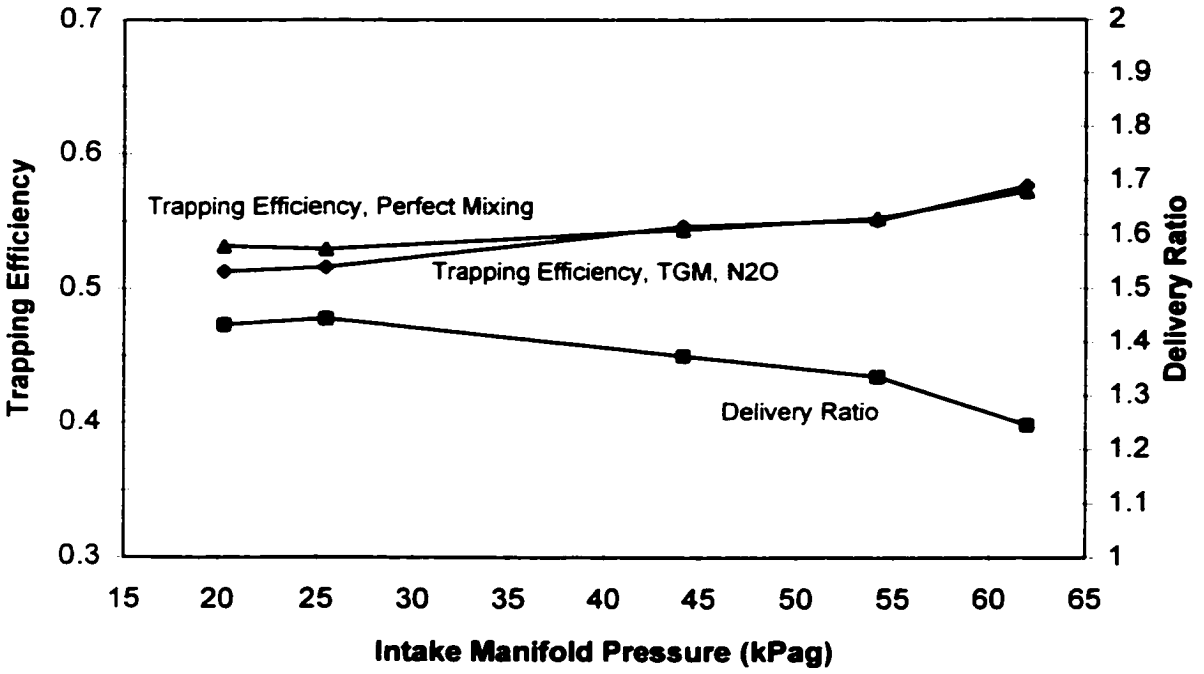

Figure 6.13 Trapping Efficiency vs. Intake Manifold Pressure

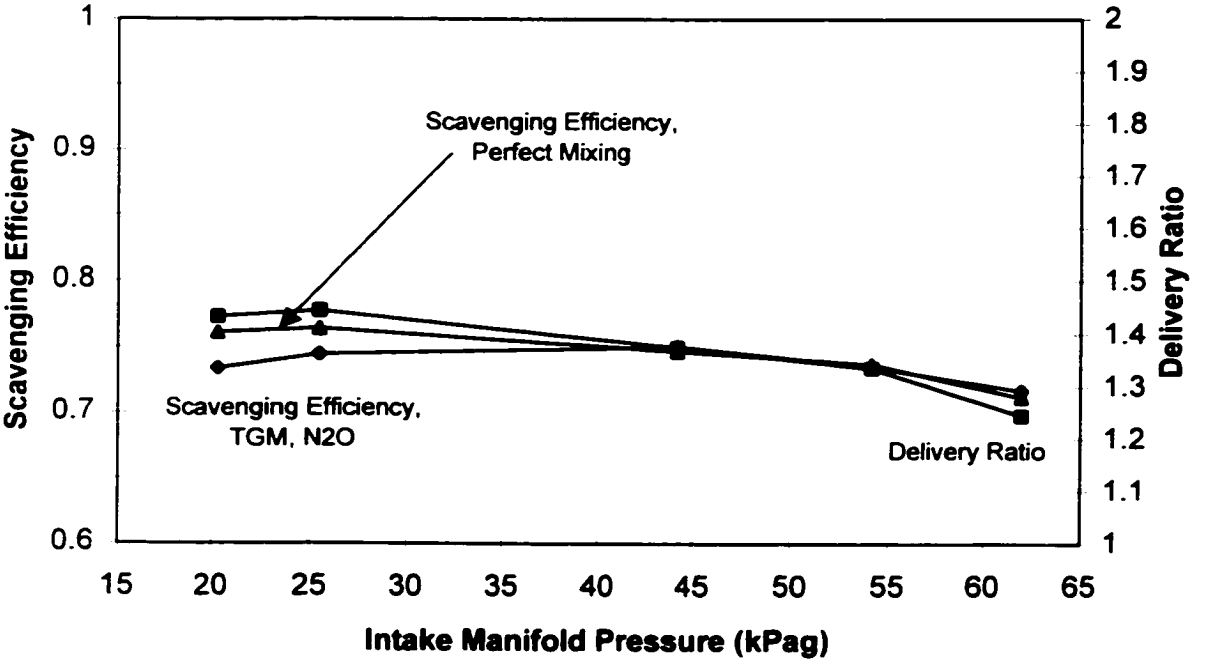

Figure 6.14 Scavenging Efficiency vs. Intake Manifold Pressure

manifold pressure of about 25 kPag, the nominal boost for the engine. The best scavenging efficiencies occur at the nominal intake manifold pressure (25 kPag) and the next highest intake manifold pressure (44 kPag) where the nitrous oxide TGM scavenging efficiencies are 0.74 and 0.75, respectively. As with the speed map, the nitrous oxide TGM data is very close to the data evaluated using the perfect mixing model. The largest discrepancy occurs at the lowest intake manifold pressure, where the perfect mixing model is about 0.03 higher than the nitrous oxide TGM data.

6.6.3 Back Pressure Variations. Changing the back pressure butterfly valve setting in the exhaust pipe influenced the delivery ratio the most. This is not surprising based on the electric circuit analogy described above. Figures 6.15, 6.16, 6.17, and 6.18 show trapping and scavenging efficiency vs. exhaust manifold pressure for variations in the back pressure valve setting at two different boost levels. The exhaust manifold pressure is a measure of the pressure drop across the back pressure butterfly valve. The delivery ratio is plotted on the second y-axis. It can be seen on all four graphs that the exhaust back pressure valve has a dramatic effect on delivery ratio, which nearly doubled as the back pressure was reduced. During testing, the torque was maintained constant at about 10 kN-m and the intake manifold pressure was held constant at 25 kPag for the first test and 34 kPag for the second test. During the tests, the fuel flow remained relatively constant while the delivery ratio was approximately doubled. The fuel flow is the variable that is adjusted to control torque. However, the fuel flow did not need to be adjusted much because in all cases a lean trapped A/F ratio is burned, which provides ample

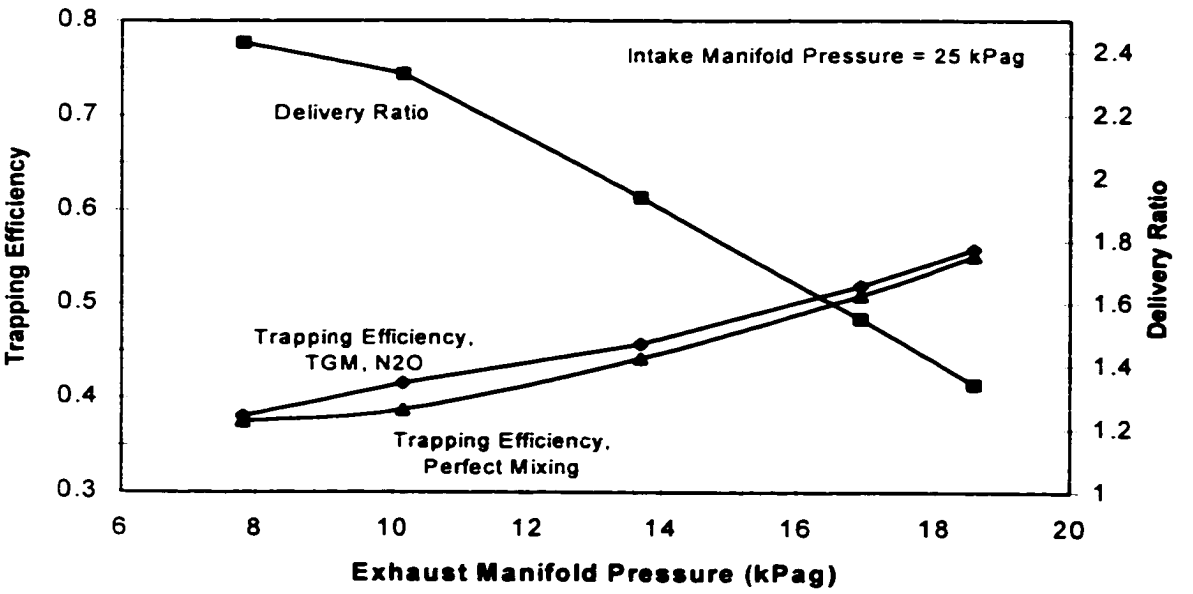

Figure 6.15 Trapping Efficiency vs. Exhaust Manifold Pressure for Back Pressure Valve Variations at Constant Intake Manifold Pressure (25 kPag)

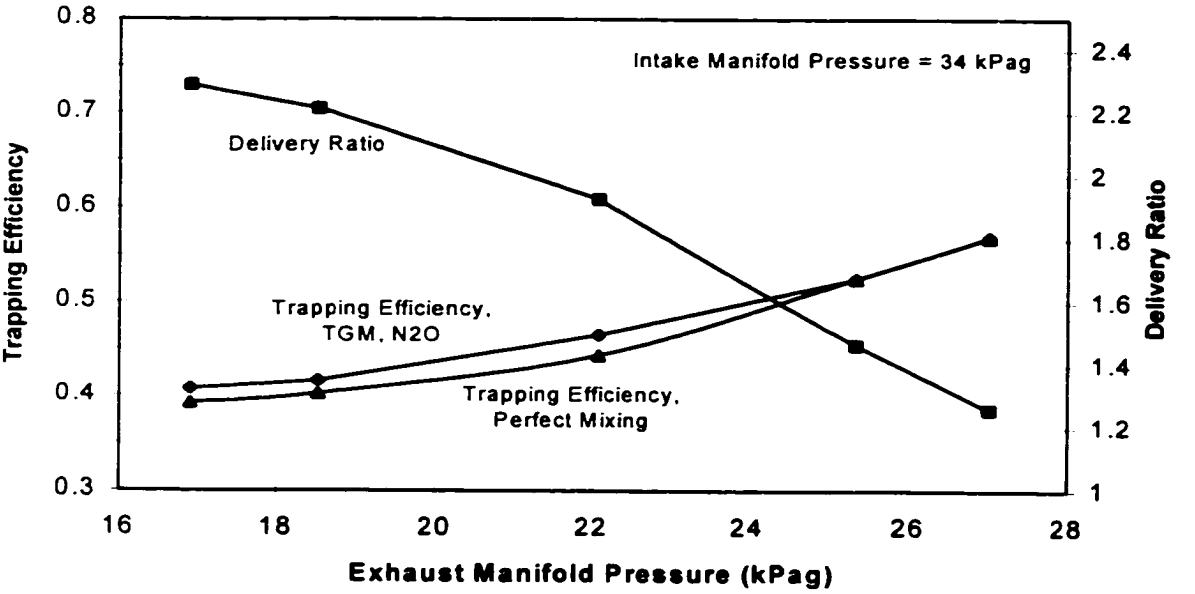

Figure 6.16 Trapping Efficiency vs. Exhaust Manifold Pressure for Back Pressure Valve Variations at Constant Intake Manifold Pressure (34 kPag)

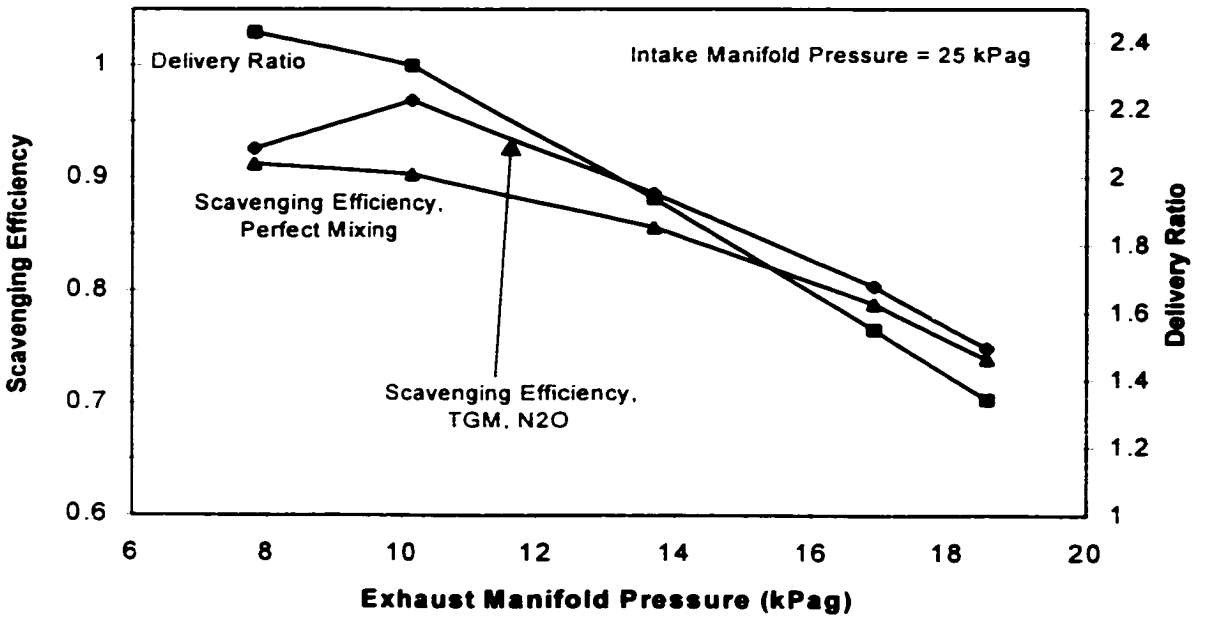

Figure 6.17 Scavenging Efficiency vs. Exhaust Manifold Pressure for Back Pressure Valve Variations at Constant Intake Manifold Pressure (25 kPag)

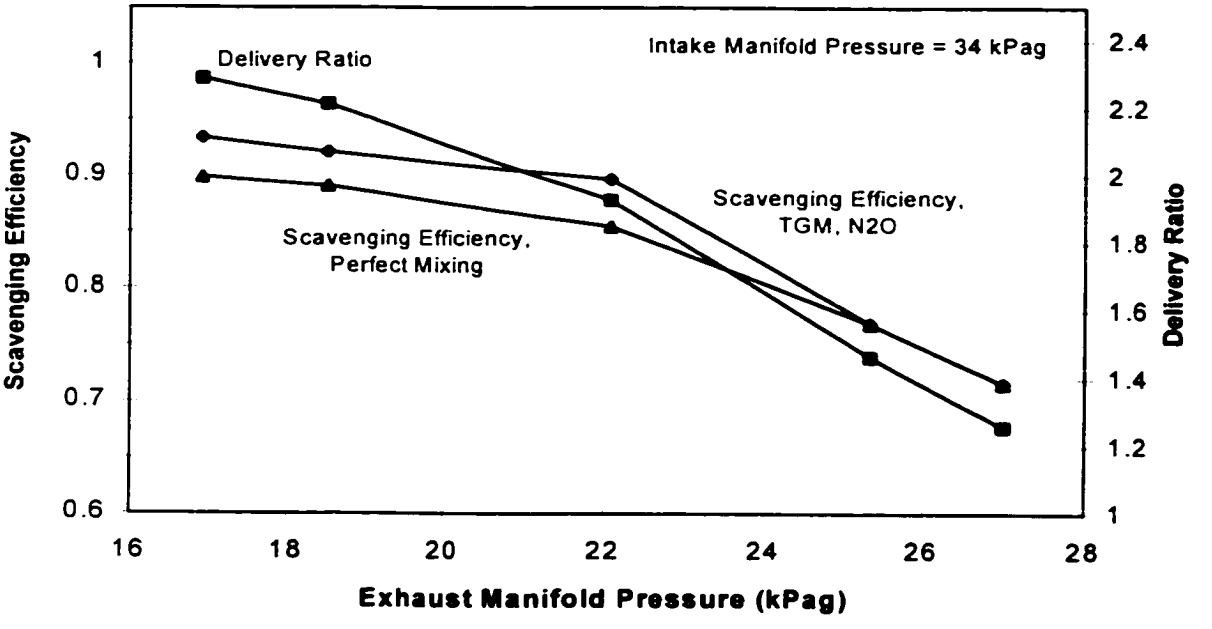

Figure 6.18 Scavenging Efficiency vs. Exhaust Manifold Pressure for Back Pressure Valve Variations at Constant Intake Manifold Pressure (34 kPag)

oxygen to oxidize the injected fuel. However, as the cylinder air purity increases with delivery ratio the potential to increase maximum power output and engine efficiency exists. Improvements to scavenging using the exhaust back pressure valve are interesting, but not practical. This is because the valve is designed to simulate the pressure drop across the exhaust turbine of a turbocharger and on real turbochargers this is not adjustable.

The same general trends of increasing trapping efficiency with increasing exhaust manifold pressure and decreasing scavenging efficiency with increasing exhaust manifold pressure are observed in the back pressure tests. These trends are directly related to the effect that the back pressure valve has on delivery ratio. The nitrous oxide TGM trapping efficiency and scavenging efficiency values are generally larger than those evaluated with perfect mixing. The trapping efficiency data tended to be closer to perfect mixing than the scavenging efficiency data. The nitrous oxide TGM trapping efficiencies range from 0.38 to 0.56 for a boost pressure of 25 kPag, and 0.41 to 0.57 for a boost pressure of 34 kPag. The nitrous oxide TGM scavenging efficiencies range from 0.75 to 0.97 for the 25 kPag boost pressure case, and 0.72 to 0.93 for the 34 kPag boost pressure case. There is very little difference in the trapping and scavenging efficiencies for the two different boost cases. Note that for high scavenging efficiencies the trapping efficiency is low, hence much of the air flow is short-circuited and is not utilized in the combustion process. This results in a penalty of excess blower power. Conversely, when the trapping efficiency is high the scavenging efficiency is low. In this case the blower power is low, but the engine may suffer from low power output and poor efficiency due to decreased scavenging efficiencies.

6.7 Trapped Equivalence Ratio

One of the main reasons to implement the tracer gas method is the information gained about the trapped equivalence ratio. The trapped equivalence ratio is calculated from Equations 1.1 and 6.1, the stoichiometric A/F ratio, the measured trapping efficiency, and overall A/F ratio calculated from exhaust gas analysis. Figures 6.19 through 6.22 show the trapped equivalence ratios evaluated from the tracer gas method measurements utilizing nitrous oxide as the tracer. Trapped equivalence ratio maps are presented for speed, boost, and back pressure. In general the equivalence ratios for this data are smaller, or leaner, then those reported in the Section 6.5.3 on the comparison of the tracer gas method with in-cylinder sampling. There are two reasons for this difference. First, the equivalence ratios evaluated with the nitrous oxide TGM for comparison with in-cylinder sampling were for cylinders 2 and 4, whereas the data presented in this section is for the entire engine. Recall that (discussed in Section 6.5.2) the 2-4 bank of the engine runs richer than the 1-3 bank, and therefore the entire engine. The second reason is that the cylinder liners were replaced between the two sets of data. The cylinder liners for the data presented in this section seemed to restrict the flow less, resulting in more airflow through the engine for the same speed, load, and boost. More airflow generally equates to better scavenging thus lower trapped equivalence ratios.

Figure 6.19 shows a gradual trend of the trapped mixture getting richer as speed is increased. The testing showed a gradual decrease in scavenging efficiency as speed increased (Figure 6.12). This explains the increase in the trapped equivalence ratio. As speed increases a lower fraction of the cylinder mass at port closure is fresh air, increasing the trapped equivalence ratio. Boost has a much stronger influence on trapped

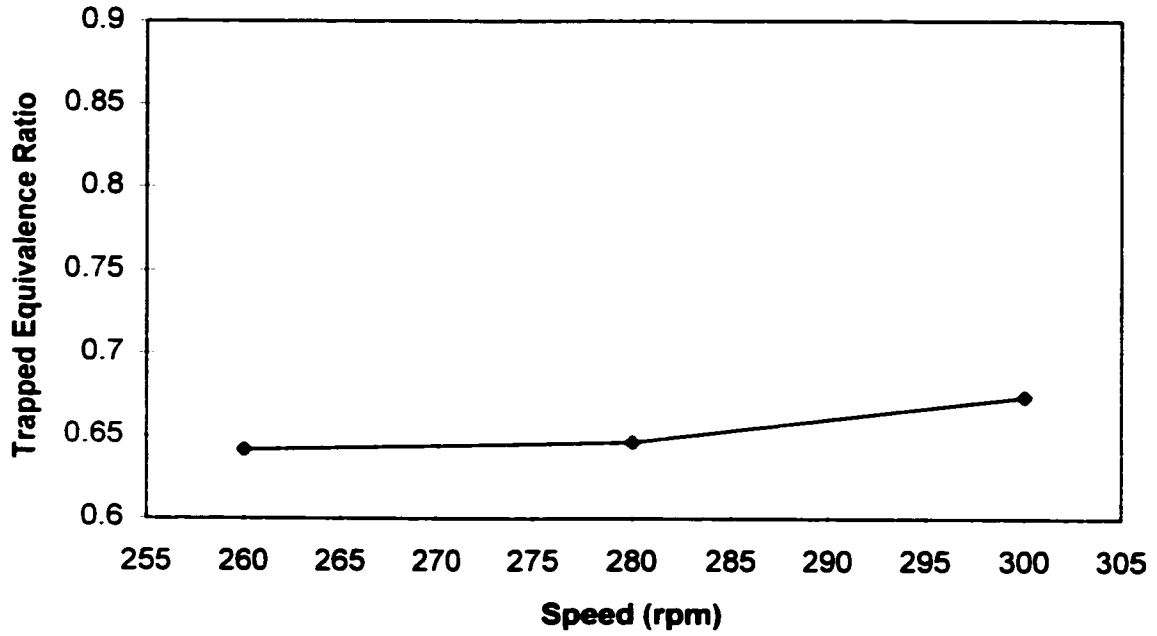

Figure 6.19 Nitrous Oxide TGM Trapped Equivalence Ratios for Variations in Speed.

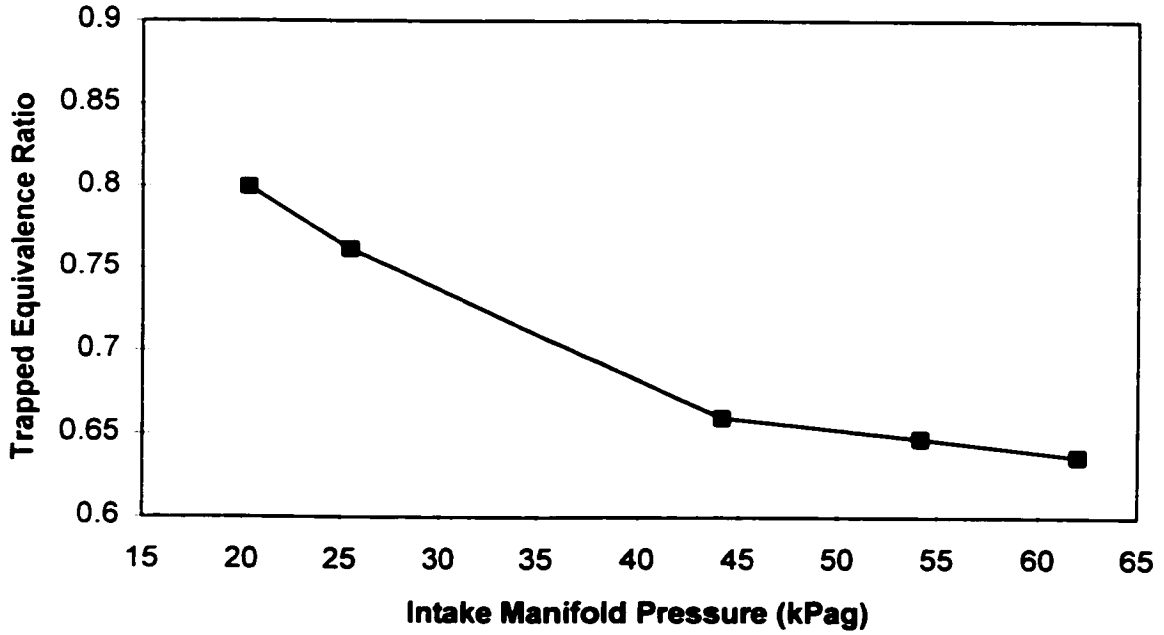

Figure 6.20 Nitrous Oxide TGM Trapped Equivalence Ratios for Variations in Intake Manifold Pressure.

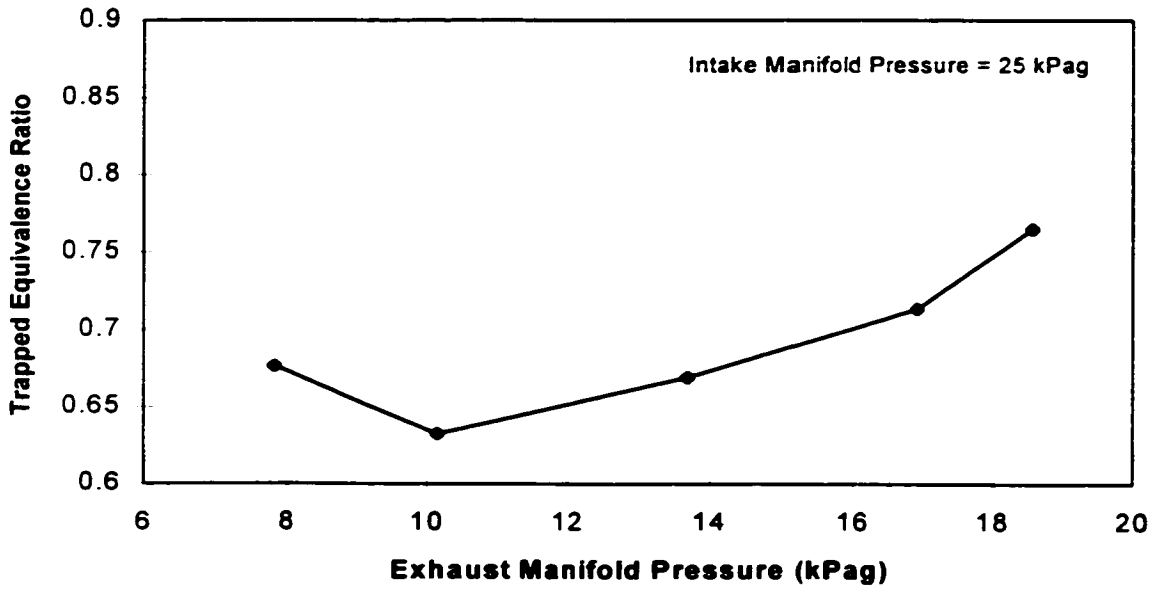

Figure 6.21 Nitrous Oxide TGM Trapped Equivalence Ratios for Variations in Exhaust Back Pressure at Constant Boost (25 kPag).

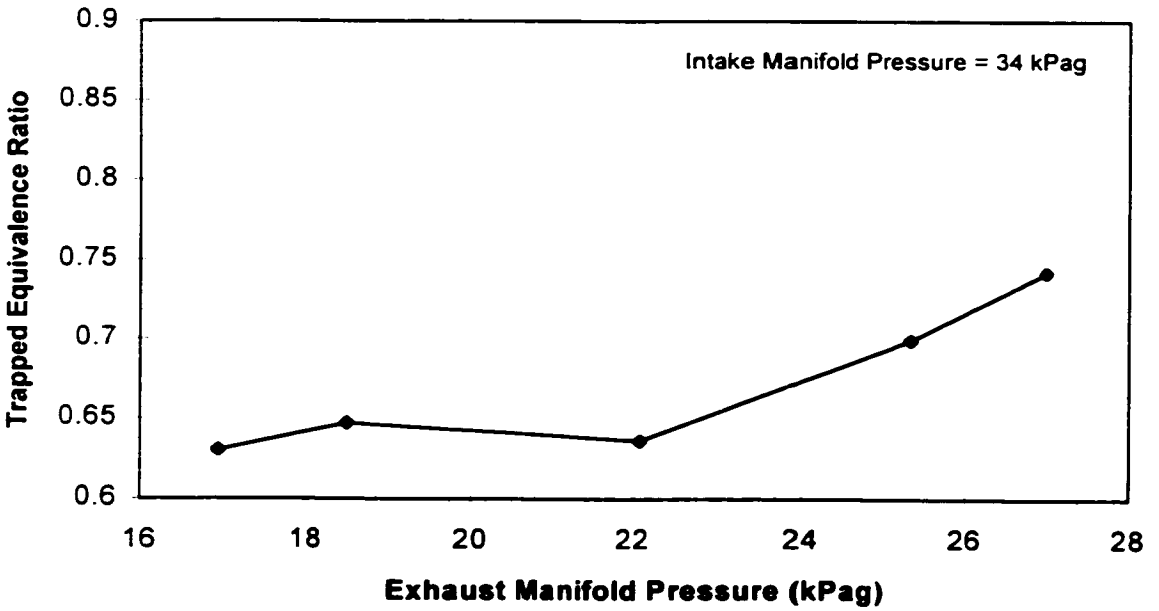

Figure 6.22 Nitrous Oxide TGM Trapped Equivalence Ratios for Variations in Exhaust Back Pressure at Constant Boost (34 kPag).

equivalence ratio (Figure 6.20) than speed. Increasing the boost at constant torque tends to decrease the equivalence ratio, resulting in a leaner mixture. The data show a significant decrease in trapped equivalence ratio as the boost increases, with a flattening trend at the higher boost levels. Referring to Figure 6.14, the scavenging efficiency actually goes down with increasing boost. Therefore, at boost levels higher than 25 kPag (nominal) the scavenging process is less effective at removing combustion products and refilling the cylinder with fresh charge. Although there is a smaller fraction of fresh charge in the cylinder at port closure, the total mass of fresh air in the cylinder is larger. That is why the charge gets leaner with increasing boost past nominal, while the scavenging efficiency decreases. Changes in fuel flow can also affect trapped equivalence ratio. Throughout the boost map the fuel flow increases with boost, which can not explain the observed trend. In fact, increasing the fuel flow increases trapped equivalence ratio. The increase in fuel flow was probably necessary to maintain constant torque to compensate for increased misfires and incomplete combustion that can be characteristic of lean equivalence ratios.

The general trend seen in the back pressure maps (Figures 6.21 and 6.22) is one of decreasing trapped equivalence ratio with decreasing exhaust manifold pressure. Referring to Figures 6.17 and 6.18, the general trend is increasing scavenging efficiency with decreasing exhaust manifold pressure. As the back pressure is reduced the scavenging efficiency increases by about 29%, from 0.75 to 0.97, for the back pressure map at 25 kPag boost; however, the final reduction in back pressure decreases the scavenging efficiency to 0.93. For the back pressure map at 34 kPag boost, the scavenging efficiency increases by about 30%, from 0.72 to 0.93. Thus, the fraction of

fresh charge in the cylinder at port closure is generally greater at lower back pressures. The fuel flow remained relatively constant throughout the test, so the effect of increasing the fraction of fresh charge is the likely cause of the reduced trapped equivalence ratios. As the back pressure drops, the trapped mass at port closure goes down and, if scavenging efficiency is constant, the mass of fresh intake air goes down as well. For a constant fuel flow, this tends to increase trapped equivalence ratio, competing with the effect of increasing the scavenging efficiency. Apparently the effect of increasing the scavenging efficiency is predominate for most of these test points, the main exception being the 8 kPag point in Figure 6.21.

6.8 The Effect of Intake Port Restriction on Scavenging and Trapped Equivalence Ratio

A test was carried out to simulate the reduction in port flow area due to carbon deposit build-up. The nitrous oxide TGM was implemented to measure the effects of port restriction on scavenging and trapped equivalence ratio. On the GMV-4TF engine the intake ports are on the outside and are much more accessible than the exhaust ports, so the area of the intake ports was reduced instead of the area of the exhaust ports. Though carbon deposit build-up typically occurs in the exhaust ports, one of the primary effects is to restrict the overall effective flow area. This can be accomplished by reducing the flow area of either set of ports. Reducing the flow area also alters gas flow patterns in the cylinder, which can affect scavenging. This is a more complex problem. No attempt was made to try and separate the effects of decreased effective flow area and the change in gas

flow patterns. This was not carried out, particularly, since plugging the intake ports is likely to alter gas flow patterns in a different way than plugging the exhaust ports.

A fixture for plugging the intake ports was developed. The fixture was designed to plug either one or two intake ports on a particular cylinder. The design of the fixture was simplified considerably by plugging a whole port, rather than reducing the area of each port. The fixture that was build is shown in Figure 6.23, and Figure 6.24 displays the fixture installed in an engine cylinder. Since there are eight intake ports, the fixture could reduce the intake port area to either 7/8 or 3/4 of the original area. The test was performed on the 2-4 bank of the engine only, thus exhaust measurements were taken from the 2-4 bank exhaust elbow rather than the stack.

Some results of the testing are presented in Figure 6.25. This test was carried out at a constant intake manifold pressure (46 kPag) and pressure drop across the engine (10 kPag). The pressure drop across the engine is controlled with the exhaust back pressure butterfly valve, as described earlier. As the level of intake port area blockage increases, the delivery ratio for the 2-4 bank decreases. This is due to an overall decrease in airflow through the engine, and a decrease in the fraction of overall airflow that flows through the 2-4 bank. The decrease in delivery ratio decreases the scavenging efficiency and increases the equivalence ratio of the 2-4 bank, resulting in a richer mixture being burned. This small increase in equivalence ratio has a significant impact on emissions, as shown in Figure 6.26. THC and CO emissions do not change significantly, however CH_2O (formaldehyde) and NO_X emissions do. CH_2O emissions increase by 8% and NO_X emissions increase by 54%. There are many things that can cause significant changes in exhaust emissions, such as ambient air conditions (humidity, temperature, etc), fuel

Figure 6.23 Fixture Implemented to Block One or Two of the Intake Ports.

Figure 6.24 Port Blockage Fixture Installed in Cylinder.

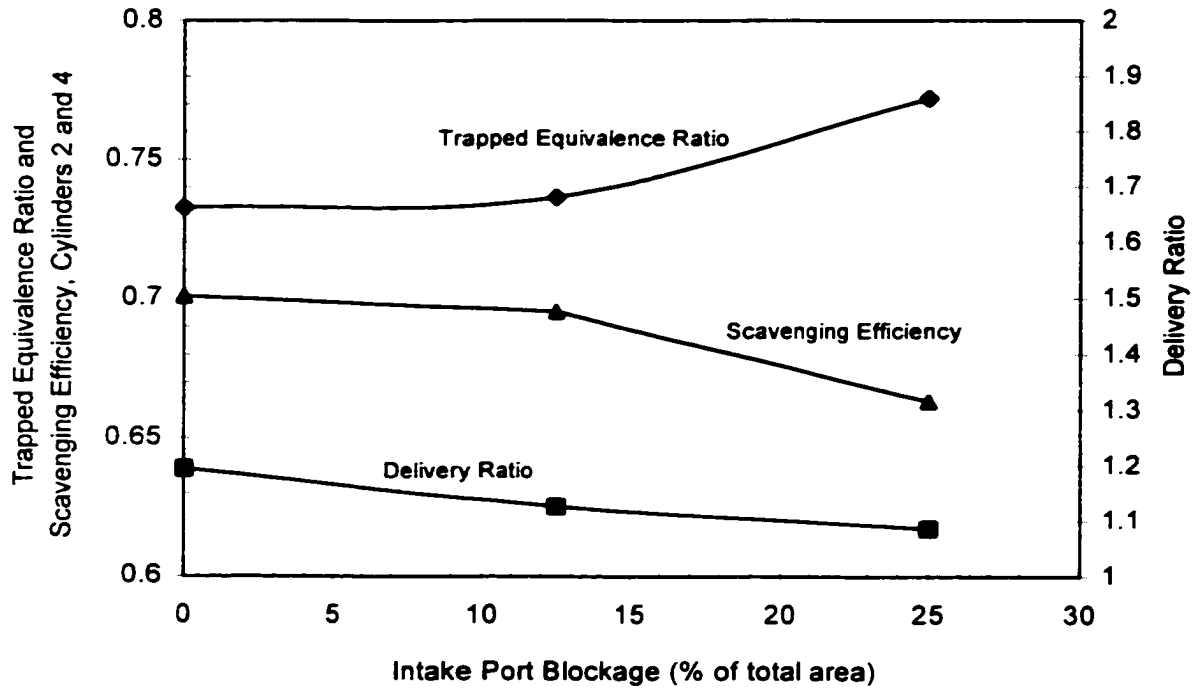

Figure 6.25 Nitrous Oxide TGM Measurements of Trapped Equivalence Ratio and Scavenging Efficiency vs. Percent of Intake Port Blockage

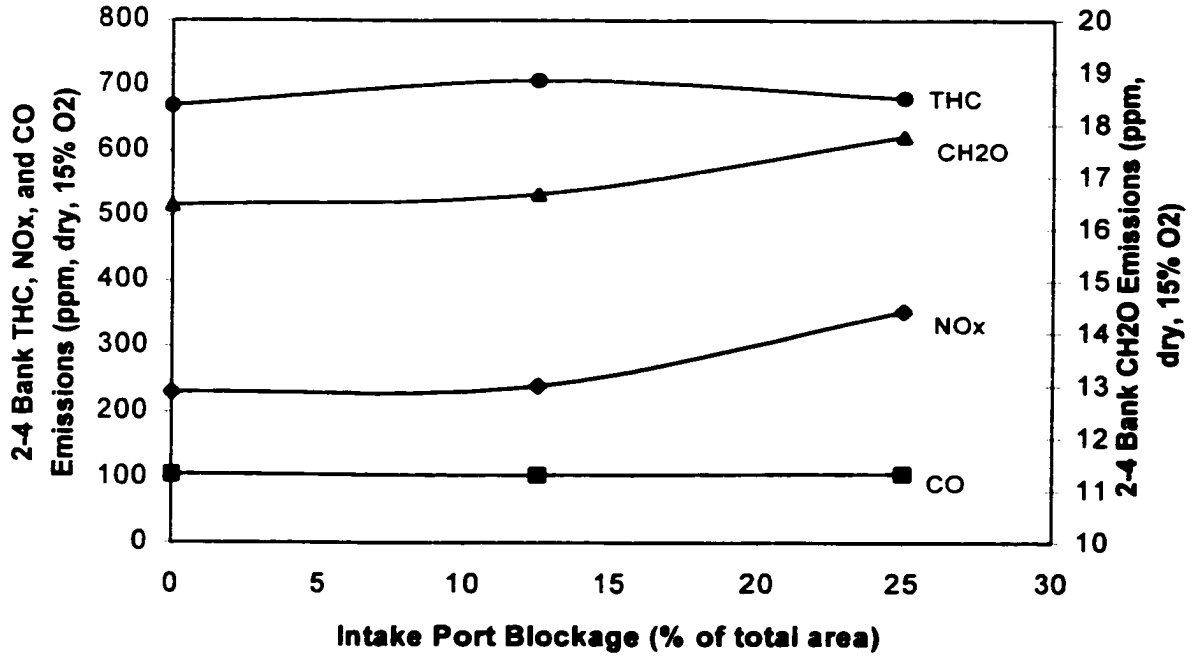

Figure 6.26 Exhaust Emissions from the 2-4 Bank vs. Intake Port Blockage.

composition, piston ring wear, and, as illustrated here, port blockage. The tracer gas method provides an additional tool for resolving emissions problems in field engines. Implementing the tracer gas method allows the scavenging characteristics to be isolated from other factors that can affect emissions.

CHAPTER 7

SUMMARY AND CONCLUSIONS

The tracer gas method was investigated as a means to measure trapping efficiency without major engine modifications. The body of literature available on the tracer gas method was reviewed, including publications on other techniques for measuring trapping efficiency. Various equations for evaluating scavenging characteristics from tracer gas measurements were developed. The equations can account for non-ideal tracer effects by correcting for (1) incomplete tracer reaction in the cylinder, (2) tracer destruction in the exhaust system, and (3) engine misfire. The criterion for tracer gas selection for a particular application was discussed. A new tracer gas, nitrous oxide, was proposed and thoroughly examined. Monomethylamine and oxygen were also considered. The research was carried out by applying the tracer gas method to two very different engines, which were a 4-stroke, carbureted, automotive size gasoline engine and a 2-stroke, fuel-injected, large bore natural gas engine. Tracer gas method investigations were carried out on these engines both through modeling and testing.

For both applications nitrous oxide was determined to be superior to the traditional tracer gas choices: monomethylamine for 2-stroke cycle engines and oxygen for 4-stroke cycle engines. The tracer gas method was best suited to 2-stroke cycle engine testing because the short-circuited fraction was much greater, which reduced sensitivity to

non-ideal tracer effects. However, the technique was successfully applied to a 4-stroke cycle engine with a small amount of short-circuiting (about 1%).

7.1 Chemical Kinetic Modeling

Chemical kinetic modeling was carried out using the chemical kinetic computer code, Chemkin II. The code was a very useful tool in predicting the stability of the tracer gases given the temperature and pressure profiles and initial composition. Actual engine test data was incorporated into the modeling input when available to help define temperature and pressure profiles. In general, temperature profiles were difficult to determine, so multiple cases were run to attempt to bracket the problem. The modeling centered around the non-ideal tracer gas effects and was separated into two problems, the consumption of the tracer in the cylinder, and the reaction of the tracer in the exhaust. A literature search was performed to find reaction mechanisms to model tracer gas chemical kinetics. A 141 step mechanism from Hwang *et al.*[26] was utilized for monomethylamine and a 13 step mechanism for nitrous oxide based on work by Glarborg *et al.*[30] was implemented.

7.1.1 Cylinder Reaction. The tracer gas cylinder reaction was fast compared to other in-cylinder phenomena such as pressure rise; near equilibrium concentrations were present within 1 ms at adiabatic flame temperatures. Monomethylamine (CH_3NH_2) was completely consumed in the cylinder for all cases run, which included high and low temperatures, with and without a combustion mechanism run in parallel with the tracer

mechanism, and for both engine cylinders. The GM 5.7 liter modeling bracketed nitrous oxide (N_2O) destruction between 97.6 and 100%, which supports the average cylinder reaction efficiency from 4-stroke cycle engines testing of 98.6%. For the GMV-4TF, the N_2O cylinder reaction efficiency was 99.7% for the high temperature case and 99.5% for the low temperature case. When a methane combustion mechanism was added to the model, 100% of the nitrous oxide was destroyed. This was higher than the measured value of 96.4%, which was expected since the modeling did not account for physical mechanisms such as protection in crevice volumes. The chemical kinetic modeling showed trace N_2O (3 ppm) forming during expansion between T = 1700 K, P = 27 atm and T = 1200 K, P = 5.4 atm in both engine cylinders. This was about the same amount of nitrous oxide measured in the exhaust of the actual engines during testing. The nitrous oxide destruction in the cylinders of both engines was dominated by third-body reactions. Of the third-body reactions in the nitrous oxide mechanism, N_2 and H_2O were the most important. The model was run for both cylinders and tracers under motored conditions, which included combustion reactions. In all cases the tracers were stable. This result indicated that misfires were a source of error to the method, and they could be accounted for by assuming that tracer in the cylinder during a misfire survives and mixes with exhaust constituents.

7.1.2 Exhaust Reaction. In general, monomethylamine was much more reactive in the exhaust than nitrous oxide for all cases. Specific results for each engine are given below.

GMV-4TF

Temperature sensitivity studies were performed for the exhaust reaction in the GMV-4TF. For CH_3NH_2 significant reaction (10%) occurred in 5 ms at temperatures greater than 1100 K. For N_2O significant reaction occurred in 5 ms at temperatures greater than 1400 K. The temperature dependence was much stronger for CH_3NH_2 than for N_2O at exhaust conditions. In other words, monomethylamine for temperatures beyond the point where 10% was consumed in 5 ms was quickly destroyed. For nitrous oxide temperatures increased beyond that point resulted in increased consumption, but the increase was much less than for monomethylamine. For the high temperature case, 100% of CH_3NH_2 and 2.6% of N_2O was consumed. For the low temperature case, no consumption for either tracer was predicted.

GM 5.7 Liter

Temperature sensitivity studies were performed for the GM 5.7 liter engine. For CH_3NH_2 significant reaction (10%) occurred in 5 ms at temperatures greater than 1100 K. For N_2O significant reaction occurred in 5 ms at temperatures greater than 1400 K. The results were nearly identical to those for the GMV-4TF. Evidently the difference in equivalence ratio and fuel type were not important at exhaust temperatures. Three exhaust temperature profile cases were run for the GM 5.7 liter. For the low temperature case 1.8% of CH_3NH_2 reacted and 0% of N_2O reacted. For the middle temperature case 11% of CH_3NH_2 was consumed, while only 0.26% of the N_2O reacted. In the high temperature runs, 57% of CH_3NH_2 reacted and 1.2% of the N_2O was destroyed.

7.2 Four-Stroke Cycle Engine Testing

Table 7.1 summarizes the advantages and disadvantages of each tracer gas evaluated for application to the GM 5.7 liter engine. The last three rows in this table are qualitative and are applicable to any engine. Based on the data in the table it was concluded that nitrous oxide was the best choice for the engine investigated. Additional conclusions which were arrived at during the 4-stroke cycle engine testing are:

- For quantitative measurement of trapping efficiency the exhaust sampling should be performed after the exhaust from all cylinders has been mixed. Sampling the exhaust near the port gives rise to significant sampling errors.
- To resolve relative differences in trapping efficiency between individual cylinders, the exhaust can be sampled near the port at equal distances away for each cylinder. Differences in exhaust tuning as well as faulty valves can result in relative differences between cylinders.
- The zero overlap cam data suggests that there are other potential mechanisms for tracer survival in the cylinder in addition to incomplete reaction in the bulk charge. It is speculated that these mechanisms are similar to many unburned hydrocarbon mechanisms.
- Monomethylamine is a good choice for a tracer gas where the maximum exhaust temperature is less than 425°C (determined by Schweitzer and Deluca[6]), because of its high cylinder reaction efficiency. The maximum exhaust temperature determined by

Tracer	N_2O	CH_3NH_2	O_2
Average Cylinder Reaction Efficiency	98.1%	99.7%	95.8%
Average Exhaust reaction	3.6%	36%	15%
Handling Concerns	Explosive	Explosive, Health, Corrosive	None
Implementation Cost	Medium	High	Low
Detectability	Excellent	Good	Excellent

Table 7.1 Tracer Gas Comparison Based on 4-Stroke Engine Testing.

Schweitzer and DeLuca[6] is supported by the exhaust reaction data from the 4-stroke engine testing.

- The tracer gas method is more applicable to engines with high short-circuited fractions. As the short-circuited fraction goes up the impact of non-ideal tracer effects are reduced.

7.3 Two-Stroke Cycle Engine Testing

The application of the tracer gas method was most successful on the 2-stroke cycle engine. In addition to evaluating exhaust reaction and cylinder reaction efficiency, the tracer gas method was applied to the engine to study scavenging characteristics at different engine operating conditions. Also the plugging of the exhaust ports with carbon deposits was simulated in the engine. The tracer gas method was used to detect and measure the impact of the reduction in port flow area. This is an illustration of a potential field application.

7.3.1 Non-Ideal Tracer Effects. The method non-ideal tracer effects were evaluated through engine testing on the GMV-4TF. The data shows that approximately 6% of monomethylamine is destroyed in the section of the exhaust system from the exhaust manifold exit to the stack. The same test showed no destruction of nitrous oxide in that section of the exhaust system. In-cylinder sampling measurements were performed to measure cylinder reaction efficiency. The in-cylinder sampling measurements were also used to evaluate the trapped equivalence ratio. In comparing these measurements with the trapped equivalence ratios from tracer gas method measurements, the total exhaust reaction was evaluated. Samples extracted during compression removed from 40 to 55% of the cylinder mass, which is considered to give an accurate representation of the average cylinder composition. In contrast, samples taken during expansion removed from 10 to 20% of the cylinder mass. A summary of non-ideal tracer effects is given in Table 7.2. A port checkvalve measurement for nitrous oxide revealed no nitrous oxide in the blowdown pulse. Thus, the cylinder reaction efficiency given in the table is a conservative value.

7.3.2 Comparison of TGM with Other Techniques. The tracer gas method was compared to other techniques for evaluating trapped equivalence ratio over a range of boost pressures. The nitrous oxide TGM compared well with the other techniques, which were in-cylinder sampling during compression and expansion, port checkvalve sampling, and the perfect mixing model. In fact, at any boost level the nitrous oxide TGM data had trapped equivalence ratios both above and below it. The other techniques for evaluating trapped equivalence have errors associated with them. Based on the data the nitrous oxide

TRACER	EXHAUST REACTION, ε_r	CYLINDER REACTION EFFICIENCY, η_{cr}
N_2O	0	0.96
CH_3NH_2	0.44	Not Measured

Table 7.2 Evaluation of Non-Ideal Tracer Effects on the GMV-4TF Engine.

TGM appears to be as accurate, if not more accurate, than the other techniques. The monomethylamine TGM gives unrealistic scavenging efficiencies (η_{sc}>1.0) due to excessive reaction in the exhaust.

7.3.3 Investigations of Scavenging Characteristics

The scavenging characteristic investigations on the GMV-4TF engine were performed with the nitrous oxide TGM for variations in engine operating conditions. For comparison purposes, perfect mixing evaluations were carried out in parallel. The nitrous oxide TGM results were compared to data in the literature for loop scavenged and cross scavenged engines, because the GMV-4TF scavenging configuration contains elements of both types of scavenging designs. The nitrous oxide TGM data fall within boundaries defined by the range of the test data reviewed.

Boost was found to have a much stronger influence on trapped equivalence ratio than speed. Increasing the boost at constant torque tended to decrease the trapped equivalence ratio, resulting in a leaner mixture. The data show a significant decrease in trapped equivalence ratio as the boost increases with a flattening trend at the higher boost levels. The scavenging efficiency goes down with increasing boost. Therefore, at boost

levels higher than 25 kPag (nominal) the scavenging process is less effective at removing combustion products and refilling the cylinder with fresh charge. However, the increase in fresh air mass due to increases in boost is the dominant effect and results in an increase in trapped A/F ratio for increasing boost.

The effect of port blockage on scavenging characteristics, trapped equivalence ratio, and emissions was examined on the 2-4 bank side of the engine. As the level of intake port area blockage increased, the delivery ratio for the 2-4 bank decreased. This was due to an overall decrease in airflow through the engine, and a decrease in the fraction of overall airflow that flowed through the 2-4 bank. The decrease in delivery ratio decreased the scavenging efficiency and increased the trapped equivalence ratio of the 2-4 bank, which resulted in a richer mixture being burned. The small increase in trapped equivalence ratio had a significant impact on emissions. THC and CO emissions did not change significantly. CH_2O emissions increased by a small amount while NO_x emissions increased by 54%.

7.4 New Contributions

The nature of this work was to further develop and update an existing IC engine measurement technique in order to fulfill a current need in engine research and development. Numerous contributions were made to extend IC engine testing and analysis capabilities, which are given below:

- The identification of corrections for non-ideal tracer gas effects.

- The development of a set of equations for calculating scavenging characteristics and trapped equivalence ratio from engine tracer gas data, incorporating corrections for non-ideal tracer gas effects.
- The development of techniques for determining tracer gas suitability using chemical kinetics considerations.
- The identification of a new tracer gas, nitrous oxide, which significantly improves accuracy and applicability of the method.
- Acquired test data on method corrections (exhaust reaction and cylinder reaction efficiency) for two different engines at various operating conditions for traditional tracer gases, monomethylamine and oxygen (4-stroke cycle engine only), and nitrous oxide.
- Updating of the tracer gas method to employ modern instrumentation and measurement techniques.
- The further development of tracer gas method test schematics, techniques, and procedures.
- The identification and development a new application of the tracer gas method for 4-stroke cycle engines with overlap cams: using the tracer gas method to detect the speed at which maximum short-circuiting occurs.
- The identification and development of a new application of the tracer gas method for 2-stroke cycle engines: using the tracer gas method as a diagnostic tool to detect port restrictions such as carbon deposits in the exhaust ports.

- The tracer gas method has been developed to a point where it is field applicable. This is largely due to the application of nitrous oxide, which is stable in the exhaust and does not require special sampling techniques near the port to sample before exhaust reaction occurs, as is required with monomethylamine.

7.5 Conclusions

The following conclusions regarding the tracer gas method can be draw:

1. The tracer gas method, when the right tracer is chosen, is an accurate technique for measuring scavenging characteristics and trapped equivalence ratio.
2. Nitrous oxide is an excellent choice for a tracer for 2-stroke cycle and 4-stroke cycle engines; it is stable in the exhaust, reacts nearly to completion in the engine cylinder, and is easy to use.
3. The tracer gas method is field applicable and requires no major engine modification.
4. The tracer gas method can be used for determining the speed where maximum short-circuiting occurs in 4-stroke engines with overlap cams, and for a diagnostic tool in 2-stroke engines to detect port restrictions, such as carbon deposits.
5. Monomethylamine is not a good choice for a tracer; it has an extremely high exhaust reaction, is highly corrosive, and is harmful if breathed or contacted with skin.

REFERENCES

[1] Heywood, J. B., "Internal Combustion Engine Fundamentals", McGraw-Hill, Inc., 1988.
[2] Mitchell, C. E. and Olsen, D. B., "Formaldehyde Formation Mechanisms in Large Bore Natural Gas Engines", ASME-ICE Conference, April, 1998.
[3] Olsen, D. B. and Mitchell, C. E., "Factors Affecting Measured CH_2O in Large Bore Natural Gas Engines", ASME-ICE Conference, April, 1998.
[4] Gunseli Sagun Shareef, Kathy R. Ferry, Mahesh Gundappa, Chad A. Leatherwood, Larry D. Ogle, Lisa M. Campbell, Gas Research Institute, GRI-96/0009.1, "Measurement of Air Toxic Emissions from Natural Gas-Fired Internal Combustion Engines at Natural Gas Transmission and Storage Facilities, Volume I", 1996.
[5] Nuti, M. and Martorano, L., "Short-Circuit Ratio Evaluation in the Scavenging of Two-Stroke S.I. Engines", SAE 850177, 1985.5
[6] Schweitzer, P. H., DeLuca, Frank Jr., "The Tracer Gas Method of Determining the Charging Efficiency of Two-Stroke-Cycle Diesel Engines", National Advisory Committee for Aeronautics (NACA), Technical Note No. 838, 1941.
[7] Irish, J.S., Karl, R.D., Keller, H.B. and Waldron, A.L., "Measurement of Scavenging Efficiency in the Two Stroke Engine: A Comparison and Analysis of Methods", Thesis, Massachusetts Institute of Technology, 1949.
[8] Isigami, S., Tanaka, Y. and Tamari, M., "The Trapping Efficiency Measurement of Two Stroke Cycle Diesel Engine by Tracer Gas Method", JSME, Vol. 6, No. 23, 1963.
[9] Huber, E.W., "Measuring the Trapping Efficiency of Internal Combustion Engines Through Continuous Exhaust Gas Analysis", SAE 710144, 1971.
[10] Bazika, V. and Rodig, J., "A New Method of Determining the Scavenging Efficiency of Oil-Engine Cylinders", Engineers' Digest, Vol. 24, No. 3, March, 1963.
[11] Wallace, F. J. and Cave, P. R., "Experimental and Analytical Scavenging Studies on a Two-Cycle Opposed Piston Diesel Engine", Society of Automotive Engineers, Paper No. 710175, 1971.
[12] Ku, P. M. and Trimble, T. F., "Scavenging Characteristics of a Two-Stroke-Cycle Engine as Determined by Skip-Cycle Operation", Journal of Research of the National Bureau of Standards, Vol. 57, No. 6, paper 2721, 1956.
[13] Tobis, B. J., Meyer, R., Yang, J., Brehob, D. D. and Anderson, R. W., "Scavenging of a Firing Two-Stroke Spark-Ignition Engine", Society of Automotive Engineers, Paper No. 940393, 1994.
[14] Kannappan, A., "A New Method for Evaluating the Scavenging Performance of Two-Stroke Diesel Engines", Society of Automotive Engineers, Paper No. 640370, 1964.
[15] Booy, R. R., "Evaluating Scavenging Efficiency of Two-Stroke Cycle Gasoline Engines", Society of Automotive Engineers, Paper No. 670029, 1967.
[16] Houtsma, C. G., *et al*, "Correlation of Scavenging Ratio and Scavenging Efficiency in 2-Stroke Compression-Ignition Engine", MIT Thesis, 1950.
[17] Cheng, W. K., Hamrin, D., Heywood, J. B., Hochgreb, S., Min, K. and Norris, M., "An Overview of Hydrocarbon Emissions Mechanisms in Spark-Ignition Engines", SAE 932708, 1993.
[18] Budavari, S. *et al.*, "The Merck Index: An Encyclopedia of Chemicals, Drugs, and Biologicals", Merck & Co., Inc., 1989.
[19] Hayhurst, A. N. and Lawrence, A. D., "Emissions of Nitrous Oxide from Combustion Sources", Progress in Energy and Combustion Science, Vol. 18, pp. 529-552, 1992.
[20] Cullis, C. F. and Isaac, I., "Structural Influences in the Oxidation of Aliphatic Amines", Transactions of the Faraday Society, Vol. 48, pp. 1023, May 1952.
[21] Cullis, C. F. and Smith, L. S. A., "The Thermal Oxidation of the Aliphatic Amines", Transactions of the Faraday Society, Vol.46, pp. 42, Aug. 1949.
[22] Jolley, L. J., "The Thermal Oxidation of Monomethylamine", Journal of the Chemical Society of London, Vol. 137, pp. 1957-1966, 1934.
[23] Cullis, C. F. and Willsher, J. P., "The thermal oxidation of methylamine", Proceedings of the Royal Society, A209, pp. 218-238, 1951.

[24] Hill, G. R. and Wilson, D. G., "A Kinetic Study of Monomethylamine Combustion", Pyrodynamics, Vol. 3, pp. 235-242, 1966.
[25] Tannenbaum, E., Coffin, E. M., and Harrison, A. J., "The Far Ultraviolet Absorption Spectra of Simple Alkyl Amines", The Journal of Chemical Physics, Vol. 21, No. 2, pp. 311, Feb. 1953.
[26] Hwang, S.M., Higashihara, T., Shin, K.S. and Gardiner Jr., W.C., "Shock Tube and Modeling Study of Monomethylamine Oxidation", J. Phys. Chem., Vol. 94, pp. 2883-2889, 1990.
[27] Hinshelwood, C. N. , "The Homogeneous Thermal Decomposition of Nitrous Oxide," Proceedings of the Royal Society of London, Series A, Volume 106, 1924.
[28] Hunter, E., "The Thermal Decomposition of Nitrous Oxide at Pressures up to 40 Atmospheres", Proceedings of the Royal Society of London, Series A, Vol. 144, 1934.
[29] Johnsson, J. E., Glarborg, P. and Dam-Johansen, K., "Thermal Dissociation of Nitrous Oxide at Medium Temperatures", Twenty-Fourth Symposium (International) on Combustion/The Combustion Institute, pp. 917-923, 1992.
[30] Glarborg, P., Johnsson, J.E. and Dam-Johansen, K., "Kinetics of Homogeneous Nitrous Oxide Decomposition", Combustion and Flame, Vol. 99, pp. 523-532, 1994.
[31] S. R. Turns, "An Introduction to Combustion", McGraw-Hill, Inc., 1996.
[32] C. Olikara and G. L. Borman, "A Computer Program for Calculating Properties of Equilibrium Combustion Products with Some Applications to I.C. Engines", SAE 750468, 1975.
[33] "JANAF Thermochemical Tables", Second Edition, The Dow Chemical Co., Midland, Michigan, 1971.
[34] Kee, R. J., Rupley, F. M. and Miller, J. A., "Chemkin-II: A Fortran Chemical Kinetics Package for the Analysis of Gas-Phase Chemical Kinetics", Sandia National Laboratories Report SAND89-8009•UC-401, 1989.
[35] A. E. Lutz, R. J. Kee, and J. A. Miller, "SENKIN: A Fortran Program for Predicting Homogeneous Gas Phase Chemical Kinetics with Sensitivity Analysis", Sandia National Laboratories, Report SAND87-8248*UC-4, Printed Feb. 1988.
[36] Caracotsios, M. and Stewart, W. E., "Sensitivity Analysis of Initial Value Problems Including ODE's and Algebraic Equations," Computers and Chemical Engineering, Vol. 9, No. 4, pp. 359-365, 1985.
[37] Mebel, A. M., Lin, M. C. and Morokuma, K., "Theoretical Study of Reactions of N_2O with NO and OH Radicals", International Journal of Chemical Kinetics, Vol. 28, 693-703, 1996.
[38] Personal communication with Peter Glarborg, Department of Chemical Engineering, Technical University of Denmark, 1997.
[39] Frenklach, M., Wang, H., Bowman, C. T., Hanson, R. K., Smith, G. P., Golden, D. M., Gardiner, W. C., and Lissianski, V., "An Optimized Kinetics Model for Natural Gas Combustion", 25th International Symposium on Combustion, Work-In-Progress Poster Session 3, Number 26, 1994.
[40] Adams, T.G., "Effect of Exhaust System Design on Engine Performance", SAE 800319, 1980.
[41] Willson, B., Hutcherson, G., Hawley, S. and Willett, K., "Relative Performance of High-Pressure Fuel Gas Delivery on Large-Bore, Two-Stroke Natural Gas Engines", PCRC Gas Machinery Conference, Austin, Texas, Oct. 6-8, 1997.
[42] Fanick, E. R., Dietzmann, H. E., and Urban, C. M., "Emissions Data for Stationary Reciprocating Engines and Gas Turbines in Use by the Gas Pipeline Transmission Industry", American Gas Association, Report No. PR-15-613, April 1988.
[43] Douglas, R., "AFR and Emissions Calculation for Two-Stroke Cycle Engines", Society of Automotive Engineers, Special Publication SP-835, Paper No. 901599, 1990.
[44] Taylor, C. F. and Rogowski, A. R., "Scavenging the 2-Stroke Engine", SAE Transactions, Vol. 62, 1954.
[45] Schoonover, R. C., "Development of a Turbocharger Simulation Package and Applications to Large Bore Engine Research", Masters Thesis, Colorado State University, 1995.
[46] Abraham, J., Maqgi, V., Macinnes, J. and Bracco, F. V., "Gas Versus Spray Injection: Which Mixes Faster?", SAE 940895, 1994.
[47] Boyer, R. L., Craig, D. R. and Miller, C. D., "A Photographic Study of Events in a 14-In. Two-Cycle Gas-Engine Cylinder", Transactions of the ASME, Paper No. 53-S-45, 1953.
[48] Potter, C. R., "The Design and Development of an Independent Large Bore, Natural Gas, Engine Test Facility", Masters Thesis, Colorado State University, 1995.

[49] Gyssler, G., "Problems Associated with Turbocharging Large Two-Stroke Diesel Engines," Proc. CIMAC, paper B.16, 1965.

APPENDIX A

N_2O DESTRUCTION MECHANISM

Reactions	A	n	E_a (cal/mol)
N2O+N2=2N2+O	5.44E+14	0	55451
N2O+O2=N2+O+O2	4.48E+14	0	55451
N2O+CO2=N2+O+CO2	9.6E+14	0	55451
N2O+H2O=N2+O+H2O	3.84E+15	0	55451
N2O+H=N2+OH	3.3E+10	0	4727
DUPLICATE			
N2O+H=N2+OH	4.4E+14	0	19244
DUPLICATE			
NH+NO=N2O+H	2.9E+14	-0.40	0
DUPLICATE			
NH+NO=N2O+H	-2.2E+13	-0.23	0
DUPLICATE			
N2O+O=NO+NO	2.9E+13	0	23137
N2O+O=N2+O2	1.4E+12	0	10794
N2O+OH=N2+HO2	1.30E-2	4.72	36600
N2O+OH=HNO+NO	1.18E-4	4.33	25100
N2O+NO=N2+NO2	5.26E+5	2.23	47000

Units are moles, cm^3, s, cal.
Units of A are dependent on stoichiometry.

APPENDIX B

CH_3NH_2 OXIDATION MECHANISM

Reactions	A	n	E_a (cal/mol)
CH3+NH2=CH3NH2	2.50E+13	0	0
CH3+NH2=CH2NH2+H	5.50E+13	0	11702.89
CH3+NH2=CH2NH+H2	6.00E+12	0	16479.58
CH3NH2=CH2NH2+H	1.00E+15	0	84069.74
CH3NH2+CH3=CH2NH2+CH4	6.52E+15	0	27704.8
CH3NH2+NH2=CH2NH2+NH3	3.25E+15	0	22211.61
CH3NH2+H=CH2NH2+H2	1.80E+13	0	5254.359
CH3NH2+H=CH3+NH3	3.90E+14	0	11464.06
CH2NH2=CH2NH+H	1.00E+13	0	42990.21
CH2NH2+H=CH2NH+H2	1.00E+13	0	0
CH2NH+M=CHNH+H+M	1.30E+17	0	65679.48
CH2NH+M=HCN+H2+M	3.30E+15	0	38213.52
CH2NH+H=CHNH+H2	5.30E+14	0	10031.05
CHNH+M=HCN+H+M	1.63E+15	0	24838.79
CHNH+H=HCN+H2	2.00E+13	0	0
CH3NH2+O2=CH2NH2+HO2	4.00E+12	0	42034.87
CH3NH2+O=CH2NH2+OH	5.40E+12	0	1671.841
CH3NH2+OH=CH2NH2+H2O	1.20E+07	2	1194.172
CH3NH2+HO2=CH2NH2+H2O2	1.60E+12	0	6448.531
CH2NH2+O2=CH2NH+HO2	9.10E+13	0	9792.214
CH2NH2+O=CH2NH+OH	5.00E+13	0	0
CH2NH2+OH=CH2NH+H2O	5.00E+13	0	0
CH2NH+O=CHNH+OH	1.60E+09	1.2	716.5035
CH2NH+OH=CHNH+H2O	6.00E+13	0	3104.848
CHNH+O=HCN+OH	3.00E+13	0	0
CHNH+OH=HCN+H2O	3.00E+13	0	0
CH3+CH3=C2H6	9.03E+16	-1.2	716.5035
CH3+CH3=C2H4+H2	6.00E+12	0	16479.58
C2H6+CH3=C2H5+CH4	5.50E-01	4	8359.207
C2H6+H=C2H5+H2	1.30E+14	0	9314.545
C2H5=C2H4+H	2.00E+13	0	39646.52
C2H5+H=CH3+CH3	3.73E+13	0	0
C2H5+H=C2H4+H2	1.70E+12	0	0
C2H4+M=C2H2+H2+M	2.60E+17	0	79293.05
C2H4+M=C2H3+H+M	2.60E+17	0	96489.13
C2H4+H=C2H3+H2	1.50E+14	0	10269.88
C2H3+H=C2H2+H2	2.00E+13	0	0
C2H2+H=C2H3	5.50E+12	0	2149.51
CH4=CH3+H	1.00E+15	0	99832.82
CH4+H=CH3+H2	2.20E+04	3	8836.876
CH4+O=CH3+OH	1.20E+07	2.1	7642.704
CH4+OH=CH3+H2O	1.60E+06	2.1	2388.345
CH3+H=CH2+H2	7.20E+14	0	15046.57

Reactions	A	n	E_a (cal/mol)
CH3+O2=CH3O+O	2.20E+14	0	33675.66
CH3+O2=CH2O+OH	3.20E+11	0	9075.711
CH3+O=CH2O+H	7.00E+13	0	0
CH3+OH=CH2+H2O	2.00E+13	0	0
CH2+H=CH+H2	3.00E+13	0	0
CH2+O2=CO+OH+H	1.30E+13	0	1433.007
CH2+O=CH+OH	8.00E+13	0	0
CH2+OH=CH+H2O	3.00E+13	0	0
CH+O2=CO+OH	2.00E+13	0	0
CH3O+M=CH2O+H+M	1.00E+14	0	25077.62
CH2O+M=CHO+H+M	5.00E+16	0	76427.04
CH2O+H=CHO+H2	2.50E+13	0	4060.186
CH2O+O=CHO+OH	3.50E+13	0	3582.517
CH2O+OH=CHO+H2O	3.00E+13	0	1194.172
CHO+M=CO+H+M	2.50E+14	0	16718.41
CHO+H=CO+H2	2.00E+14	0	0
CHO+O2=CO+HO2	3.00E+12	0	0
CHO+O=CO+OH	3.00E+13	0	0
CHO+OH=CO+H2O	5.00E+13	0	0
C2H6+O=C2H5+OH	3.00E+07	2	5015.524
C2H6+OH=C2H5+H2O	6.30E+06	2	716.5035
C2H4+O=CH3+CHO	1.60E+09	1.2	716.5035
C2H4+OH=C2H3+H2O	5.00E+13	0	6687.366
C2H3+O2=CH2O+CHO	4.00E+12	0	-238.834
C2H2+O=CH2+CO	4.10E+08	1.5	1671.841
C2H2+O=C2HO+H	4.30E+14	0	12180.56
C2H2+OH=C2H2O+H	1.00E+14	0	11464.06
C2H2O+M=CH2+CO+M	3.60E+15	0	59230.95
C2HO+H=CH2+CO	3.00E+13	0	0
NH2+NH2=N2H2+H2	4.00E+13	0	11702.89
NH2+NH=N2H2+H	3.20E+13	0	955.338
N2H2+M=N2H+H+M	1.00E+16	0	49916.41
N2H2+H=N2H+H2	5.00E+13	0	955.338
NH3+M=NH2+H+M	2.50E+16	0	93623.12
NH3+H=NH2+H2	1.30E+14	0	21495.1
NH3+O=NH2+OH	2.20E+13	0	8836.876
NH3+OH=NH2+H2O	5.80E+13	0	8120.373
NH2+H=NH+H2	1.90E+13	0	0
NH2+O2=HNO+OH	1.51E+12	-0.4	36064.01
NH2+HO2=NH2O+OH	2.95E+13	0	21972.77
NH2+NO=N2H+OH	8.82E+15	-1.25	0
NH2+NO=N2+H2O	6.30E+19	-2.5	1910.676
NH2+O=HNO+H	8.94E+14	-0.5	238.8345

Reactions	A	n	E_a (cal/mol)
NH2+O=NH+OH	6.90E+11	0.4	-238.834
NH2+OH=NH+H2O	5.00E+11	0.5	1910.676
NH+H=N+H2	1.00E+14	0	0
NH+O2=NO+OH	1.40E+11	0	1910.676
NH+O2=HNO+O	1.00E+13	0	11941.72
NH+NO=N2O+H	1.70E+14	-0.5	0
NH+O=NO+H	6.30E+11	0.5	0
NH+OH=HNO+H	1.50E+12	0.5	1910.676
NH+OH=N+H2O	5.00E+11	0.5	1910.676
NH2O+M=HNO+H+M	3.55E+13	0	25077.62
N+O2=NO+O	6.00E+09	1	6209.697
N2+O=N+NO	1.84E+14	0	76188.2
NO+H=N+OH	1.70E+14	0	48722.24
HNO+M=H+NO+M	1.90E+16	0	48722.24
HNO+H=NO+H2	1.30E+13	0	4060.186
HNO+OH=NO+H2O	3.60E+13	0	0
N2H+M=N2+H+M	2.00E+14	0	5970.862
N2H+NO=N2+HNO	2.50E+12	0	0
N2O+M=N2+O+M	6.92E+23	-2.5	64962.98
N2O+H=N2+OH	7.60E+13	0	15046.57
N2O+O=NO+NO	1.00E+14	0	27943.64
HCN+O=CN+OH	5.00E+13	0	21972.77
HCN+O=NCO+H	1.74E+08	1.5	7403.869
HCN+O=NH+CO	2.20E+13	0	15285.41
HCN+OH=CN+H2O	4.40E+12	0	9075.711
CN+H2=HCN+H	2.50E+02	3.62	1910.676
CN+O2=NCO+O	5.60E+12	0	0
CN+O=CO+N	2.04E+13	0	477.669
CN+OH=NCO+H	5.60E+13	0	0
NCO+M=CO+N+M	6.31E+16	-0.5	47766.9
NCO+H2=HNCO+H	3.00E+13	0	5254.359
NCO+H=NH+CO	4.00E+13	0	0
NCO+NO=N2O+CO	1.00E+13	0	-477.669
NCO+O=NO+CO	5.80E+13	0	0
HNCO+M=NH+CO+M	5.00E+13	0	69978.5
HNCO+H=NH2+CO	2.00E+13	0	3104.848
HNCO+O2=NCO+HO2	1.00E+13	0	69978.5
H2+M=H+H+M	2.20E+14	0	96011.46
H+O2=OH+O	2.20E+14	0	16718.41
O+H2=OH+H	1.50E+07	2	7642.704
OH+H2=H2O+H	1.00E+08	1.6	3343.683
OH+OH=H2O+O	1.50E+09	1.14	0
H+O2+M=HO2+M	7.50E+23	-2.6	0

Reactions	A	n	E_a (cal/mol)
HO2+H=OH+OH	2.50E+14	0	1910.676
HO2+H=H2+O2	2.50E+13	0	716.5035
HO2+OH=H2O+O2	2.00E+13	0	0
HO2+O=OH+O2	2.00E+13	0	0
HO2+HO2=H2O2+O2	2.00E+12	0	0
H2O2+M=OH+OH+M	1.20E+17	0	45378.55
CO+OH=CO2+H	4.40E+06	1.5	-716.503
CH3+NO=HCN+H2O	4.30E+12	0	20300.93
CH2+NO=HCN+OH	1.40E+12	0	-1194.17
CH+NO=HCN+O	1.20E+14	0	0
CH+N2=HCN+N	2.10E+12	0	16718.41

Units are moles, cm^3, s, cal.
Units of A are dependent on stoichiometry.

APPENDIX C

GRI-Mech Version 1.2: A NATURAL GAS COMBUSTION MECHANISM

Reactions	A	n	E_a (cal/mol)
2O+M<=>O2+M	1.200E+17	-1.000	0.00
H2/ 2.40/ H2O/15.40/ CH4/ 2.00/ CO/ 1.75/ CO2/ 3.60/ C2H6/ 3.00/ AR/ 0.83/			
O+H+M<=>OH+M	5.000E+17	-1.000	0.00
H2/2.00/ H2O/6.00/ CH4/2.00/ CO/1.50/ CO2/2.00/ C2H6/3.00/ AR/0.70/			
O+H2<=>H+OH	5.000E+04	2.670	6290.00
O+HO2<=>OH+	2.000E+13	0.000	0.00
O+H2O2<=>OH+HO2	9.630E+06	2.000	4000.00
O+CH<=>H+CO	5.700E+13	0.000	0.00
O+CH2<=>H+HCO	8.000E+13	0.000	0.00
O+CH2(S)<=>H2+CO	1.500E+13	0.000	0.00
O+CH2(S)<=>H+HCO	1.500E+13	0.000	0.00
O+CH3<=>H+CH2O	8.430E+13	0.000	0.00
O+CH4<=>OH+CH3	1.020E+09	1.500	8600.00
O+CO+M<=>CO2+M	6.020E+14	0.000	3000.00
H2/2.00/ O2/6.00/ H2O/6.00/ CH4/2.00/ CO/1.50/ CO2/3.50/ C2H6/3.00/ AR/0.50/			
O+HCO<=>OH+CO	3.000E+13	0.000	0.00
O+HCO<=>H+CO2	3.000E+13	0.000	0.00
O+CH2O<=>OH+HCO	3.900E+13	0.000	3540.00
O+CH2OH<=>OH+CH2O	1.000E+13	0.000	0.00
O+CH3O<=>OH+CH2O	1.000E+13	0.000	0.00
O+CH3OH<=>OH+CH2OH	3.880E+05	2.500	3100.00
O+CH3OH<=>OH+CH3O	1.300E+05	2.500	5000.00
O+C2H<=>CH+CO	5.000E+13	0.000	0.00
O+C2H2<=>H+HCCO	1.020E+07	2.000	1900.00
O+C2H2<=>OH+C2H	4.600E+19	-1.410	28950.00
O+C2H2<=>CO+CH2	1.020E+07	2.000	1900.00
O+C2H3<=>H+CH2CO	3.000E+13	0.000	0.00
O+C2H4<=>CH3+HCO	1.920E+07	1.830	220.00
O+C2H5<=>CH3+CH2O	1.320E+14	0.000	0.00
O+C2H6<=>OH+C2H5	8.980E+07	1.920	5690.00
O+HCCO<=>H+2CO	1.000E+14	0.000	0.00
O+CH2CO<=>OH+HCCO	1.000E+13	0.000	8000.00
O+CH2CO<=>CH2+CO2	1.750E+12	0.000	1350.00
O2+CO<=>O+CO2	2.500E+12	0.000	47800.00
O2+CH2O<=>HO2+HCO	1.000E+14	0.000	40000.00
H+O2+M<=>HO2+M	2.800E+18	-0.860	0.00
O2/0.00/ H2O/0.00/ CO/0.75/ CO2/1.50/ C2H6/1.50/ N2/0.00/ AR/0.00/			
H+2O2<=>HO2+O2	3.000E+20	-1.720	0.00
H+O2+H2O<=>HO2+H2O	9.380E+18	-0.760	0.00
H+O2+N2<=>HO2+N2	3.750E+20	-1.720	0.00
H+O2+AR<=>HO2+AR	7.000E+17	-0.800	0.00
H+O2<=>O+OH	8.300E+13	0.000	14413.00

Reactions	A	n	E_a (cal/mol)
2H+M<=>H2+M	1.000E+18	-1.000	0.00
H2/0.00/ H2O/0.00/ CH4/2.00/ CO2/0.00/ C2H6/3.00/ AR/0.63/			
2H+H2<=>2H2	9.000E+16	-0.600	0.00
2H+H2O<=>H2+H2O	6.000E+19	-1.250	0.00
2H+CO2<=>H2+CO2	5.500E+20	-2.000	0.00
H+OH+M<=>H2O+M	2.200E+22	-2.000	0.00
H2/0.73/ H2O/3.65/ CH4/2.00/ C2H6/3.00/ AR/0.38/			
H+HO2<=>O+H2O	3.970E+12	0.000	671.00
H+HO2<=>O2+H2	2.800E+13	0.000	1068.00
H+HO2<=>2OH	1.340E+14	0.000	635.00
H+H2O2<=>HO2+H2	1.210E+07	2.000	5200.00
H+H2O2<=>OH+H2O	1.000E+13	0.000	3600.00
H+CH<=>C+H2	1.100E+14	0.000	0.00
H+CH2(+M)<=>CH3(+M)	2.500E+16	-0.800	0.00
LOW / 3.200E+27 -3.140 1230.00/			
TROE/ 0.6800 78.00 1995.00 5590.00 /			
H2/2.00/ H2O/6.00/ CH4/2.00/ CO/1.50/ CO2/2.00/ C2H6/3.00/ AR/0.70/			
H+CH2(S)<=>CH+H2	3.000E+13	0.000	0.00
H+CH3(+M)<=>CH4(+M)	1.270E+16	-0.630	383.00
LOW / 2.477E+33 -4.760 2440.00/			
TROE/ 0.7830 74.00 2941.00 6964.00 /			
H2/2.00/ H2O/6.00/ CH4/2.00/ CO/1.50/ CO2/2.00/ C2H6/3.00/ AR/0.70/			
H+CH4<=>CH3+H2	6.600E+08	1.620	10840.00
H+HCO(+M)<=>CH2O(+M)	1.090E+12	0.480	-260.00
LOW / 1.350E+24 -2.570 1425.00/			
TROE/ 0.7824 271.00 2755.00 6570.00 /			
H2/2.00/ H2O/6.00/ CH4/2.00/ CO/1.50/ CO2/2.00/ C2H6/3.00/ AR/0.70/			
H+HCO<=>H2+CO	7.340E+13	0.000	0.00
H+CH2O(+M)<=>CH2OH(+M)	5.400E+11	0.454	3600.00
LOW / 1.270E+32 -4.820 6530.00/			
TROE/ 0.7187 103.00 1291.00 4160.00 /			
H2/2.00/ H2O/6.00/ CH4/2.00/ CO/1.50/ CO2/2.00/ C2H6/3.00/			
H+CH2O(+M)<=>CH3O(+M)	5.400E+11	0.454	2600.00
LOW / 2.200E+30 -4.800 5560.00/			
TROE/ 0.7580 94.00 1555.00 4200.00 /			
H2/2.00/ H2O/6.00/ CH4/2.00/ CO/1.50/ CO2/2.00/ C2H6/3.00/			
H+CH2O<=>HCO+H2	2.300E+10	1.050	3275.00
H+CH2OH(+M)<=>CH3OH(+M)	1.800E+13	0.000	0.00
LOW / 3.000E+31 -4.800 3300.00/			
TROE/ 0.7679 338.00 1812.00 5081.00 /			
H2/2.00/ H2O/6.00/ CH4/2.00/ CO/1.50/ CO2/2.00/ C2H6/3.00/			
H+CH2OH<=>H2+CH2O	2.000E+13	0.000	0.00
H+CH2OH<=>OH+CH3	1.200E+13	0.000	0.00

Reactions	A	n	E_a (cal/mol)
H+CH2OH<=>CH2(S)+H2O	6.000E+12	0.000	0.00
H+CH3O(+M)<=>CH3OH(+M)	5.000E+13	0.000	0.00
LOW / 8.600E+28 -4.000 3025.00/			
TROE/ 0.8902 144.00 2838.00 45569.00 /			
H2/2.00/ H2O/6.00/ CH4/2.00/ CO/1.50/ CO2/2.00/ C2H6/3.00/			
H+CH3O<=>H+CH2OH	3.400E+06	1.600	0.00
H+CH3O<=>H2+CH2O	2.000E+13	0.000	0.00
H+CH3O<=>OH+CH3	3.200E+13	0.000	0.00
H+CH3O<=>CH2(S)+H2O	1.600E+13	0.000	0.00
H+CH3OH<=>CH2OH+H2	1.700E+07	2.100	4870.00
H+CH3OH<=>CH3O+H2	4.200E+06	2.100	4870.00
H+C2H(+M)<=>C2H2(+M)	1.000E+17	-1.000	0.00
LOW / 3.750E+33 -4.800 1900.00/			
TROE/ 0.6464 132.00 1315.00 5566.00 /			
H2/2.00/ H2O/6.00/ CH4/2.00/ CO/1.50/ CO2/2.00/ C2H6/3.00/ AR/0.70/			
H+C2H2(+M)<=>C2H3(+M)	5.600E+12	0.000	2400.00
LOW / 3.800E+40 -7.270 7220.00/			
TROE/ 0.7507 98.50 1302.00 4167.00 /			
H2/2.00/ H2O/6.00/ CH4/2.00/ CO/1.50/ CO2/2.00/ C2H6/3.00/ AR/0.70/			
H+C2H3(+M)<=>C2H4(+M)	6.080E+12	0.270	280.00
LOW / 1.400E+30 -3.860 3320.00/			
TROE/ 0.7820 207.50 2663.00 6095.00 /			
H2/2.00/ H2O/6.00/ CH4/2.00/ CO/1.50/ CO2/2.00/ C2H6/3.00/ AR/0.70/			
H+C2H3<=>H2+C2H2	3.000E+13	0.000	0.00
H+C2H4(+M)<=>C2H5(+M)	1.080E+12	0.454	1820.00
LOW / 1.200E+42 -7.620 6970.00/			
TROE/ 0.9753 210.00 984.00 4374.00 /			
H2/2.00/ H2O/6.00/ CH4/2.00/ CO/1.50/ CO2/2.00/ C2H6/3.00/ AR/0.70/			
H+C2H4<=>C2H3+H2	1.325E+06	2.530	12240.00
H+C2H5(+M)<=>C2H6(+M)	5.210E+17	-0.990	1580.00
LOW / 1.990E+41 -7.080 6685.00/			
TROE/ 0.8422 125.00 2219.00 6882.00 /			
H2/2.00/ H2O/6.00/ CH4/2.00/ CO/1.50/ CO2/2.00/ C2H6/3.00/ AR/0.70/			
H+C2H5<=>H2+C2H4	2.000E+12	0.000	0.00
H+C2H6<=>C2H5+H2	1.150E+08	1.900	7530.00
H+HCCO<=>CH2(S)+CO	1.000E+14	0.000	0.00
H+CH2CO<=>HCCO+H2	5.000E+13	0.000	8000.00
H+CH2CO<=>CH3+CO	1.130E+13	0.000	3428.00
H+HCCOH<=>H+CH2CO	1.000E+13	0.000	0.00
H2+CO(+M)<=>CH2O(+M)	4.300E+07	1.500	79600.00
LOW / 5.070E+27 -3.420 84350.00/			
TROE/ 0.9320 197.00 1540.00 10300.00 /			
H2/2.00/ H2O/6.00/ CH4/2.00/ CO/1.50/ CO2/2.00/ C2H6/3.00/ AR/0.70/			

Reactions	A	n	E_a (cal/mol)
OH+H2<=>H+H2O	2.160E+08	1.510	3430.00
2OH(+M)<=>H2O2(+M)	7.400E+13	-0.370	0.00
LOW / 2.300E+18 -0.900 -1700.00/			
TROE/ 0.7346 94.00 1756.00 5182.00 /			
H2/2.00/ H2O/6.00/ CH4/2.00/ CO/1.50/ CO2/2.00/ C2H6/3.00/ AR/0.70/			
2OH<=>O+H2O	3.570E+04	2.400	-2110.00
OH+HO2<=>O2+H2O	2.900E+13	0.000	-500.00
OH+H2O2<=>HO2+H2O	1.750E+12	0.000	320.00
DUPLICATE			
OH+H2O2<=>HO2+H2O	5.800E+14	0.000	9560.00
DUPLICATE			
OH+C<=>H+CO	5.000E+13	0.000	0.00
OH+CH<=>H+HCO	3.000E+13	0.000	0.00
OH+CH2<=>H+CH2O	2.000E+13	0.000	0.00
OH+CH2<=>CH+H2O	1.130E+07	2.000	3000.00
OH+CH2(S)<=>H+CH2O	3.000E+13	0.000	0.00
OH+CH3(+M)<=>CH3OH(+M)	6.300E+13	0.000	0.00
LOW / 2.700E+38 -6.300 3100.00/			
TROE/ 0.2105 83.50 5398.00 8370.00 /			
H2/2.00/ H2O/6.00/ CH4/2.00/ CO/1.50/ CO2/2.00/ C2H6/3.00/			
OH+CH3<=>CH2+H2O	5.600E+07	1.600	5420.00
OH+CH3<=>CH2(S)+H2O	2.501E+13	0.000	0.00
OH+CH4<=>CH3+H2O	1.000E+08	1.600	3120.00
OH+CO<=>H+CO2	4.760E+07	1.228	70.00
OH+HCO<=>H2O+CO	5.000E+13	0.000	0.00
OH+CH2O<=>HCO+H2O	3.430E+09	1.180	-447.00
OH+CH2OH<=>H2O+CH2O	5.000E+12	0.000	0.00
OH+CH3O<=>H2O+CH2O	5.000E+12	0.000	0.00
OH+CH3OH<=>CH2OH+H2O	1.440E+06	2.000	-840.00
OH+CH3OH<=>CH3O+H2O	6.300E+06	2.000	1500.00
OH+C2H<=>H+HCCO	2.000E+13	0.000	0.00
OH+C2H2<=>H+CH2CO	2.180E-04	4.500	-1000.00
OH+C2H2<=>H+HCCOH	5.040E+05	2.300	13500.00
OH+C2H2<=>C2H+H2O	3.370E+07	2.000	14000.00
OH+C2H2<=>CH3+CO	4.830E-04	4.000	-2000.00
OH+C2H3<=>H2O+C2H2	5.000E+12	0.000	0.00
OH+C2H4<=>C2H3+H2O	3.600E+06	2.000	2500.00
OH+C2H6<=>C2H5+H2O	3.540E+06	2.120	870.00
OH+CH2CO<=>HCCO+H2O	7.500E+12	0.000	2000.00
2HO2<=>O2+H2O2	1.300E+11	0.000	-1630.00
DUPLICATE			
2HO2<=>O2+H2O2	4.200E+14	0.000	12000.00
DUPLICATE			

Reactions	A	n	E_a (cal/mol)
HO2+CH2<=>OH+CH2O	2.000E+13	0.000	0.00
HO2+CH3<=>O2+CH4	1.000E+12	0.000	0.00
HO2+CH3<=>OH+CH3O	2.000E+13	0.000	0.00
HO2+CO<=>OH+CO2	1.500E+14	0.000	23600.00
HO2+CH2O<=>HCO+H2O2	1.000E+12	0.000	8000.00
C+O2<=>O+CO	5.800E+13	0.000	576.00
C+CH2<=>H+C2H	5.000E+13	0.000	0.00
C+CH3<=>H+C2H2	5.000E+13	0.000	0.00
CH+O2<=>O+HCO	3.300E+13	0.000	0.00
CH+H2<=>H+CH2	1.107E+08	1.790	1670.00
CH+H2O<=>H+CH2O	5.710E+12	0.000	-755.00
CH+CH2<=>H+C2H2	4.000E+13	0.000	0.00
CH+CH3<=>H+C2H3	3.000E+13	0.000	0.00
CH+CH4<=>H+C2H4	6.000E+13	0.000	0.00
CH+CO(+M)<=>HCCO(+M)	5.000E+13	0.000	0.00
LOW / 2.690E+28 -3.740 1936.00/			
TROE/ 0.5757 237.00 1652.00 5069.00 /			
H2/2.00/ H2O/6.00/ CH4/2.00/ CO/1.50/ CO2/2.00/ C2H6/3.00/ AR/0.70/			
CH+CO2<=>HCO+CO	3.400E+12	0.000	690.00
CH+CH2O<=>H+CH2CO	9.460E+13	0.000	-515.00
CH+HCCO<=>CO+C2H2	5.000E+13	0.000	0.00
CH2+O2<=>OH+HCO	1.320E+13	0.000	1500.00
CH2+H2<=>H+CH3	5.000E+05	2.000	7230.00
2CH2<=>H2+C2H2	3.200E+13	0.000	0.00
CH2+CH3<=>H+C2H4	4.000E+13	0.000	0.00
CH2+CH4<=>2CH3	2.460E+06	2.000	8270.00
CH2+CO(+M)<=>CH2CO(+M)	8.100E+11	0.500	4510.00
LOW / 2.690E+33 -5.110 7095.00/			
TROE/ 0.5907 275.00 1226.00 5185.00 /			
H2/2.00/ H2O/6.00/ CH4/2.00/ CO/1.50/ CO2/2.00/ C2H6/3.00/ AR/0.70/			
CH2+HCCO<=>C2H3+CO	3.000E+13	0.000	0.00
CH2(S)+N2<=>CH2+N2	1.500E+13	0.000	600.00
CH2(S)+AR<=>CH2+AR	9.000E+12	0.000	600.00
CH2(S)+O2<=>H+OH+CO	2.800E+13	0.000	0.00
CH2(S)+O2<=>CO+H2O	1.200E+13	0.000	0.00
CH2(S)+H2<=>CH3+H	7.000E+13	0.000	0.00
CH2(S)+H2O(+M)<=>CH3OH(+M)	2.000E+13	0.000	0.00
LOW / 2.700E+38 -6.300 3100.00/			
TROE/ 0.1507 134.00 2383.00 7265.00 /			
H2/2.00/ H2O/6.00/ CH4/2.00/ CO/1.50/ CO2/2.00/ C2H6/3.00/			
CH2(S)+H2O<=>CH2+H2O	3.000E+13	0.000	0.00
CH2(S)+CH3<=>H+C2H4	1.200E+13	0.000	-570.00
CH2(S)+CH4<=>2CH3	1.600E+13	0.000	-570.00

Reactions	A	n	E_a (cal/mol)
CH2(S)+CO<=>CH2+CO	9.000E+12	0.000	0.00
CH2(S)+CO2<=>CH2+CO2	7.000E+12	0.000	0.00
CH2(S)+CO2<=>CO+CH2O	1.400E+13	0.000	0.00
CH2(S)+C2H6<=>CH3+C2H5	4.000E+13	0.000	-550.00
CH3+O2<=>O+CH3O	2.675E+13	0.000	28800.00
CH3+O2<=>OH+CH2O	3.600E+10	0.000	8940.00
CH3+H2O2<=>HO2+CH4	2.450E+04	2.470	5180.00
2CH3(+M)<=>C2H6(+M)	2.120E+16	-0.970	620.00
LOW / 1.770E+50 -9.670 6220.00/			
TROE/ 0.5325 151.00 1038.00 4970.00 /			
H2/2.00/ H2O/6.00/ CH4/2.00/ CO/1.50/ CO2/2.00/ C2H6/3.00/ AR/0.70/			
2CH3<=>H+C2H5	4.990E+12	0.100	10600.00
CH3+HCO<=>CH4+CO	2.648E+13	0.000	0.00
CH3+CH2O<=>HCO+CH4	3.320E+03	2.810	5860.00
CH3+CH3OH<=>CH2OH+CH4	3.000E+07	1.500	9940.00
CH3+CH3OH<=>CH3O+CH4	1.000E+07	1.500	9940.00
CH3+C2H4<=>C2H3+CH4	2.270E+05	2.000	9200.00
CH3+C2H6<=>C2H5+CH4	6.140E+06	1.740	10450.00
HCO+H2O<=>H+CO+H2O	2.244E+18	-1.000	17000.00
HCO+M<=>H+CO+M	1.870E+17	-1.000	17000.00
H2/2.00/ H2O/0.00/ CH4/2.00/ CO/1.50/ CO2/2.00/ C2H6/3.00/			
HCO+O2<=>HO2+CO	7.600E+12	0.000	400.00
CH2OH+O2<=>HO2+CH2O	1.800E+13	0.000	900.00
CH3O+O2<=>HO2+CH2O	4.280E-13	7.600	-3530.00
C2H+O2<=>HCO+CO	5.000E+13	0.000	1500.00
C2H+H2<=>H+C2H2	4.070E+05	2.400	200.00
C2H3+O2<=>HCO+CH2O	3.980E+12	0.000	-240.00
C2H4(+M)<=>H2+C2H2(+M)	8.000E+12	0.440	88770.00
LOW / 7.000E+50 -9.310 99860.00/			
TROE/ 0.7345 180.00 1035.00 5417.00 /			
H2/2.00/ H2O/6.00/ CH4/2.00/ CO/1.50/ CO2/2.00/ C2H6/3.00/ AR/0.70/			
C2H5+O2<=>HO2+C2H4	8.400E+11	0.000	3875.00
HCCO+O2<=>OH+2CO	1.600E+12	0.000	854.00
2HCCO<=>2CO+C2H2	1.000E+13	0.000	0.00

Units are moles, cm^3, s, cal.
Units of A are dependent on stoichiometry.

APPENDIX D

EES COMPUTER PROGRAMS FOR CALCULATING A/F RATIO FROM EXHAUST EMISSIONS

{A/F RATIO ANALYSIS BASED ON DRY EXHAUST EMISSIONS FROM 5-GAS EMISSIONS BENCH}

{INPUT: intake temperature, pressure, and relative humidity}
Tairman=(110-32)*5/9+273.15
Pboost=(5.4845+25)*101.3/29.92 {in this case Pboost is AMP, the pressure at the RH sensor}
Hrel=26.43 {%}

{INPUT: Dry Emissions from 5-gas Rack}
co2dry%=4.447
codryppm=98.23
noxdryppm=1383
thcdryppm=753.9

{INPUT: For error evaluation}
o2dry%=12.56 {dry O2 from 5-Gas Rack}
h2oppm=110616 {wet H2O from FTIR}

{Assume the following reaction:}
{1[(1-j-k-l)CxHy + jCO2 + kN2 +lO2] + a[O2 + 3.76N2 + bH2O] ------> cH2O + dCO2 + eCO + fNOr + gO2 + hN2 + iCHz}

{Fuel composition}
x=1.169
y=4.337
j=.0262
k=.0068
l=.0003
r=1.1 {assume NOx is all NO}
z=y/x {assume all unburned hydrocarbons are same compostion as fuel}

{Molecular Weights}
MWf=(1-j-k-l)*(12.011*x+1.008*y)+j*(12.011+MWo2)+k*MWn2+l*MWo2
MWo2=15.9994*2
MWn2=14.0067*2
MWh2o=2*1.008+15.9994
MWa=(MWo2+2.76*MWn2+b*MWh2o)/(1+2.76+b)

{Mole fraction of inlet air moisture from inlet air relative humidity (%)}
Hrel=100*Pboost*h2oin/pressure(WATER, X=.5, T=Tairman)

h2oin=a*b/a/(1+3.76+b)

{Dry emission mole fractions in terms of stoichiometric coefficients}
co2dry%=d*100/(N-c)
codryppm=e*1e6/(N-c)
noxdryppm=f*1e6/(N-c)
o2%drycalc=g*100/(N-c)
thcdryppm=i*1e6/(N-c)
h2ocalcppm=c*1e6/N

{How close are the O2 and H2O calculations?}
o2%delta=-o2dry%+o2%drycalc
h2o%error=100*(h2ocalcppm-h2oppm)/h2oppm
comb%err=abs(h2o%error)+abs(100*o2%delta/o2dry%)

{Atom balances}

x*(1-j-k-l) + j = d +e+i	{Carbon}
y*(1-j-k-l) +2*a*b=2*c+i*z	{Hydrogen}
j*2+l*2+2*a+a*b=c+2*d+2*g+e+f*r	{Oxygen}
2*k+2*3.76*a=2*h+f	{Nitrogen}
N=c+d+g+h+e+f+i	{total moles in exhaust}

{A/F Ratio}
a*(1+3.76+b)=AFratio*MWf/Mwa

{A/F RATIO ANALYSIS BASED ON WET EXHAUST EMISSIONS FROM FTIR}

{INPUT: intake temperature, pressure, and relative humidity}
Tairman=(110-32)*5/9+273.15
Pboost=(13.496+25)*101.3/29.92 {in this case Pboost is AMP, the pressure at the RH sensor}
Hrel=33.44 {%}

{INPUT: Wet Emissions from FTIR}
co2wetppm=44258
cowetppm=133.3
noxwetppm=444.1
thcwetppm=856.5

{INPUT: for comparison purposes}
h2oppm=106824 {from FTIR}
o2dry%=12.592 {dry, from 5-Gas Rack}

{Assume the following reaction:}
{1[(1-j-k-l)CxHy + jCO2 + kN2 +lO2] + a[O2 + 3.76N2 + bH2O] ------> cH2O + dCO2 + eCO + fNOr + gO2 + hN2 + iCHz}

{Fuel composition}
x=1.169
y=4.337
j=.0262
k=.0068
l=.0003
r=1.1 {assume NOx has an O/N ratio of r}
z=y/x {assume all unburned hydrocarbons are same compostion as fuel}

{Molecular Weights}
MWf=(1-j-k-l)*(12.011*x+1.008*y)+j*(12.011+MWo2)+k*MWn2+l*MWo2
MWo2=15.9994*2
MWn2=14.0067*2
MWh2o=2*1.008+15.9994
MWa=(MWo2+2.76*MWn2+b*MWh2o)/(1+2.76+b)

{Calculate mole fraction of inlet moisture from inlet air relative humidity (%)}
Psat=pressure(WATER, X=.5, T=Tairman)
Hrel=100*Pboost*h2oin/Psat
h2oin=a*b/a/(1+3.76+b)

{Relate dry and wet emissions}

co2dry%=co2wetppm*100/(1e6-h2oppm)
codryppm=cowetppm*1e6/(1e6-h2oppm)
noxdryppm=noxwetppm*1e6/(1e6-h2oppm)
thcdryppm=thcwetppm*1e6/(1e6-h2oppm)

{Dry emission mole fractions in terms of stoichiometric coefficients}
co2dry%=d*100/(N-c)
codryppm=e*1e6/(N-c)
noxdryppm=f*1e6/(N-c)
o2%drycalc=g*100/(N-c)
thcdryppm=i*1e6/(N-c)
h2ocalcppm=c*1e6/N

{How close are the calculated O2 and H2O values?}
o2%delta=-o2dry%+o2%drycalc
h2o%error=100*(h2ocalcppm-h2oppm)/h2oppm
comb%err=abs(h2o%error)+abs(100*o2%delta/o2dry%)

{Atom balances}

x*(1-j-k-l) + j = d +e+i	{Carbon}
y*(1-j-k-l) +2*a*b=2*c+i*z	{Hydrogen}
j*2+l*2+2*a+a*b=c+2*d+2*g+e+f*r	{Oxygen}
2*k+2*3.76*a=2*h+f	{Nitrogen}
N=c+d+g+h+e+f+i	{total moles in exhaust}

{A/F Ratio}
a*(1+3.76+b)=AFratio*MWf/MWa